2012

Identification of spatiotemporal nutrient patterns and associated ecohydrological trends in the tampa bay coastal region

Brent Wimberly
University of Central Florida

IDENTIFICATION OF SPATIOTEMPORAL NUTRIENT PATTERNS AND ASSOCIATED ECOHYDROLOGICAL TRENDS IN THE TAMPA BAY COASTAL REGION

by

BRENT E. WIMBERLY

A thesis submitted in partial fulfillment of the requirements
for the Honors in the Major Program in Civil Engineering
in the College of Engineering and Computer Science
and in The Burnett Honors College
at the University of Central Florida
Orlando, Florida

Spring Term 2012

Thesis Chair: Dr. Ni-Bin Chang, Ph. D

ABSTRACT

The comprehensive assessment techniques for monitoring of water quality of a coastal bay can be diversified via an extensive investigation of the spatiotemporal nutrient patterns and the associated eco-hydrological trends in a coastal urban region. With this work, it is intended to thoroughly investigate the spatiotemporal nutrient patterns and associated eco-hydrological trends via a two part inquiry of the watershed and its adjacent coastal bay. The findings show that the onset of drought lags the crest of the evapotranspiration and precipitation curve during each year of drought. During the transition year, ET and precipitation appears to start to shift back into the analogous temporal pattern as the 2005 wet year. NDVI shows a flat receding tail for the September crest in 2005 due to the hurricane impact signifying that the hurricane event in October dampening the severity of the winter dry season in which alludes to relative system memory. The k-means model with 8 clusters is the optimal choice, in which cluster 2 at Lower Tampa Bay had the minimum values of total nitrogen (TN) concentrations, chlorophyll *a* (Chl-*a*) concentrations, and ocean color values in every season as well as the minimum concentration of total phosphorus (TP) in three consecutive seasons in 2008. Cluster 5, located in Middle Tampa Bay, displayed elevated TN concentrations, ocean color values, and Chl-*a* concentrations, suggesting that high colored dissolved organic matter values are linked with some nutrient sources. The data presented by the gravity modeling analysis indicate that the Alafia River Basin is the major contributor of nutrients in terms of both TP and TN values in all seasons. Such ecohydrological evaluation can be applied for supporting the LULC management of climatic vulnerable regions as well as further enrich the comprehensive assessment techniques for estimating and examining the multi-temporal impacts and dynamic influence of urban land use

and land cover. Improvements for environmental monitoring and assessment were achieved to advance our understanding of sea–land interactions and nutrient cycling in a coastal bay.

DEDICATIONS

This is for my mother and family for all of their love, encouragement, and support over the years, all of my teachers and colleagues who aided and pressed me to complete this effort, and all of my friends who stuck around all these years.

I don’t think I could have done it without you,

Thank you.

ACKNOWLEDGMENTS

First and foremost, I would like to express my sincere gratitude to my committee members who all have enabled this project reach its full potential. Special thanks go to my thesis chair, Dr. Ni-Bin Chang, for his exceptional guidance, time, and patience; without his spirited drive, this paper would not have been possible. Special thanks are also owed to my other committee members, Dr. Keveh Madani and Dr. Michael Georgiopoublos. First, I would like to thank my department committee member, Dr. Keveh Madani, for his guidance, enthusiastic interest in my academic career, and for taking the time to sit on my committee. Thanks also to my out-of-department committee member, Dr. Michael Georgiopoulos, for providing his valuable time and comments to improve this work.

TABLE OF CONTENTS

LIST OF FIGURES

LIST OF TABLES

CHAPTER 1: INTRODUCTION

1.1. Overview

Urbanized regions are more vulnerable to the impacts of climate change. Urban sprawl has led to an increase in impervious area as well as a decrease in the vegetation cover, which has weakened urban infiltration and flood control capacity; these implications of urbanization have increased the vulnerability of urban region to climate change impacts. Recently, exploring extreme climatic events in urban regions has received wide attention due to an observation of the possible increase in regularity and magnitude of hurricane and drought events, and an increase in deaths and economic losses due to these events (Karl and Easterling, 1999). The recent occurrences of extreme drought events in the east and southeast regions of the United States in Maryland and the Chesapeake Bay area in 2001–2002, the Peace River and Lake Okeechobee in South Florida in 2006, and Lake Lanier in Atlanta, Georgia in 2007; the occurrence of droughts in several regions has led to studies on their impact, mostly on water availability or water shortage in regard to public needs and ecosystem conservation (Haase, 2009). Drought stresses the regions ecosystems by causing increases in the amount of higher concentrated and warmer polluted runoff in the receiving waters resulting in an increase in cases of eutrophication of surface waters.

Nutrient over-enrichment, or eutrophication, in coastal regions alters algal community structure directly by altering competition among the dominant phytoplankton species for nutrients. About 65% of United States estuaries have moderate to high eutrophic conditions[1]; the most eutrophic estuaries are in the Gulf of Mexico (National Oceanic and Atmospheric

Administration, 2011). Eutrophication of coastal water has been considered one of the major threats to the health status of marine ecosystems for more than 40 years because of the various well-documented damaging impacts (Ryther and Dunstan, 1971; Cloern, 2001; Conley, Markager, Andersen, Ellermann, and Svendsen, 2002). During the conduction of a national assessment the consequences of coastal eutrophication, symptoms have been found to become more apparent over the years, including extensive SAV (submerged aquatic vegetation) loss, the associated loss of fish habitat, worsening episodes of low dissolved oxygen in coastal systems, and longer lasting or first-time nuisance/toxic algal blooms (Bricker, Longstaff, Dennison, Jones, Boicourt, Wicks, and Woerner, 2007; Bricker, Clement, Pirhalla, Orlando, and Farrow, 1999). Enrichment of nutrients such as nitrogen and phosphorus, which frequently occur in the forms of nitrite, ammonia, and phosphate, is one of the major causes of cyanobacteria blooms (also known as blue-green algae) in water bodies; cyanobacteria blooms has been linked to human and animal illnesses around the world (Bobbin and Recknagel 2001; Wei, Sugiura, and Maekawa, 2001). Nutrient over-enrichment is not the only major threat to coastal estuaries but also regions of limited nutrient levels may also have adverse effects on coastal estuaries. These changes in the composition of water quality can directly affect various algal species, which may rely on these nutrients for survival.

The comprehensive assessment techniques for monitoring of water quality of a coastal bay can be diversified via an extensive investigation of the spatiotemporal nutrient patterns and the associated eco-hydrological trends in a coastal urban region. To verify such patterns, the urban region of Tampa Bay, located in Florida (south-eastern United States) was selected as a study site; a region in which has grown large enough to affect the hydrological characteristics of

the area due to continuous urban sprawl and expansion. With this work, it is intended to thoroughly investigate the spatiotemporal nutrient patterns and associated eco-hydrological trends via a two part inquiry of the major impacts of water quality status in a coastal expanse.

The first segment of the study will examine how an urban region's watershed, which has grown large enough to affect the hydrological characteristics of the area, affects ecological and hydrological nutrient patterns. This response is due to urbanization increases the impervious area and decreases the vegetation cover, which weakens the infiltration and flood storage capacity. During this section, the impacts of major weather events, e.g., a hurricane event as well as a drought event will also be investigated in order to determine how these incidents affect the spatiotemporal ecohydrological patterns of a coastal region. In this examination, the interactions between various watershed parameters such as the vegetation cover, land surface temperature (LST), evapotranspiration (ET), and precipitation will be explored, e.g., parameters such as evapotranspiration can be affected by both water and energy balances in the system in which involve many complex processes in the hydrological cycle and ecosystem dynamics at the earth's surface.

In the second segment of the study, the linkage between the watershed nutrient input and the spatiotemporal nutrient patterns within a coastal bay will be comprehensively explored via a novel integrated k-means clustering and gravity distribution model. Through the utilization of the k-means clustering analysis ability to partition a set of data into a user-specified number of subsets composed of related objects into clusters it is possible to discover spatiotemporal patterns of water quality hidden within a bay. When the k-means clustering analysis is used in

conjunction with gravity modeling it is possible to estimate and examine the impacts of major watershed nutrient loading locations on the generated clusters. To observe how these patterns change due to impacts of major meteorological conditions previously discussed, this model will be used for one year during the hurricane occurrence and one year during a drought incident.

1.2. Objectives

This work is intended to thoroughly investigate the spatiotemporal nutrient patterns and associated eco-hydrological trends via a two part inquiry of the major impacts of water quality status in a coastal expanse, there are several important scientific questions needed to be address with this study. The following are the key research questions for this study:

1. How does nutrient input from major watershed basins affect the spatiotemporal patterns of nutrients in a coastal bay?
2. What is the spatiotemporal trends and correlation between LST, NDVI, ET, and precipitation?
3. Are there any prevalent association between urbanization and spatiotemporal variation between LST, NDVI, ET, and Precipitation?
4. What are the ecohydrological implications of changes in influential watershed parameters such as normalized difference vegetation index (NDVI), land surface temperature (LST), evapotranspiration (ET), and precipitation?
5. How do major weather events, e.g., hurricane and drought occurrences affect the spatiotemporal nutrient patterns and ecohydrological trends of a coastal region?
6. Can the k-means clustering technique be used to discover spatiotemporal patterns of water quality in a coastal bay?

7. Can the k-means clustering technique be used to ascertain how the water quality changes over the course of a year in a coastal bay?

8. Can a gravity model analysis be deployed to estimate the impacts of watershed nutrient input on the clusters generated by the k-means clustering analysis?

9. Can a gravity model analysis be used to deploy a spatial distribution analysis to estimate the dispersion of watershed nutrient mass input in a coastal bay?

1.3. Limitations

The methodology presented in this paper can be applied in any geographical region and its primary limitations are related to data availability. One problem associated with the study of a region like Tampa Bay is that a large volume of water moves in and out of the bay on each tide causing the volume to fluctuate over time in a cycle. Samples of water taken at one period in time are now displaced at another location in the bay or swept out into the Gulf of Mexico; as a result, the water is always mixing and changing. The dynamics of coastal bay water is very complex so to help make the effects of water motion, seabed topography, and other effects not considered negligible, seasonal averages of all parameters were produced. In addition, the mixing of fresh and seawater in an estuary provides water with a range of salinities and other related properties (Ketchum, 1955). Another problem associated with this study is there exists no data for minor canals and streams in which also input nutrients into the bay. Although these sources of nutrients are much smaller in comparison to major input locations such as the major river basins around the bay, they are still a source of nutrients not taken into consideration for the model.

CHAPTER 2: SPATIOTEMPORAL VARIABLILITY OF ECOHYDROLOGICAL PATTERNS IN THE TAMPA BAY WATERSHED, FLORIDA UNDER THE IMPACTS OF HURRICANES AND DROUGHTS

2.1. Introduction

Urban regions are more vulnerable to climate change impacts. Many of these urban regions have developed over an area large enough to affect the hydrological characteristics because of continuous urban sprawl and rural expansion. An increase in impervious area and a decrease the vegetation cover has led to weakened urban infiltration and flood control capacity. These implications of urbanization have increased the vulnerability of urban region to climate change impacts. In-turn, urbanization has developed a necessity for flood as well as drought management, urban drainage, and drainage infrastructure. Recently, exploring variations and trends of extreme climatic events in urban regions has received wide attention due to an observation of the possible increase in regularity and magnitude of hurricane and drought events, and an increase in deaths and economic losses due to these events (Karl and Easterling, 1999). For example, in 2004, there were 15 named storms including 9 hurricanes in the Atlantic Basin (NCDC, 2004). Among the 9 hurricanes during 2004, 5 made landfall, 4 of them battering the state of Florida (Southeast United States) with devastating results in which Hurricane Charley; is deemed the most powerful hurricane to make landfall in the United States since the category 5 Hurricane Andrew made landfall south of Miami in 1992 (Sallenger et al., 2006). On the opposite end of the spectrum, there have been recent occurrences of extreme drought events in the east and southeast regions of the United States in Maryland and the Chesapeake Bay area in

2001–2002, the Peace River and Lake Okeechobee in South Florida in 2006, and Lake Lanier in Atlanta, Georgia in 2007; the occurrence of droughts in several regions has led to studies on their impact, mostly on water availability or water shortage in regard to public needs and ecosystem conservation (Haase, 2009). A complete review of the potential impacts of climatic change is provided in the Intergovernmental Panel on Climate Change (IPCC) (IPCC, 1996).

Urbanization also leads to more intense heat exchange that augments heat retention and produces more heat than the natural ecological environment; this impact illuminates the causes of urban heat island effect (UHI) as well as an evident increase in evapotranspiration (ET). Urban heat island effect have caused changes in urban precipitation and temperature that are at least similar to, or greater than, those predicted to develop over the next 100 years by global change models (Changnon, 1992). Research on the trends of surface temperatures at rapidly growing urban sites in the United States during the last 30 to 50 years suggests that significant UHI effects have caused the temperatures at these sites to rise by 1° to 2° C (Cayan and Douglas, 1984; Karl et al., 1988).Urban heat island effect stresses the regions ecosystems by causing increases in the amount of warmer polluted runoff in the receiving waters resulting in an increase in cases of eutrophication of surface waters. During a national assessment the consequences of coastal eutrophication, symptoms have been found to become more apparent over the years, including extensive SAV (submerged aquatic vegetation) loss, the associated loss of fish habitat, worsening episodes of low dissolved oxygen in coastal systems, and longer lasting or first-time nuisance/toxic algal blooms (Bricker et. al., 2007; Bricker et. al., 1999). In order to better understand urban land use and land cover (LULC) dynamics and water sustainability in urban regions, resilience theory offers insights into the behavior of complex systems and characterizes

the importance of system criteria such as system memory, self-organization, and diversity (Adger et. al., 2005; Allenby et. al., 2005). The relationship between land surface temperature (LST) and land cover in Guangzhou and in the urban clusters in the Zhujiang Delta, China was investigated by Weng (2001, 2003). Weng (2004) also derived an estimation of the land surface temperature and vegetation abundance relationship for urban heat island studies. In spite of significant contributions, the event-based assessment of ecohydrological effects and urban heat island effect in urban regions integrating such important ecohydrological parameters including ET, vegetation cover, precipitation, and LST during extreme climatic events is rather limited.

Burn and Hag Elnur (2002) conducted studies and developed a procedure that identifies trends in hydrologic variables via the utilization of the Mann–Kendall non-parametric test to detect trends; within this context, a permutation approach was used to estimate the test distribution, and account for the correlation structure in the data for determining the significance level of the test results based on 18 hydrologic variables collected from a point-measurement network of 248 Canadian catchments. The emergence of remote sensing technologies and spatial statistics has brought up novel means to engage in the event-based assessment of ecohydrological effects in urban regions. Conventionally, studies on UHI have been conducted for isolated locations with in-situ measurements of air temperatures. The advent of satellite remote sensing technology has made it possible to study UHI remotely on urban, regional, continental or even global scales (Streutker, 2002). Due to the complexity and ever-changing of ecohydrological system dynamics, periodic point measurements may not be representative. As of in the last couple decades, studies on the UHI phenomenon using satellite derived LST measurements were conducted primarily using the data collected by the *Advanced Very High*

Resolution Radiometer (*AVHRR*) and the Moderate Resolution Imaging Spectroradiometer (MODIS) (Balling and Brazell, 1988; Gallo et al., 1993; Gallo and Owen, 1998; Kidder and Wu, 1987; Roth et al., 1989; Streutker, 2002).

The utilization of computational intelligence and/or spatial statistics in support of the information retrieval via remote sensing to discover hidden spatiotemporal patterns, variations, and trends for the ecological, hydrological, and thermal cycles at the surface of the Earth is required to realize some key scientific questions in this study: (1) "What is the spatiotemporal trends and correlation between LST, NDVI, ET, and precipitation?" (2) "What effect does extreme climatic events such as hurricanes and droughts on the spatiotemporal patterns within a watershed?" (3) "Are there any prevalent association between urbanization and spatiotemporal variation between LST, NDVI, ET, and Precipitation?" (4) "What are the ecohydrological implications of changes in influential watershed parameters such as NDVI, LST, ET, and precipitation?"

On a long-term basis, the integration of urban hydrology with remote sensing technologies may provide us with quantitative and qualitative ways to measure urban system adaptive capability relative to system memory, self-organization, and temporal diversity on a seasonal temporal scale and identify emergent threshold limits in the assessment of ecosystem resilience in urban regions (Blackmore and Plant, 2008). The objective of this study is to investigate the spatiotemporal variability of ecohydrological patterns and the impact of UHI effect in the urbanized Tampa Bay Watershed, Florida under major climatic events, in particular, hurricanes and droughts. All these weather events impact ecosystem processes and services

triggering a need for advanced ecohydrological studies, especially in coastal urban regions where most of the population lives. As a consequence, urban hydrology or hydrometeorology is playing a pivotal role on regional water balance and conservation in this Tampa Bay region. This study particularly examined hurricane Wilma that made landfall in south Florida on October 24th, 2005, drought events in 2007, and the wet year in 2008 such that the effects of a transition year between drought and wet years as well as between hurricane and wet years can be comparatively elucidated. We hypothesize that "there exists changing spatial clustering across these selected ecohydrological parameters in Tampa Bay Watershed that holistically entails the interactions among ecological, hydrological, and thermal cycles under natural hazard impact. The spatiotemporal distribution of fundamental ecohydrological variables including ET, NDVI, precipitation, and LST affected by both water and energy equilibriums in the soil-vegetation-atmosphere system was derived via the use of several spatial statics techniques. It leads to the realization of the temporal and spatial correlation structure of the data in connection with the distribution and intensification of ecohydrological parameters and the spatiotemporal assessment of urban LULC components with respect to ecohydrological features. Although, there exists an assortment of other regional parameters of a system with sea–land interactions, which should be also considered, the parameters stated herein have been deemed vital to gain a better understanding and more sophisticated picture of the coupled bay and watershed system. Such ecohydrological evaluation can be applied for supporting the urban planning in response to land use and cover change (LUCC) in association with major climatic events vulnerable to the region as well as enriching the comprehensive assessment techniques for estimating and examining the impacts and dynamic influence of natural hazards on urban LULC.

2.2. Materials and methods

This study comprehensively inspected the potential spatiotemporal variability of ecohydrological patterns and the impact of UHI effect in an urbanized coastal region under major climatic events. The interactions between various watershed ecohydrological parameters including the NDVI, LST, ET, and precipitation under these conditions was also examined for knowledge discovery. The investigation was partitioned into three primary steps: (1) the first step encompassed the examination of monthly temporal pairwise-plots in order to pin down subtle changes for each parameter and investigated the hidden relationships and identified the ecohydrological implications during extreme climatic events. (2) the second step incorporated the employment of the spatial statistic method coefficient of variation (CoV) analysis in order to ascertain the degree of spatial variation; the values for each parameter spatial patterns via maps was examined for relevant knowledge discovery. (3) the final step contained Moran's I, a multi-dimensional measure of spatial autocorrelation, to establish the similarity between observations as a function of the time separation between them. With the inclusion of these three unified efforts stepwise, the comprehensive assessment of the spatiotemporal variability of ecohydrological patterns and the impact of UHI effect in the urbanized Tampa Bay Watershed, Florida under major climatic events was realized.

2.2.1. Study site

The study area chosen is the urbanized region Tampa Bay, Florida (Southeast United States), which is the economic and environmental hub of a rapidly growing coastal region supporting almost three million people (Figure 2.1). It is Florida's largest open-water estuary, with a surface area of 1,031 km^2 and on average, 3.7 m deep. More than 100 tributaries flow into

Tampa Bay, including dozens of meandering, brackish water creeks and four major rivers: Hillsborough River, Alafia River, Manatee River, and Little Manatee River (Russell et. al.). Such strong sea-land interactions can be seen in many coastal cities in the rest of the world as urbanization effect deeply affect the LULC changes in urban regions. This type of routine air-sea-land interactions can intimately tie four coastal river basins, including Hillsborough River, Alafia River, Little Manatee River and Manatee River, to the four bay segments to form a complex environmental system in which the ecohydrological study is in an acute need. There are 16 standard land use classes as classified by the United States Geological Survey (USGS) in the following LULC map. They include open water, barren land, cultivated crops, deciduous forest, developed area with high intensity, developed area with medium intensity, developed area with low intensity, developed area with open space, emergent herbaceous wetlands, evergreen forest, hay/pasture, herbaceous land, mixed forest, perennial snow/ice, shrub/scrub, and woody wetlands. The urban and developed areas are mainly distributed at north Tampa Bay and lower south Tampa Bay. Most of the grassland (herbaceous land) is located at upstream of Hillsborough and Alafia catchments (Figure 2.1).

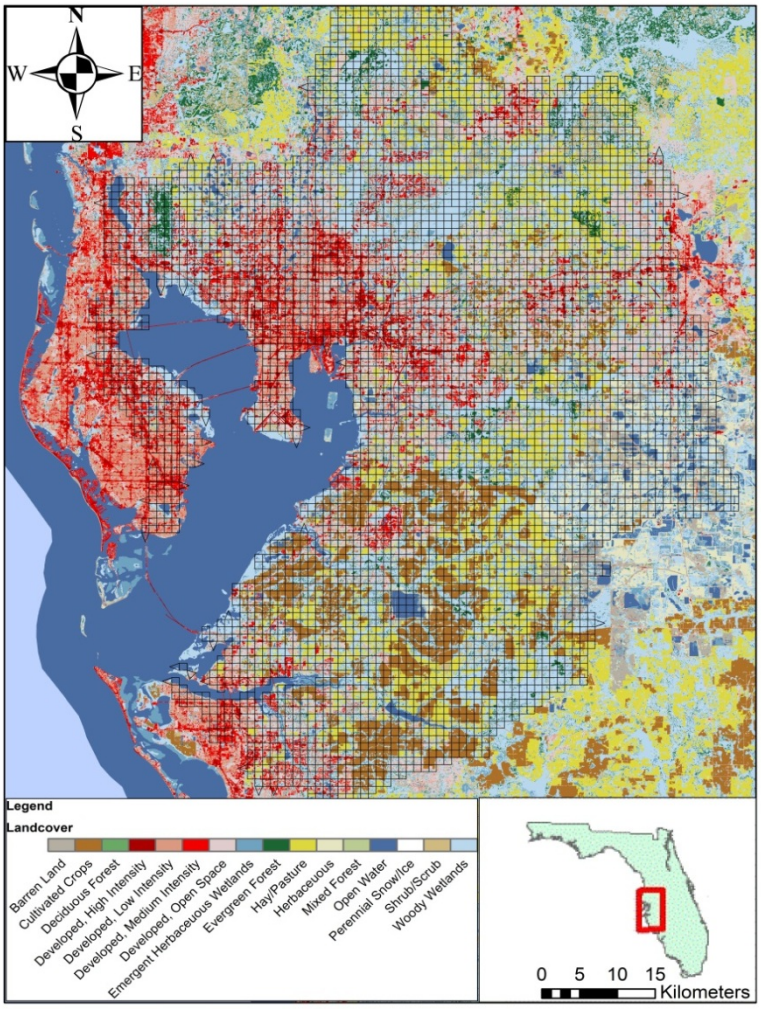

Figure 2.1 Land use and land cover (LULC) map displaying the classes of LULC as classified by the United States Geological Survey (USGS).

2.2.2. Data collection

This study was conducted on data collected from January 1, 2005 to December 31, 2005 and January 1, 2007 to December 31, 2008; the year of 2005 was investigated for the impacts of hurricane events; the year 2007 was analyzed for the effects of drought events and the year 2008

was examined for the effects of a transition year between drought and wet years. The multispectral remote sensing imageries were acquired from the MODIS, an advanced multi-purpose sensor and a key instrument aboard the Terra (Earth Observation System (EOS)-AM) satellite operated by the National Aeronautics and Space Administration (NASA). Surface reflectance, LST/emissivity, and vegetation indices (NDVI) of the MODIS satellite data are available from NASA. The precipitation data was retrieved via the Next-Generation Radar (NEXRAD) in which is a network of high-resolution Doppler weather radars operated by the National Weather Service (NWS), an agency under the National Oceanic and Atmospheric Administration (NOAA). The time series ET data were derived via the Geostationary Operational Environmental Satellite (GOES) data and retrieved directly from the United States Geological Survey (USGS) web site (i.e., USGS spatiotemporal GOES-based data, http://hdwp.er.usgs.gov/et.asp). USGS produced retrospective potential evapotranspiration (PET) and reference evapotranspiration (RET) estimates throughout Florida at a 2 km and daily resolution using a combination of satellite (NOAA GOES) and land-based (weather stations) methods to compute ET. Once the selected parameters were gathered, the data were divided temporally based on a monthly temporal scale; hence, the differences in the composition of the data taken were more evident across a monthly temporal scale.

2.2.3. Variable selection

The selection of input variables was obtained through searching the preeminent available parameters and data. Four parameters were selected for the examination of spatiotemporal patterns and associated ecohydrological trends of the watershed: NDVI, LST, ET, and precipitation. The criterion to include or exclude a variable was based upon their effect on the

hydrological cycle and the ecosystem dynamics at the earth's surface. LST is a good indicator of the energy balance at the Earth's surface and urban heat island effect because it is one of the crucial parameters in the behavior of land-surface processes. It combines the results of surface-atmosphere interactions and energy fluxes between the atmosphere and the ground (Sellers et al., 1988). Consequently, LST is utilized in a variety of climate, hydrologic, ecological, and biogeochemical studies (Camillo, 1991; Running, 1991; Zhang et al., 1995).

Vegetation indices have been developed to qualitatively and quantitatively assess vegetation cover using spectral measurements (Bannari et al., 1995). The uses of the red and near-infrared spectral bands of the sensors on board satellites are suitable for assessing vegetation covers (Weier and Herring, 2006). The green vegetation strongly absorbs red light (Landsat band 3) through the photosynthetic pigments, such as chlorophyll *a*. In contrast, the near-infrared wavelengths are half reflected by and half passed through the leaf tissue, regardless of their color (USDA-ARS, 2006). There are more than 35 vegetation indices derived (Bannari et al., 1995); most use the red and the near-infrared bands, while others incorporate additional parameters to compensate for atmospheric and/or soil background corrections. Selecting the right vegetation index might greatly affect the accuracy of change detection of vegetation cover. The NDVI is a normalized ratio from −1 to +1, calculated as the difference between the NIR and red bands by their sum:

$$NDVI = \left(\frac{NIR - RED}{NIR + RED}\right) \quad (1)$$

Although studies have found NDVI is chlorophyll sensitive, and other indies such as the Enhanced Vegetation Index (EVI) are more responsive to canopy structural variations, including

canopy type, plant physiognomy, canopy architecture, and improved vegetation monitoring through a de-coupling of the canopy background signal, and a reduction in atmosphere influences (Huete et al., 1999); for this flat and relatively homogeneous urbanized region, such as Tampa Bay region, NDVI was deemed satisfactory.

The USGS produced retrospective PET and RET estimates throughout Florida at a 2 km and daily resolution derived by the GOES data and calibrated by land-based (weather stations) methods in the context of a hydrologic model to compute ET (Table 2.1). The overall effort may provide gridded estimates of solar radiation, net radiation, PET, RET, and actual ET at a (2km × 2km) grid scale and a daily time scale from 2002 to 2008 for the entire state of Florida. The satellite-derived solar insolation dataset required calibration to correct for biases embedded in temporal-, seasonal-, and cloudiness-related models (Jacobs et al., 2008). This was achieved through a comparison with available ground-based pyranometer measurements (Jacobs et al., 2008). Upon calibration, the quality of the solar insolation product was improved (Jacobs et al., 2008). Because RET is used mainly for agricultural use, PET data were downloaded for the first day of each month during the study period to retrieve the ET monthly maps. To harmonize the overall consistency in terms of spatial resolution, ET data were finally resampled at a 1-km by 1-km scale to be comparable with LST and NDVI datasets (Table 2.1). Precipitation data provided by Next Generation Radar (NEXRAD) were used for this analysis too (Table 2.1).

Table 2.1 Collected parameters used in the examination of the watershed; their provider, product, notation, and unit.

Parameter	Provider	Product	Notation	Units
Enhanced Vegetation index	MODIS	16-Day	NDVI	Unitless
Land Surface Temperature	MODIS	8-Day	LST	°C
Evapotranspiration	GOES	1-Day	ET	mm/day
Precipitation	NEXRAD	Month-to-Date	N/A	mm/day

2.2.4. Theory

2.2.4.1. Interpolation methods.

This section presents a brief overview of the interpolation methods utilized to interpolate and project values for precipitation and evapotranspiration to harmonize the overall consistency in terms of spatial resolution at a 1-km x 1-km scale. This process is required in order for precipitation and evapotranspiration to be comparable with LST and NDVI datasets. Kriging methods are an assembly of geostatistical techniques used to interpolate the values of a random field as a function of an unobserved location from observations of its value at nearby locations. (Kriging Krige, 1951). The use of the available data Z(u) at n points for a user specified search neighborhood to determine the values at unsampled locations Z(u), where the Z(u) value is a realization of a stationary random function that comprises n + 1 random variables (Wackernagel, 2003; Goovaerts, 1997; Isaaks and Srivastava, 1989). Ordinary Kriging (OK) accounts for local variation of the mean as it uses a local neighborhood w(u) centered on the location (u) being estimated. This method of Kriging considers the trend component to be stationary, thus this linear estimation can be expressed as a linear arrangement of the random variables $Z(u_x)$ and the mean value m:

$$Z(u) = \sum_{x=1}^{n(u)} \lambda_x(u) Z(u_x) \quad (2)$$

where,

$$\sum_{x=1}^{n(u)} \lambda_x(u) = 1. \quad (3)$$

Therefore, these equations enable the method of Ordinary Kriging to be arranged in terms of the semivariogram (Goovaerts, 1997; Wackernagel, 2003):

$$\begin{cases} \sum_{y=1}^{n(u)} \lambda_y(u)\,\gamma(u_x - u_y) - \mu(u) = \gamma(u_x - u); for\ x = 1, \dots, n(u). \\ \sum_{y=1}^{n(u)} \lambda_y(u) = 1 \end{cases} \quad (4)$$

where, μ(u) is a Lagrange parameter employed to limit the weights and $\gamma(u_x - u)$ represents the semivariogram for various lags; the term $\gamma(u_x - u)$ displays the distinctions between each data point (u_x) and the estimation point (u), while λ_y(u) represents the weight values gained by solving equation (4), which are then utilized in equation (2) to resolve Z(u).

2.2.4.2. Pearson Product-Moment Correlation Coefficient (R).

In statistics, the Pearson product-moment correlation coefficient is an indicator of the strength of linear dependence between two variables or data sets; the theoretical range for the Pearson correlation coefficient is from -1 < R < 1; where -1 is perfect negative correlation, 0 is no correlation, and 1 is perfect positive correlation. In the study, the Pearson product-moment coefficient is used to analyze the time dependence relationships between the ecohydrological parameters investigated. The Pearson product-moment correlation coefficient is defined by the formula:

$$R = \frac{\sum_{i=1}^{n}(x_i - \bar{x})(y_i - \bar{y})}{\sqrt{\sum_{i=1}^{n}(x_i - \bar{x})^2\,(y_i - \bar{y})^2}} \quad (5)$$

where, x and y are two variables and $\bar{x}$ and $\bar{y}$ are the means of the two variables.

2.2.4.3. Coefficient of Variation.

To analyze the spatiotemporal trends and patterns of LST, NDVI, ET, and precipitation, some spatial statistic methods such as the CoV were employed in this analysis. In statistics, the coefficient of variation is computed as the standard deviation (σ) divided by the mean (μ) of the time series data (Sun et. al., 2010; Milich and Weiss, 2000; Vicente-Serrano et. al., 2006) and the formula is as follows:

$$CoV = \frac{\sigma}{\mu} = \frac{\sqrt{\frac{1}{n}\sum_{i=1}^{n}(X_i - \bar{X})}}{\frac{1}{n}\sum_{i-1}^{n} X_i} \quad (6)$$

where n is the total number of the pixels utilized in the remote sensing images in our study, x is the random variable of interest, and $\bar{x}$ is the mean of the variable of interest.

2.2.4.4. Moran's Autocorrelation Coefficient I.

Moran's autocorrelation coefficient (often denoted as I) is an extension of Pearson product-moment correlation coefficient to a univariate series (Cliff and Ord, 1973; Moran, 1950). Moran's I is a measure of spatial autocorrelation developed by Patrick A.P. Moran; which characterizes the correlation by a signal from nearby locations in space (Moran, 1950). The theoretical range for the Moran's autocorrelation coefficient is from -1 < I < 1; where -1 is perfect negative spatial correlation indicating perfect dispersion in space, 0 is no correlation indicating a random spatial pattern, and 1 is perfect positive correlation in space. One of the primary assumptions in the theory is that close observations in space is going to be more similar than observations further apart; it is very common to use weights to each pair of observations in space in order to quantify this parameter (Cliff and Ord, 1981). Spatial autocorrelation is

considered to be much more complex than one-dimensional autocorrelation because spatial correlation is multidimensional, usually considering 2 or 3 dimensions in space. The Moran's I formula is defined as follows:

$$I = \frac{N}{\sum_i \sum_j w_{ij}} \left[\frac{\sum_i \sum_j w_{ij} (x_i - \bar{x})(x_j - \bar{x})}{\sum_i (x_i - \bar{x})^2} \right] \quad (7)$$

where, N is the number of spatial units in a matrix of i by j, x is the variable of interest, and $\bar{x}$ is the mean of the variable of interest.

2.2.4.5. Z-Scores.

In statistics, a z-score also known as a standard score describes how many standard deviations for an observation is above or below the mean of the population. In this study, the z-score value will be utilized to determine the significance of Moran's autocorrelation coefficient.

$$Z = \frac{(x - \mu)}{\sigma} \quad (8)$$

where, x is raw score to be standardized, μ is the mean of the population, and σ is the standard deviation of the population.

2.3. Results and discussion

To clarify the application potential, this dsicussion is composed of (1) the investigation of the monthly temporal pairwise-plots in order to pin down subtle changes for each parameter and investigate the hidden relationships and identify the ecohydrological implications during extreme climatic events, (2) the employment of the spatial statistics method, CoV analysis, in order to ascertain the degree of variation spatially; the values for each parameter spatial patterns

via maps will be examined for relevant knowledge discovery, and (3) the spatial autocorrelation analysis via Moran's I assessment to establish the similarity between observations as a function of the separation between them.

2.3.1. Temporal Trend Analysis

2.3.1.1. Temporal trends of ecohydrological parameters.

The temporal interaction between ecohydrological parameters introduces stimulating findings. Temporal trends for LST during the years of 2005, 2007, and 2008 in Tampa Bay, Florida generally are lowest in February and peak in May and June (Figure 2.2). LST displays minimum values in the month of February and maximum values during the month of May during the drought year event (2007). In addition, NDVI displayed an inconsistent sinusoidal behavior over time. In the comparison of the 2007 drought year to the 2005 wet year and 2008 transition year, 2007 displayed sharper transitions and higher amplitude between crests and sags in the sinusoidal curve while the wet and transition year display a flat sinusoidal behavior. This observation suggests that LST and NDVI are more variable during a dry year than a wet year (Figures 2.2 – 2.3). During October of 2005, in which encompasses the hurricane event, you can see a drop in the LST value while in 2007 and 2008 there is generally a crest in LST temporal trend (Figure 2.2). This suggests that during a hurricane event there is a general decrease in LST, which could be a result of an increase in precipitation across a large portion of the watershed area. NDVI shows a flat receding tail for the September crest in 2005 while the years of 2007 and 2008 demonstrated an exponential drop after a crest in the curve signifying that the hurricane event in October dampened the severity of the winter dry season in which alludes to relative

system memory. In addition, the ET temporal pattern is rather homogeneous over the wet-dry season pattern but in the month a sudden change in the normal temporal pattern in the month of November for the ET variable can be observed (Figure 2.4). It should be noted that ET displays a lag effect when compared to precipitation, therefore, shortly after Hurricane Wilma made landfall in Florida on October 24th, 2005, ET exhibited a sudden, sharp increase in magnitude in November; his abnormal increase in magnitude is feasibly the result of the increase in precipitation. Consequently, an increase in rainwater leads to an increase in vegetation cover and ET; therefore, this observation accentuates the essential relationship between LST, precipitation, vegetation cover, and ET in the soil-vegetation-atmospheric system. These intriguing findings display some of the significant ecohydrological repercussions of an extreme hurricane event.

An interesting abnormality displayed in the ET and precipitation data can be detected in Figures 2.4 and 2.5 as a result of the drought event. The year 2008 was a transition year between dry and wet seasons in which occurred in the middle of the year. Figure 2.4 indicates that the onset of drought lags the first crest of the ET curve during a year by approximately one month every year of drought. In the middle of 2008, the transition between dry and wet years had commenced and ET appears to start to shift back into the analogous temporal pattern as the 2005 wet year. Figure 2.5 expresses a similar behavior as the ET curve. The maximum crest in the precipitation curve is lagged between 2005 and 2007 by approximately two months and then demonstrates a sudden swift transition back to the similar temporal pattern as a typical wet year in 2008. These fascinating irregularities display some of the key ecohydrological implications of an extreme drought event.

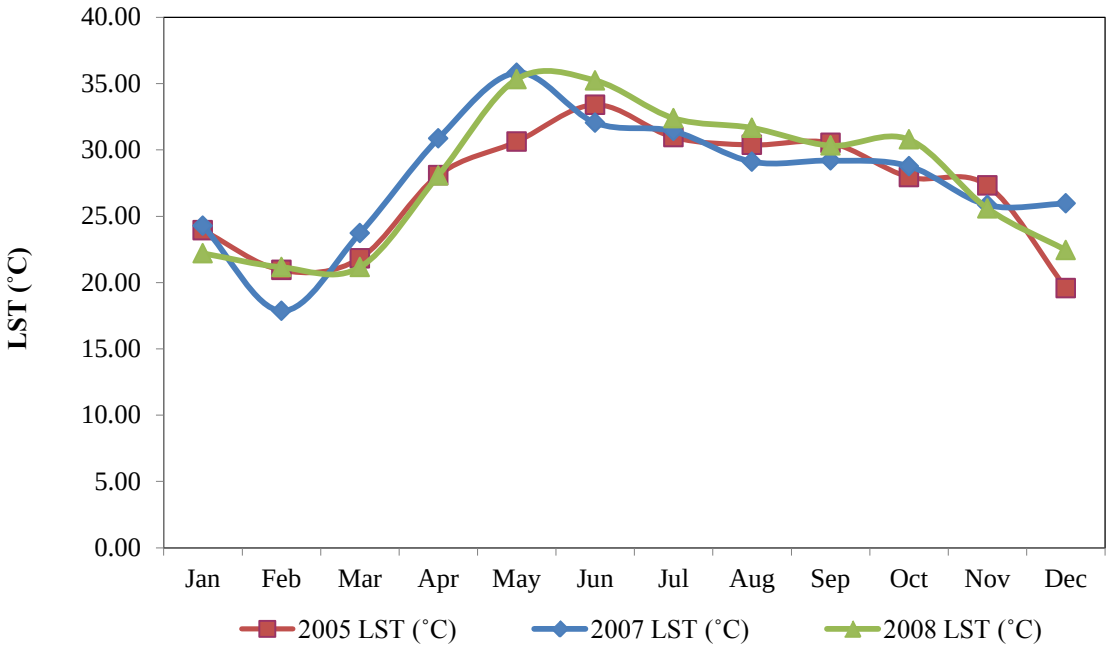

Figure 2.2 Temporal trends of LST in °C for 2005, 2007, and 2008.

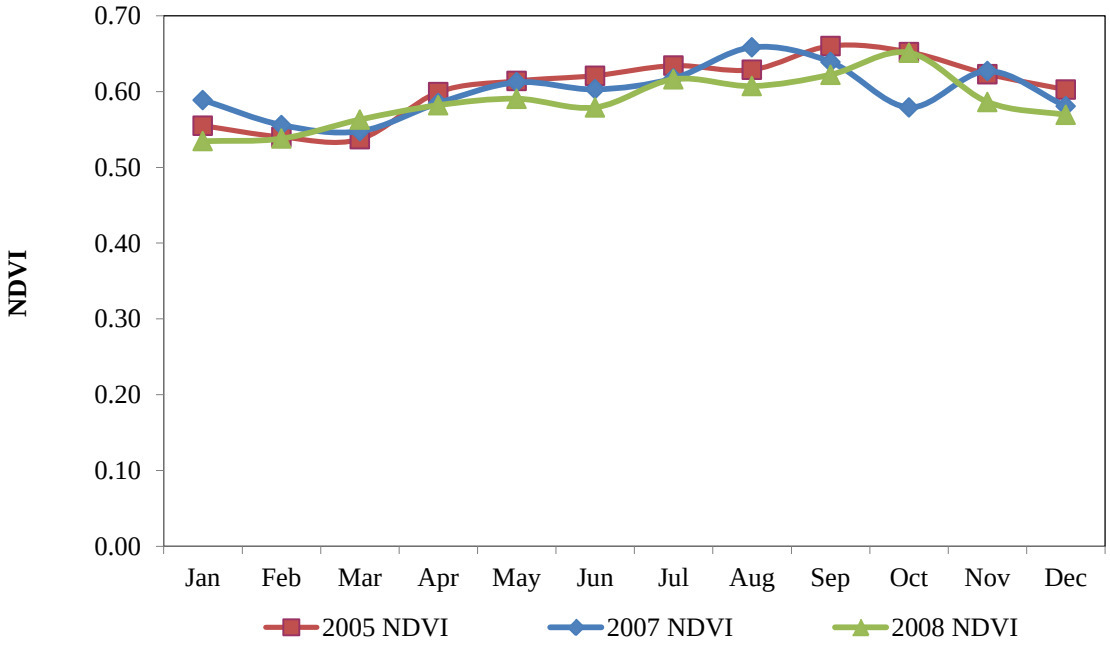

Figure 2.3 Temporal trends of NDVI for 2005, 2007, and 2008.

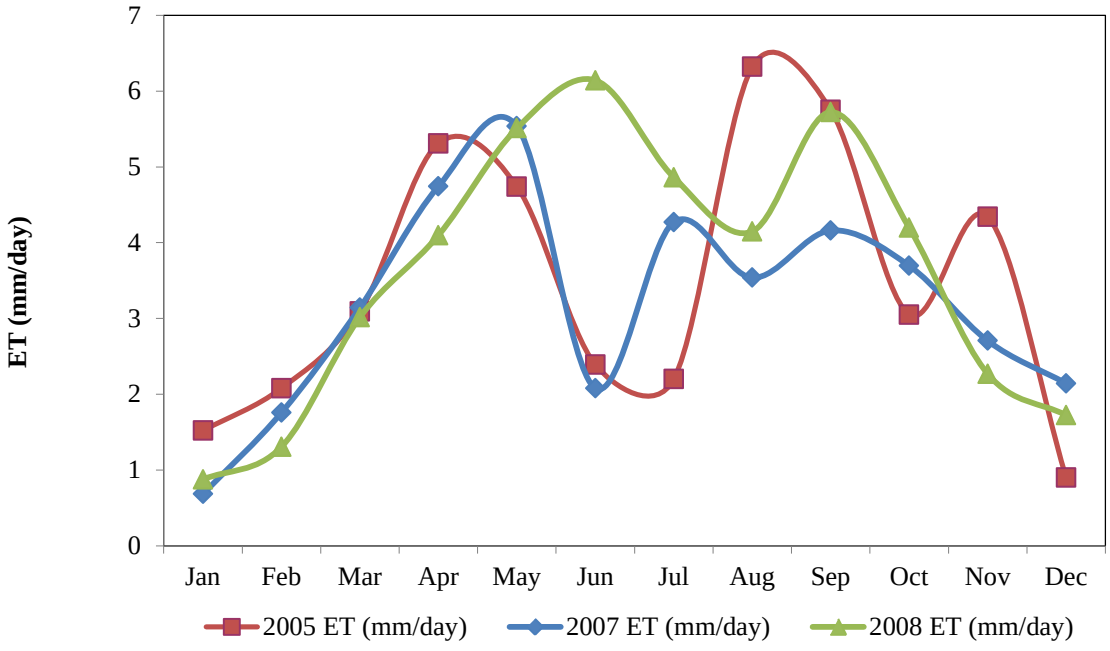

Figure 2.4 Temporal trends of evapotranspiration in mm/day for 2005, 2007, and 2008.

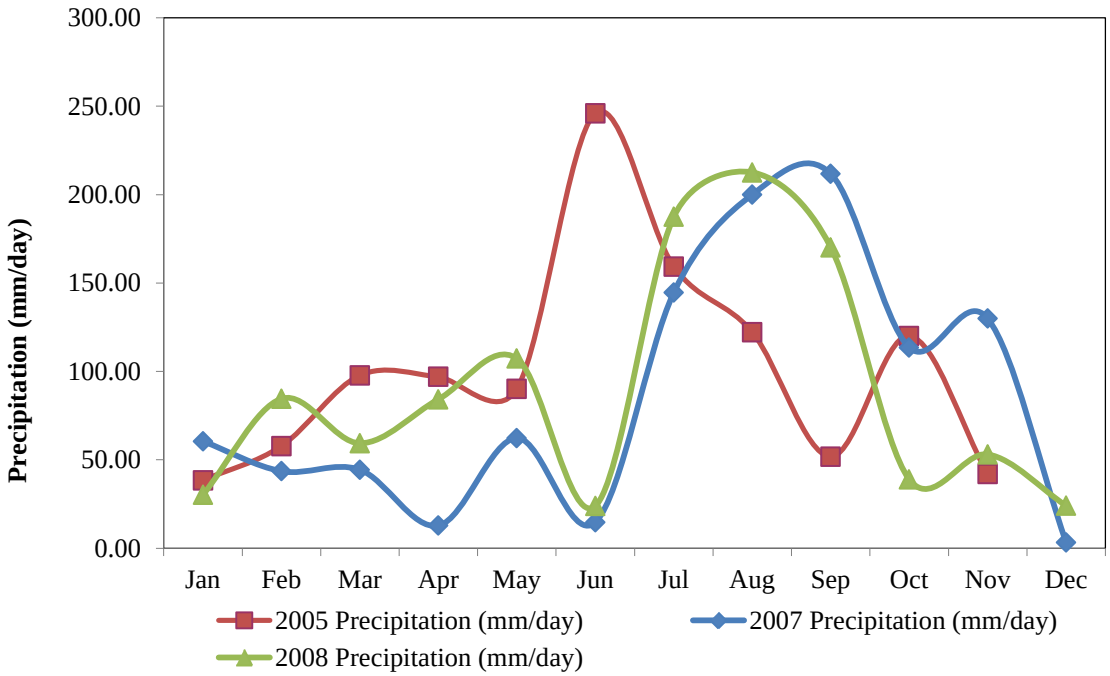

Figure 2.5 Temporal trends of precipitation in mm/day for 2005, 2007, and 2008.

2.3.1.2. Interactions and Temporal Trends between Ecohydrological Parameters.

There are various intriguing interactions and temporal trends between the ecohydrological parameters investigated (Figures 2.6 – 2.8). First, higher correlation values are observed for NDVI versus LST as well as NDVI versus ET during the 2005 wet year and the 2008 transition year; this proposes that vegetation cover is more dependent on LST and ET is dependent on NDVI when there is ample precipitation for growth (Table 2.2); in Figure 2.6(a) and Figure 2.8(a). Similar temporal interactions between LST and ET can be observed; where there is a sharp increase in ET, there also exists an increase in LST (Figure 2.6(b) and Figure 2.8(b). In contrast, higher correlation values for NDVI and precipitation was detected for the drought year suggesting that vegetation cover is more dependent on precipitation during drought than during wet years (Figure 2.8(a); most likely, this fact is the direct result of the vegetation's shift into survival mode and first priority for survival is the necessity for water. In addition, the correlation between precipitation and ET remained relatively low and unchanged during the years investigated; this may be primarily due to the fact that ET variations might be dominated collectively by other parameters such as LST, surface heterogeneity, and the aerodynamic resistance impact. The lag effect between precipitation and ET can be seen in the pair-wise plots of Precipitation and ET in Figure 2.6(f), Figure 2.7(f), and Figure 2.8(f); in light of the lag effect between these two hydrological parameters, there is a stronger correlation between the two.

The minimum correlation coefficient value observed was 0.159 in 2007 for LST and precipitation but slightly higher correlation for 2005 and 2008 was observed. In Figures 2.6(c), Figure 2.7(c), Figure 2.8(c), when there is a sharp increase in precipitation, a decrease in LST can be witnessed. This relationship across the watershed can be perceived to be a direct influence

of the urbanization of the region due to the complexity of building canopy effect and heterogeneity of the landscape ecology. For example, the increase in impervious area and, consequently, a decrease the pervious area and vegetation cover has led to urban heat island effect. The impervious area heated by the sun is rapidly cooled to significantly lower temperatures while pervious, vegetation covered, areas are not as influenced during the event of a substantial rainstorm.

Last, the maximum value observed during this segment of the study was 0.905 occurring between LST and ET. The correlation coefficient between LST and ET was observed to display an exponential increasing trend over time (Table 2.2). This finding cannot be confirmed as a consistent long term trend for such a short time period during this study, therefore, the increasing correlation trend between LST and ET might deserve an extended long-term investigation in the future.

Table 2.2 Summary table of Pearson's product-moment correlation coefficient for LST, NDVI, ET, and precipitation.

2005				
Correlation Coefficient (R)	NDVI	LST (˚C)	ET (mm/day)	Precipitation (mm/day)
NDVI	-	0.726	0.443	0.482
LST (˚C)		-	0.543	0.624
ET (mm/day)			-	0.303
Precipitation (mm/day)				-

2007				
Correlation Coefficient (R)	NDVI	LST (˚C)	ET (mm/day)	Precipitation (mm/day)
NDVI	-	0.533	0.334	0.757
LST (˚C)		-	0.709	0.159
ET (mm/day)			-	0.310
Precipitation (mm/day)				-

2008				
Correlation Coefficient (R)	NDVI	LST (˚C)	ET (mm/day)	Precipitation (mm/day)
NDVI	-	0.665	0.668	0.435
LST (˚C)		-	0.905	0.413
ET (mm/day)			-	0.426
Precipitation (mm/day)				-

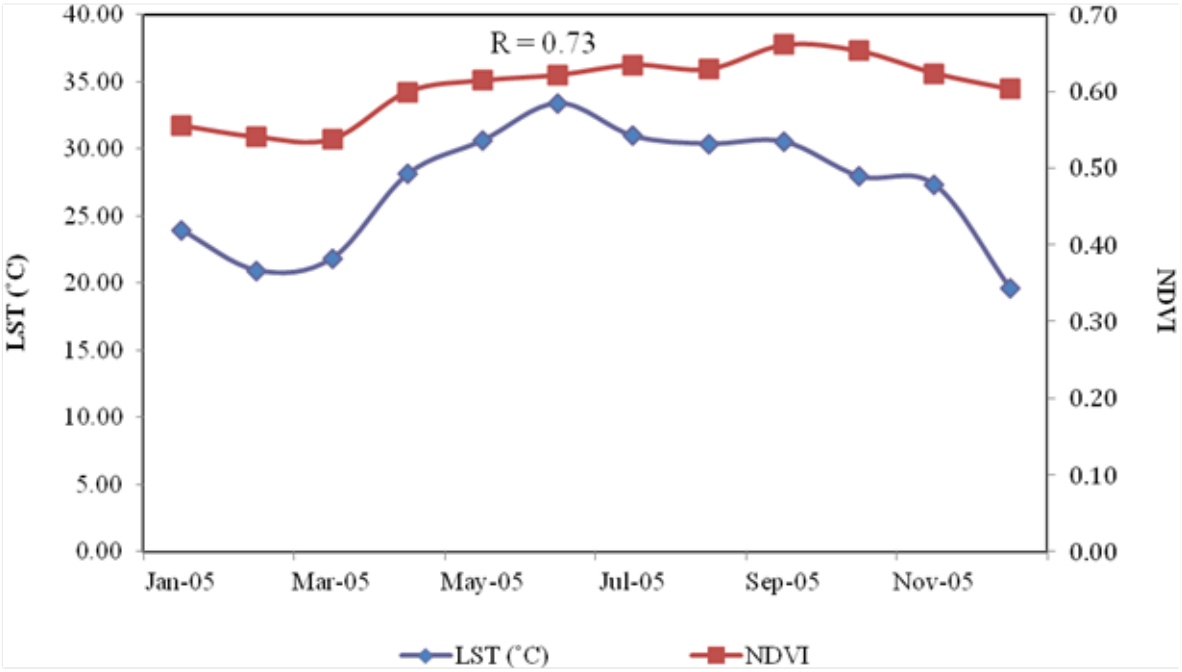

(a) Temporal trends and interactions between LST and NDVI.

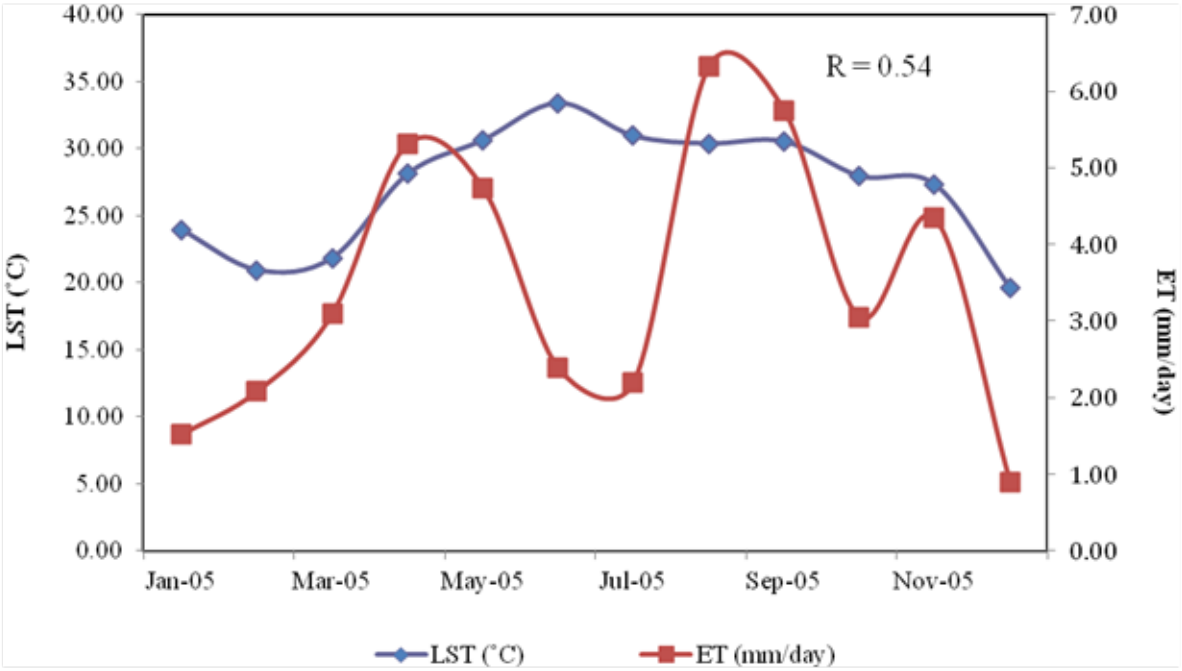

(b) Temporal trends and interactions between LST and ET.

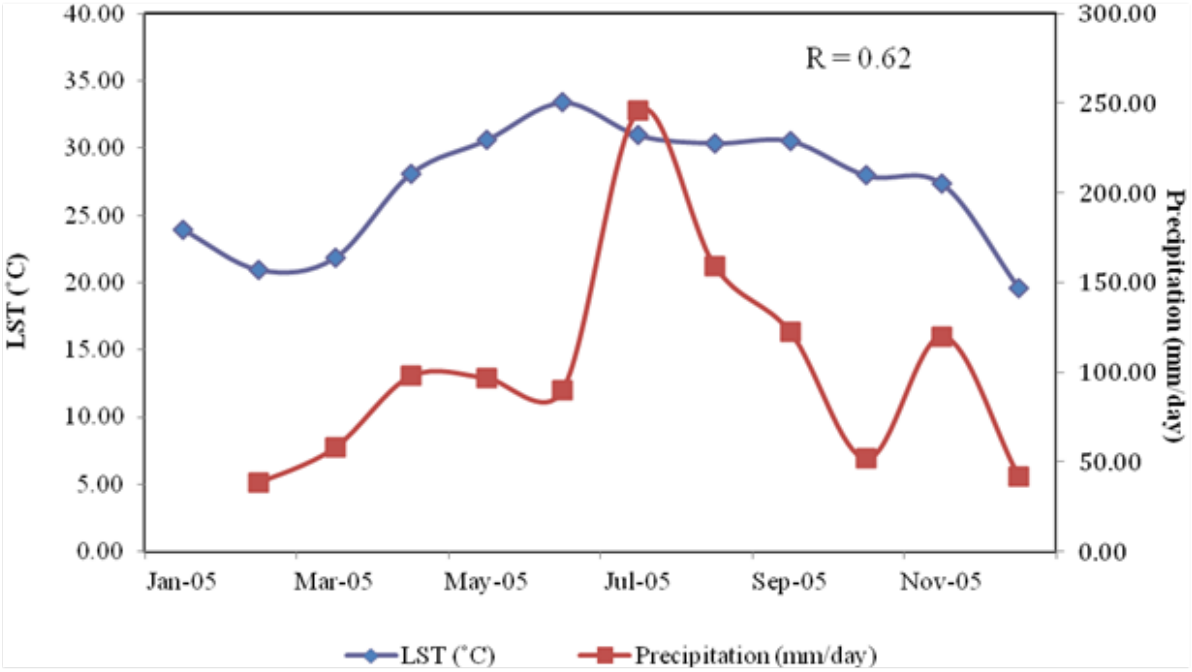

(c) Temporal trends and interactions between LST and precipitation.

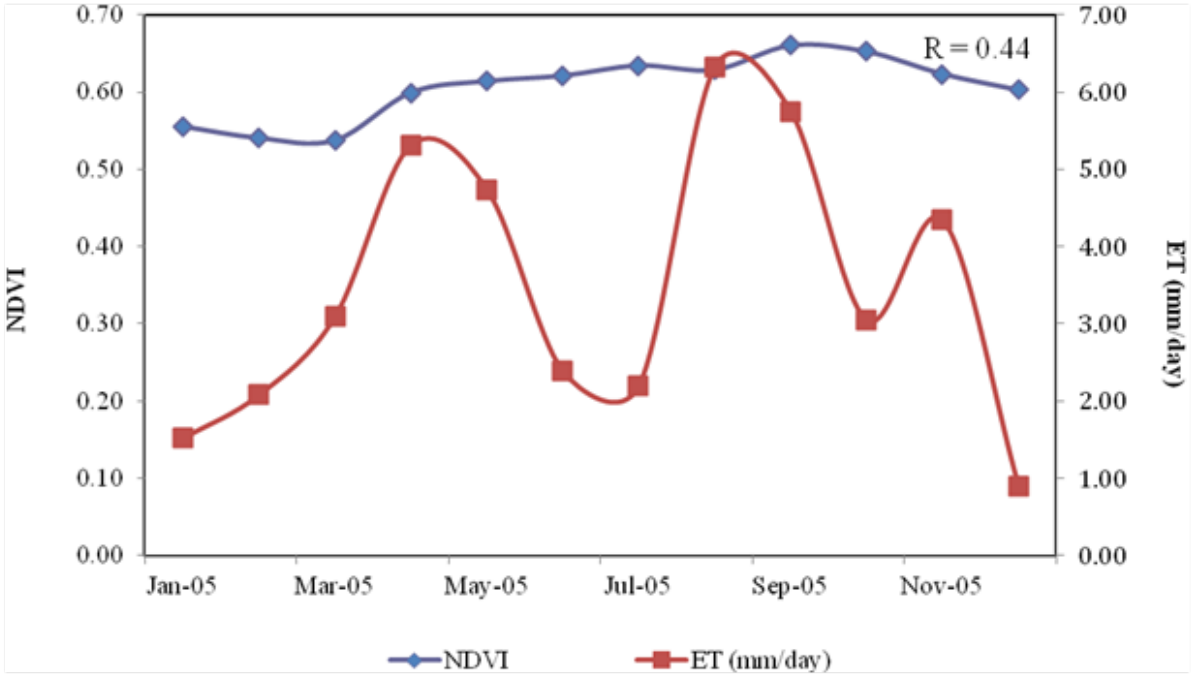

(d) Temporal trends and interactions between NDVI and ET.

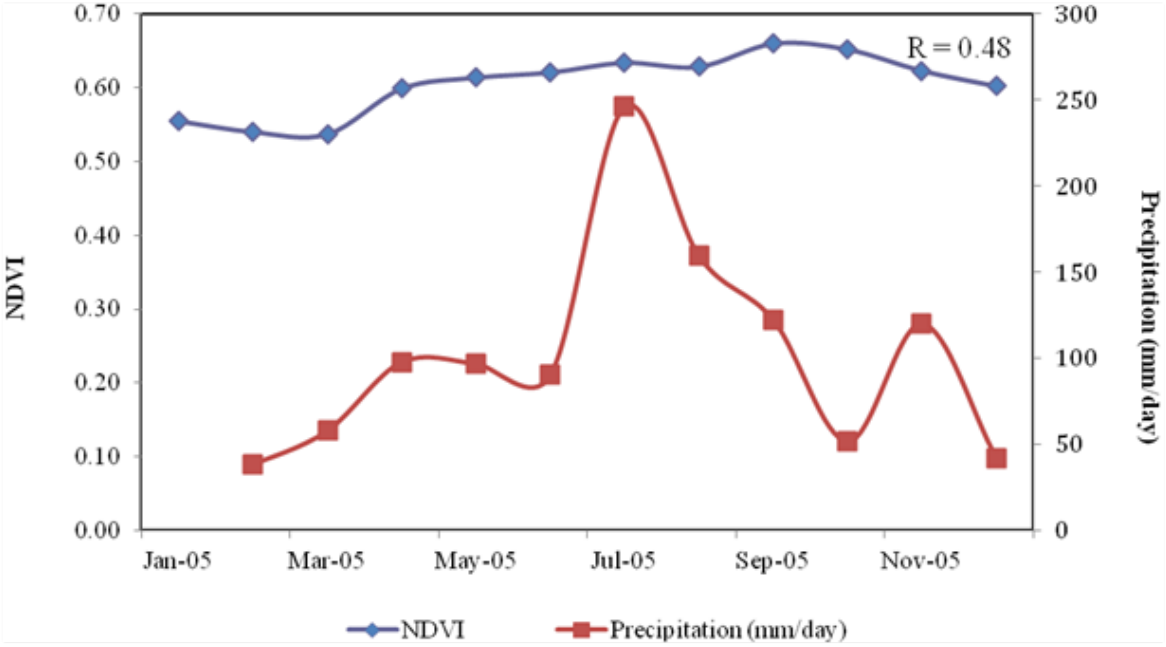

(e) Temporal trends and interactions between NDVI and precipitation.

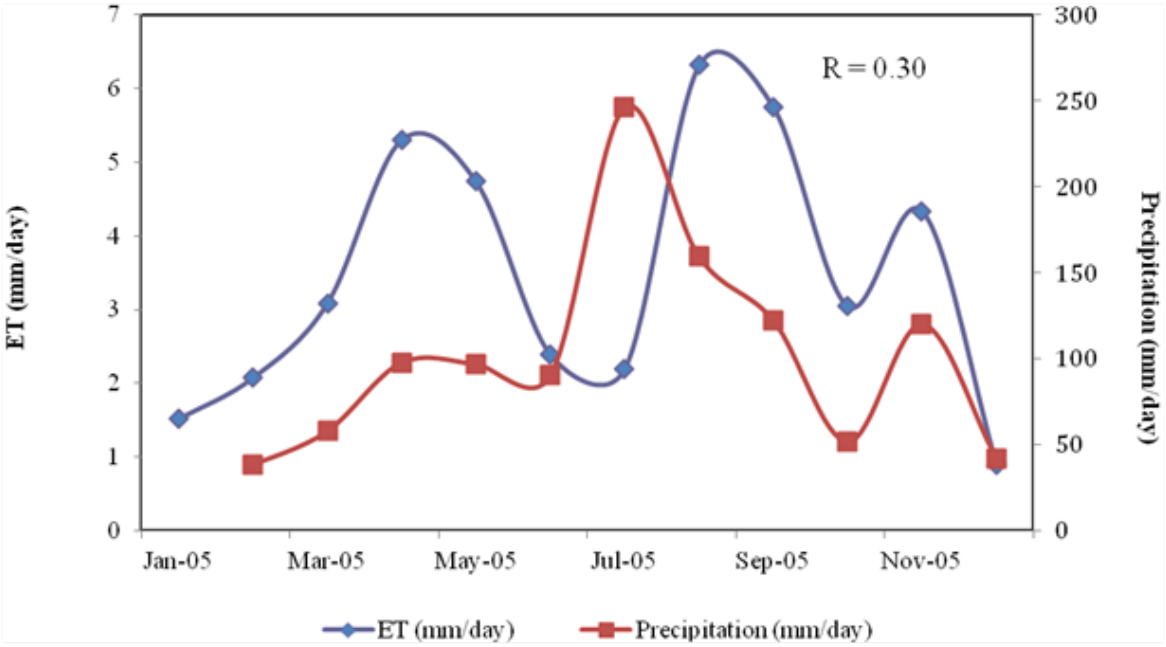

(f) Temporal trends and interactions between ET and Precipitation.

Figure 2.6 Time-series pair-wise plots among LST, NDVI, ET, and Precipitation for 2005.

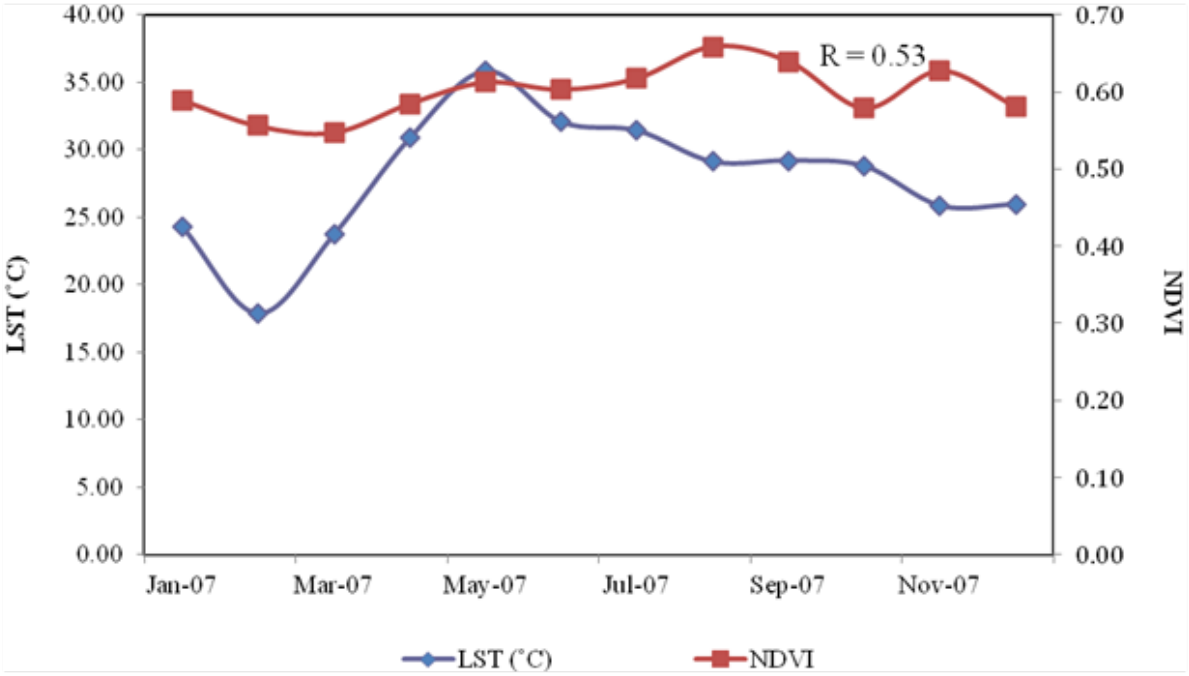

(a) Temporal trends and interactions between LST and NDVI.

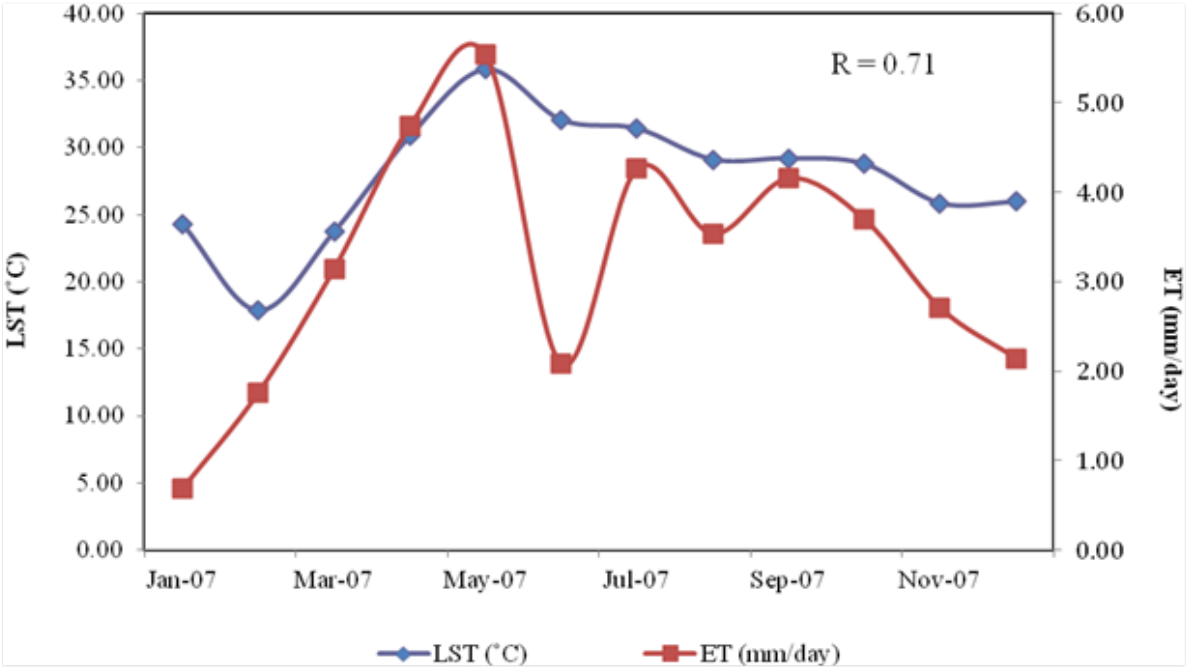

(b) Temporal trends and interactions between LST and ET.

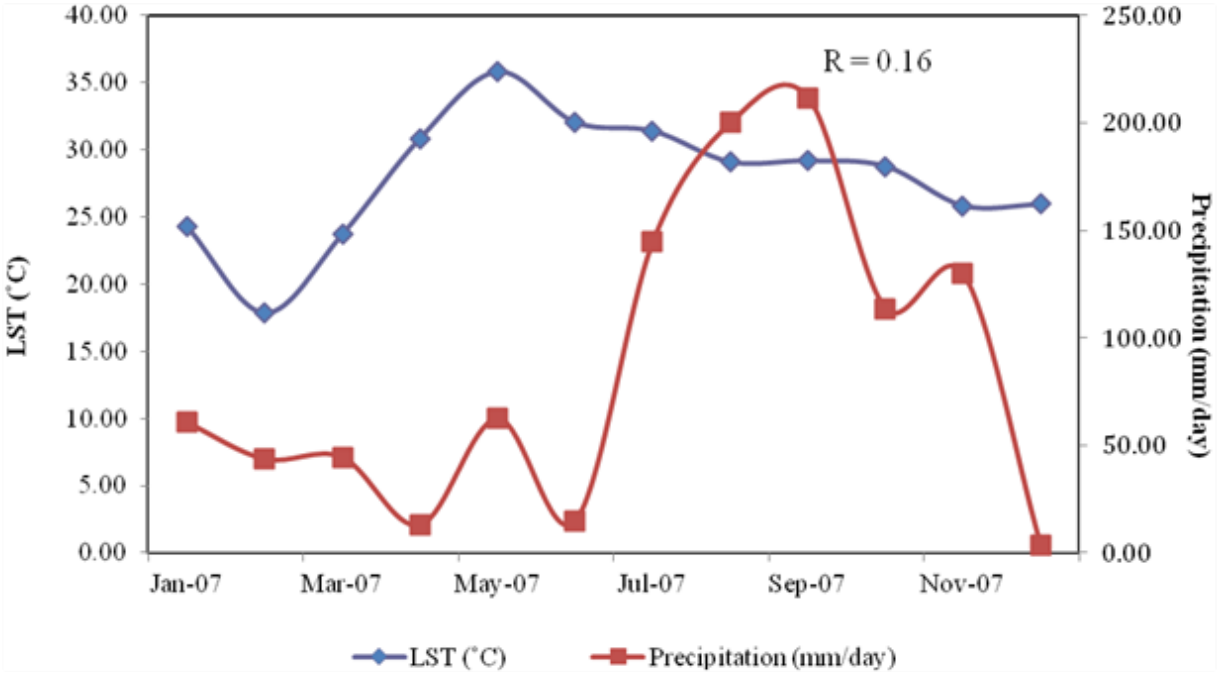

(c) Temporal trends and interactions between LST and precipitation.

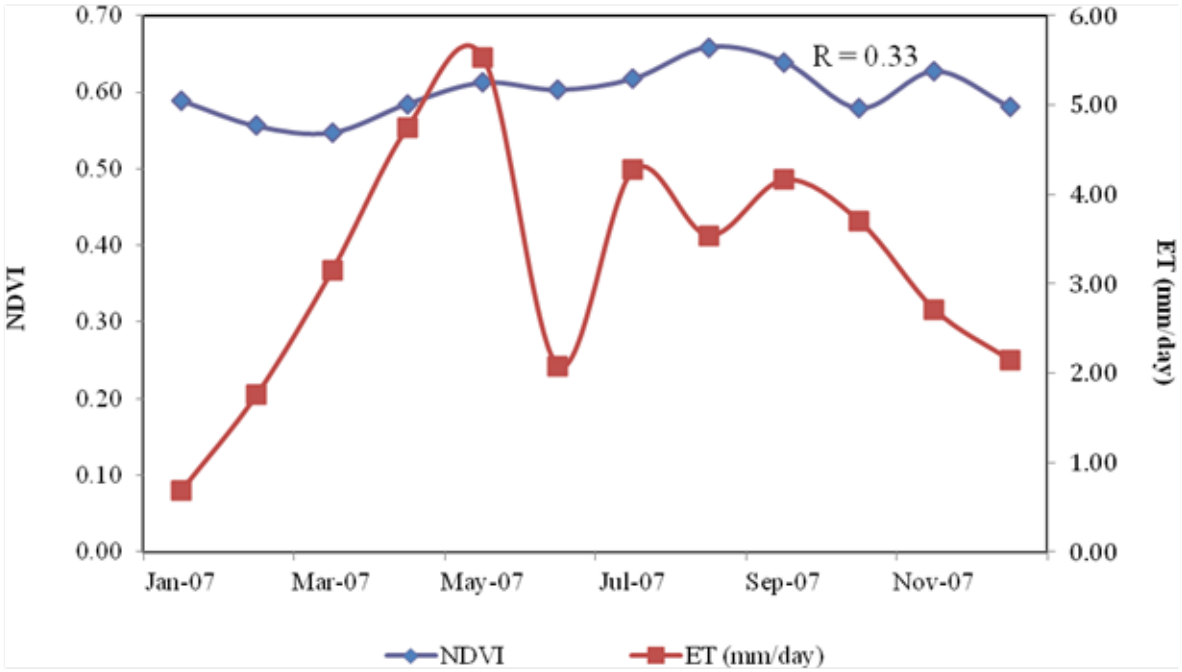

(d) Temporal trends and interactions between NDVI and ET.

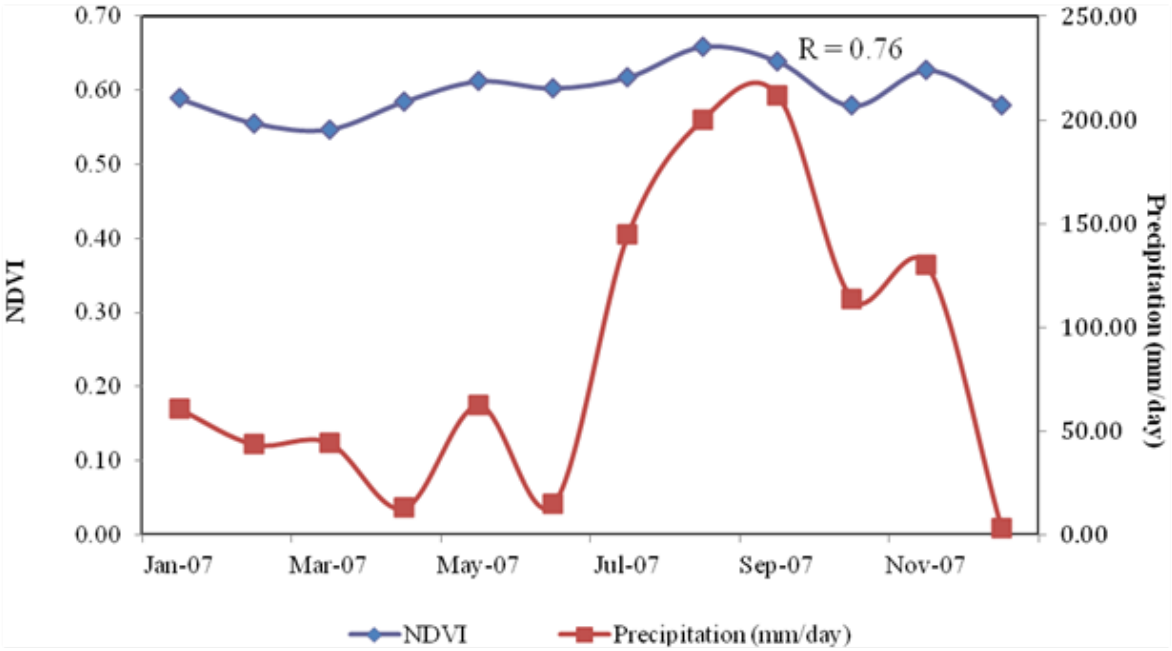

(e) Temporal trends and interactions between NDVI and precipitation.

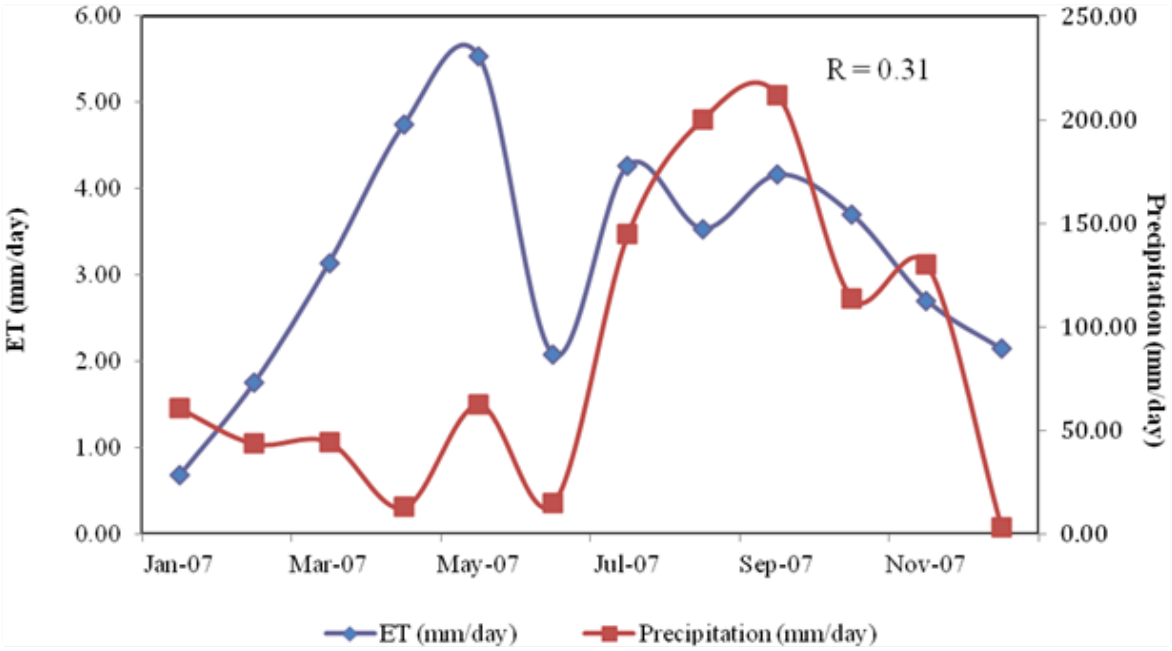

(f) Temporal trends and interactions between ET and Precipitation.

Figure 2.7 Time-series pair-wise plots among LST, NDVI, ET, and Precipitation for 2007.

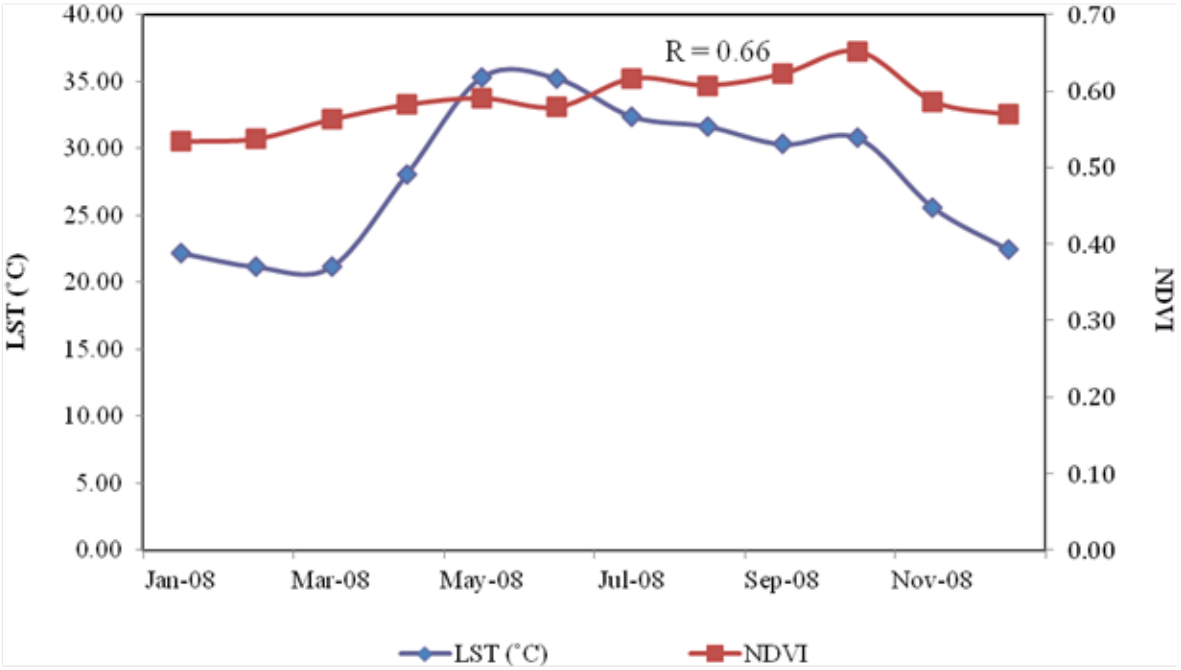

(a) Temporal trends and interactions between LST and NDVI.

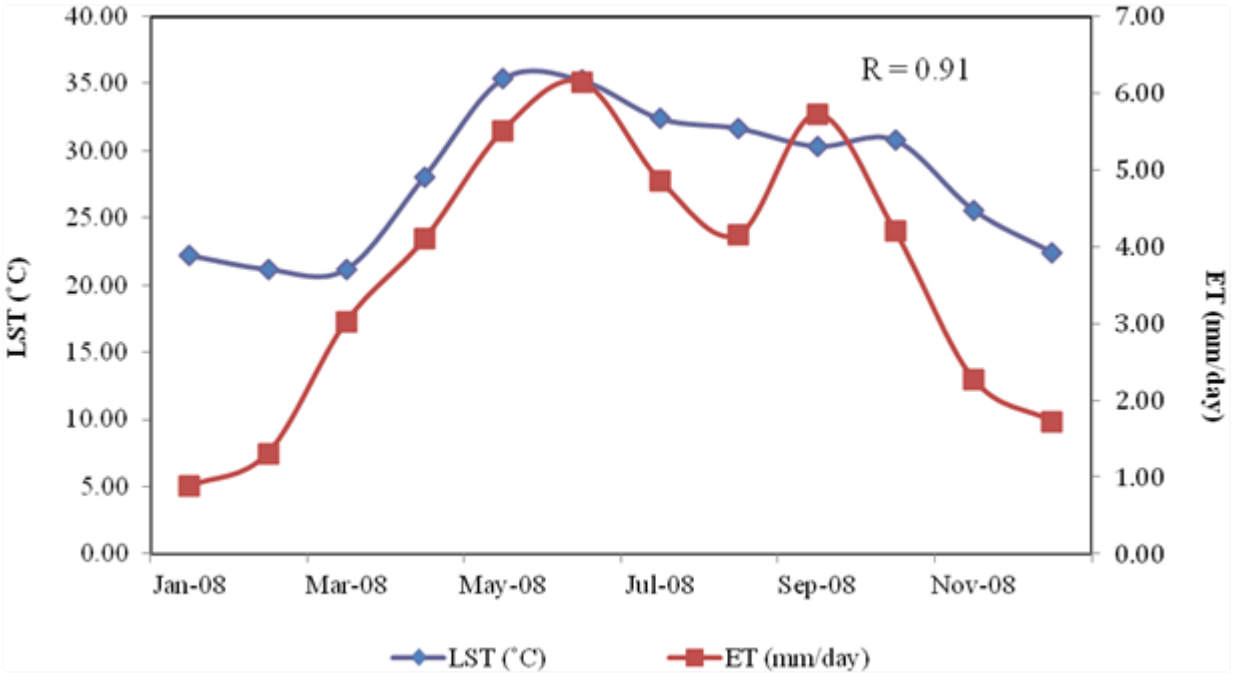

(b) Temporal trends and interactions between LST and ET.

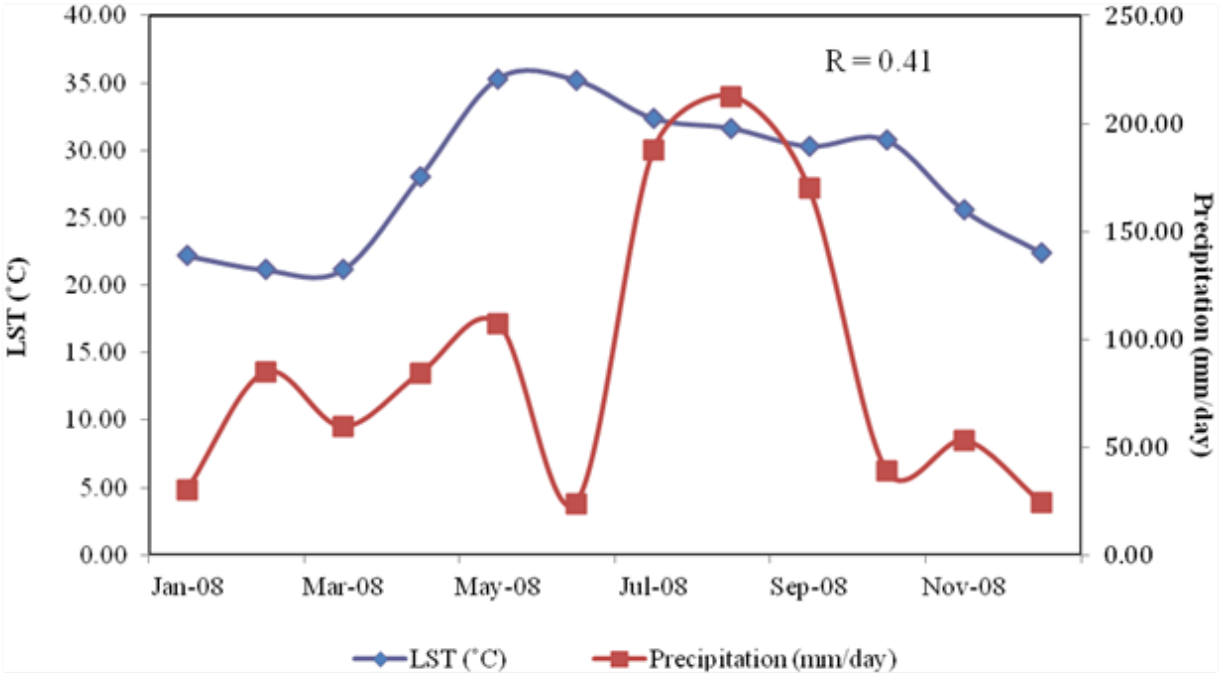

(c) Temporal trends and interactions between LST and precipitation.

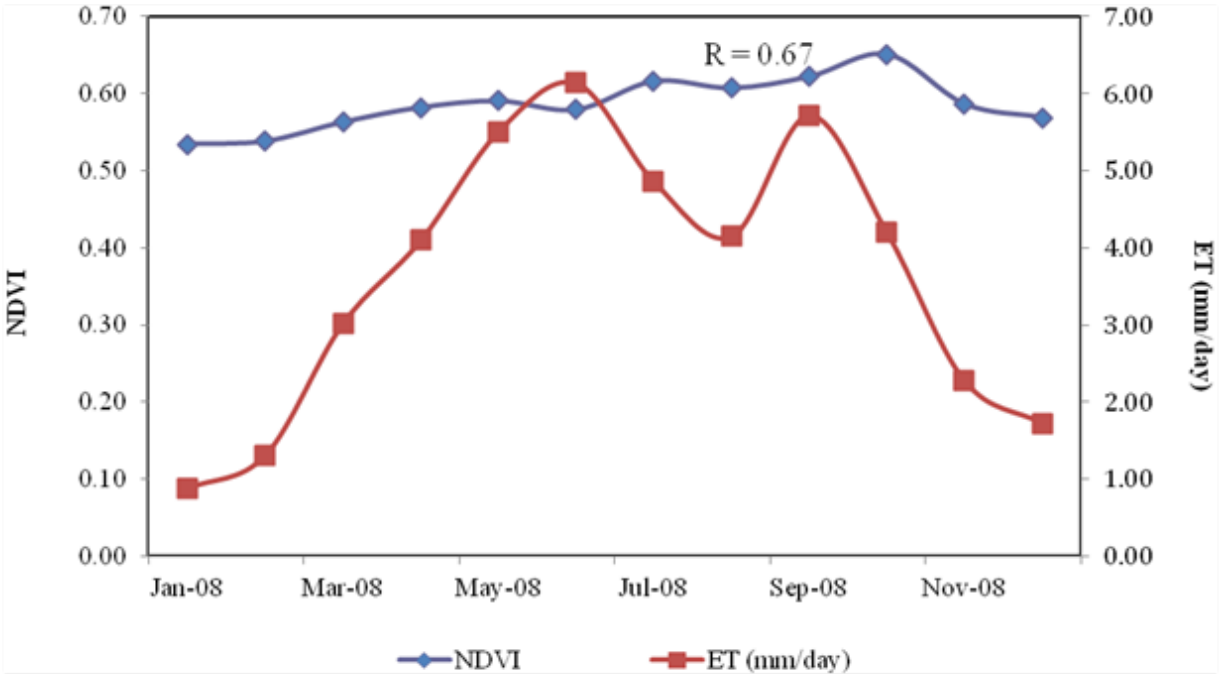

(d) Temporal trends and interactions between NDVI and ET.

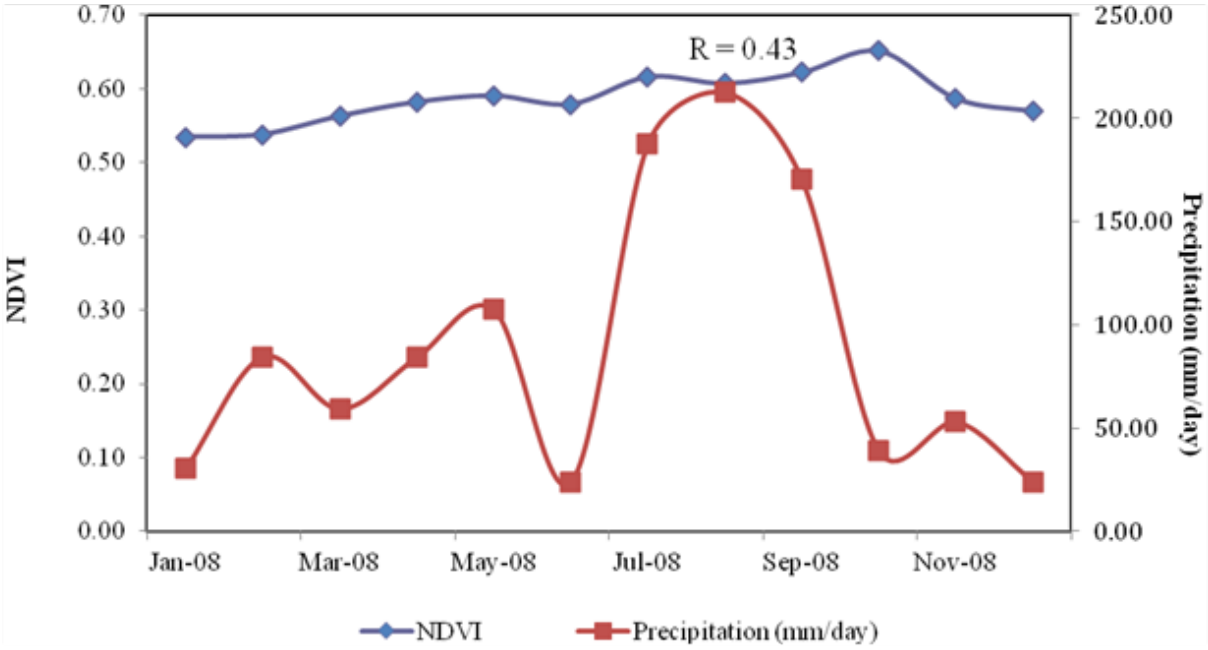

(e) Temporal trends and interactions between NDVI and precipitation.

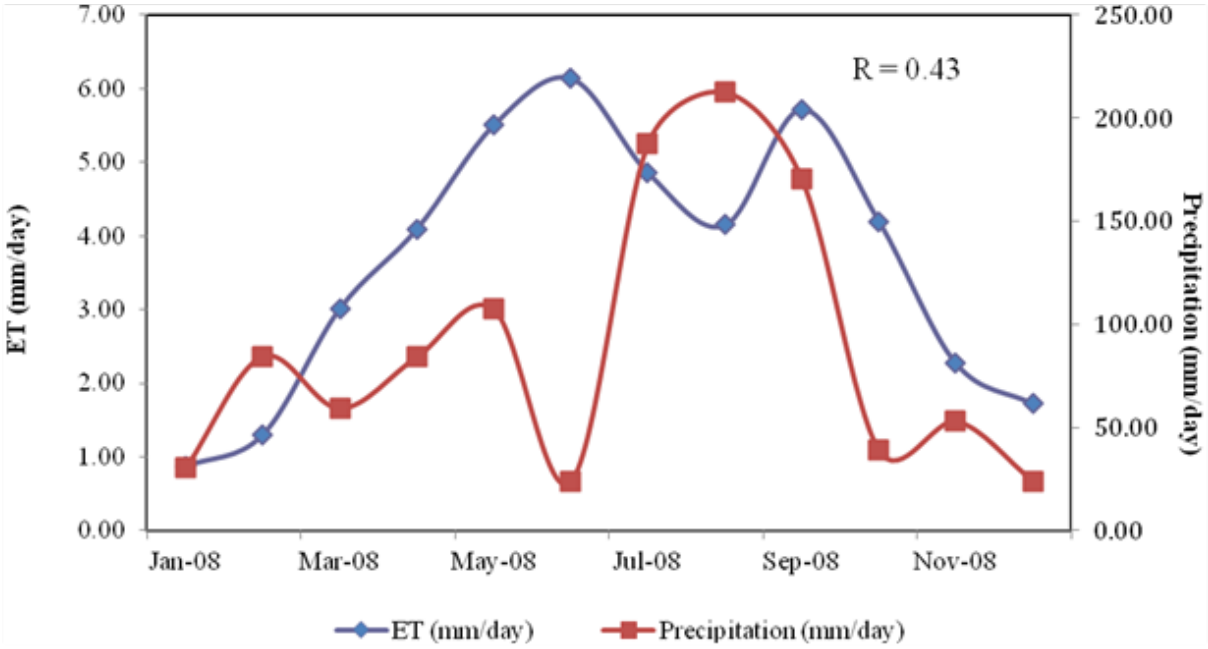

(f) Temporal trends and interactions between ET and Precipitation.

Figure 2.8 Time-series pair-wise plots among LST, NDVI, ET, and Precipitation for 2008.

2.3.2. Spatiotemporal Variation Analysis

Maps were created showing the results of the CoV analysis for each variable and for each of the three study periods; each map depicts the spatiotemporal pattern for the coefficient of variation (Figures 2.9 - 2.11). Seasonal changes over different locations are caused by a series of complex factors in the ecological, hydrological, and thermal cycles at the surface of the Earth. Four data sets associated with three time periods were generated across the entire watershed in order to retrieve the means of LST, NDVI, ET, and precipitation. The factors affecting on ecohydrological variations are intricate and their spatial and temporal changes are diverse at the even the annual scale, thus, the CoV for of each pixel were calculated over the watershed as depicted in Figures 2.9, 2.10, and 2.11 for each year. The spatiotemporal variation analysis revealed some interesting finds in regard to variations in ecohydrological parameters during extreme climatic events.

The CoV analysis revealed some unseen findings in data in regard to variations of LST during 2005, 2007, and 2008. The minimum value for the LST CoV was 0.14 and the maximum value for the CoV was 0.76 in which occurred during the hurricane event year of 2005. Inspection of the spatial distribution of the CoV for 2005 revealed that significant variation, primarily composed of values ranging from 0.16 to 0.30, is found across a large portion of the watershed area. Examination of 2007 and 2008 CoV maps exposes that there is an association between high variations in rainfall and LST; where high variations in rainfall exists, there also exists high variations in LST. These observations lead to the proposition that a hurricane event increases variation in LST at a larger scale than isolated areas across all LULC classifications; the interactions and temporal trends between the LST and precipitation ecohydrological

parameters and CoV maps can confirm this hypothesis. Inspection of the spatial distribution for the LST CoV revealed that significant variation is found in areas where the LULC classification is considered to be “developed” areas of varying intensity. This continuous trend on a long-term basis may partially support the influence of urban heat island effect in respect to the possible reason causing the variations in vegetation cover and precipitation in which reflects UVI’s direct influence on the variations in the coastal region to a significant extent.

The minimum value for the NDVI CoV was 0.02 and the maximum value for the CoV was 1.30 occurring in the drought year of 2007. During all years of the analysis, assessment of the NDVI maps divulges that areas where the LULC classification is considered to be “developed” areas of varying intensity there is a significant increase in variation values. During the drought year, comparing LST, NDVI, and precipitation shows that they all have a similar spatial pattern. There appears to be high variation right above Hillsborough Bay in the urbanized city of Tampa and radiates north in a cone pattern. Higher variation can also be observed in areas where the LULC classification is considered to be “wetlands.” Another interesting finding was that where greater values for the ET CoV occurred, there are diminutive variation in vegetation cover is observed.

The CoV value for ET and precipitation varied spatially from year to year and displayed a random pattern. For ET, the minimum CoV value was 0.41 and the maximum CoV value was 0.59 in which both occurred during the hurricane event year, 2005. During the 2005 and 2008 wet years, significantly higher variation was observed in which occurred in locations along the major river basins; Hillsborough River and Little Manatee River in 2005 and the Little Manatee

River and some of the Alafia River basin during 2008. Comparison of the ET maps for all years shows that the Alafia River basin displays lower CoV values along the river during all years. During the wet years, the Manatee River basin also displays a similar behavior as the Alafia River but during the dry year, it displayed higher values of variation. One explanation for this phenomenon is that the Alafia River may still have possessed significant flow during the drought year. Changes in precipitation varied spatially as well as temporally across the watershed from year to year. The maximum and minimum values for the CoV value both occurred during the wet year of 2005 with a range from 0.49 to 3.1. The higher values were observed to primarily occur in the south-eastern corner of the watershed while minimum values occurred across the center of the watershed in a diagonal pattern. During 2007 and 2008, higher variations in precipitation were observed in areas considered to possess “developed” LULC classification with varying intensities, in particular, 2007. This observation may bring the discussion of the implications of UHI has been observed in previous studies such as Changnon (1992). This observation suggests that drought events may in fact increase rainfall events in urbanized regions compared to years considered to be wet years.

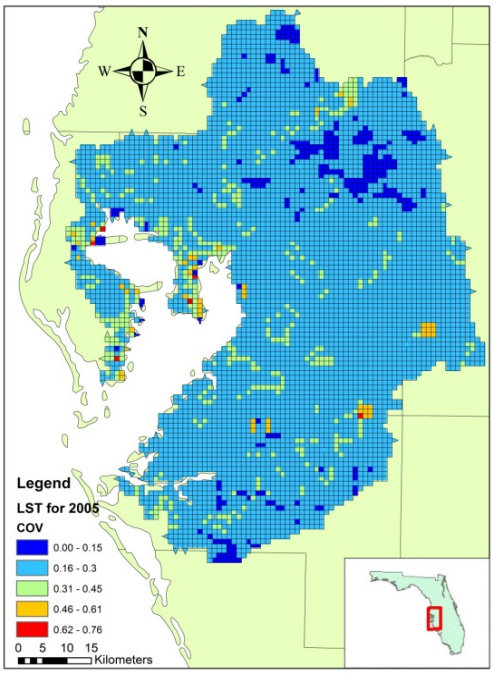
N
W
E
S
Legend
LST for 2005
COV
0.00 - 0.15
0.16 - 0.3
0.31 - 0.45
0.46 - 0.61
0.62 - 0.76
0 5 10 15
Kilometers

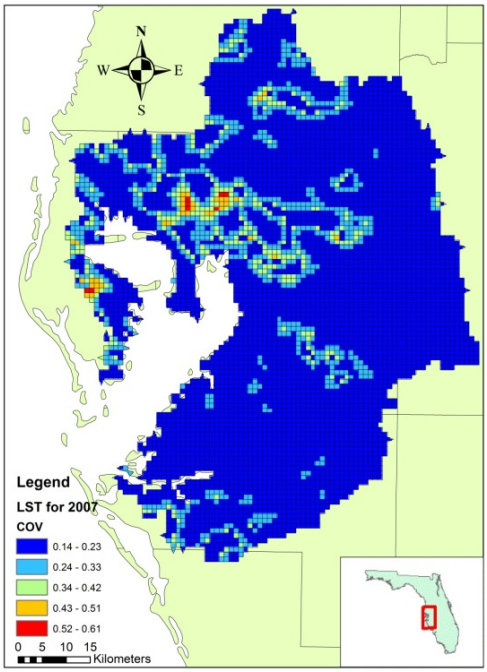
N
W
E
S
Legend
LST for 2007
COV
0.14 - 0.23
0.24 - 0.33
0.34 - 0.42
0.43 - 0.51
0.52 - 0.61
0 5 10 15
Kilometers

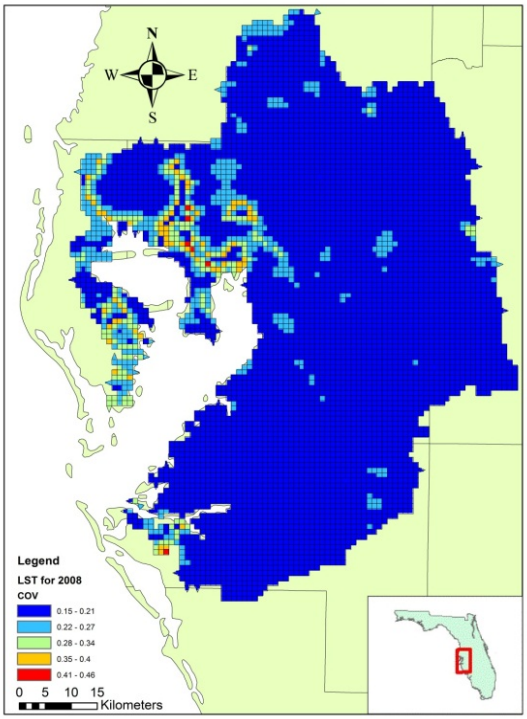

Figure 2.9 CoV analysis maps for LST (2005, 2007, and 2008).

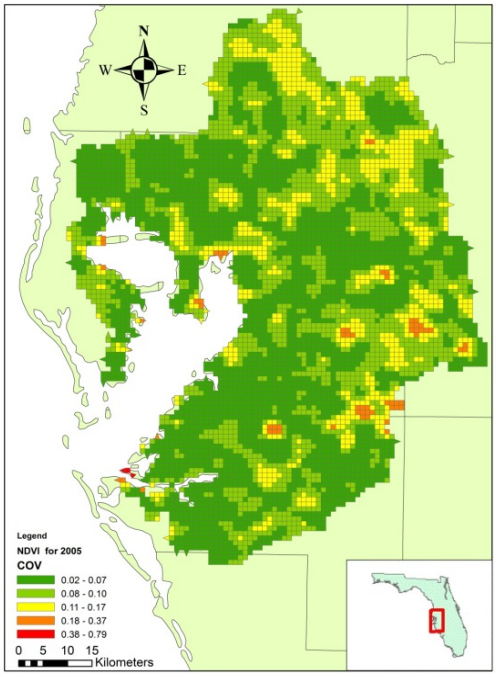
N
W
E
S
Legend
NDVI for 2005
COV
0.02 - 0.07
0.08 - 0.10
0.11 - 0.17
0.18 - 0.37
0.38 - 0.79
0 5 10 15
Kilometers

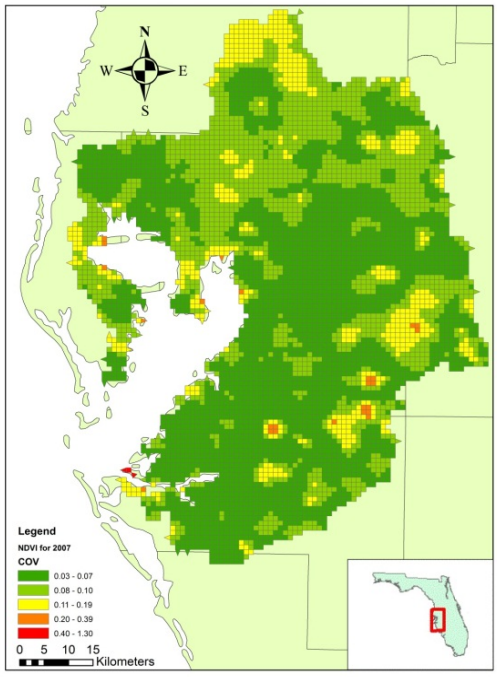
N
W
E
S
Legend
NDVI for 2007
COV
0.03 - 0.07
0.08 - 0.10
0.11 - 0.19
0.20 - 0.39
0.40 - 1.30
0 5 10 15
Kilometers

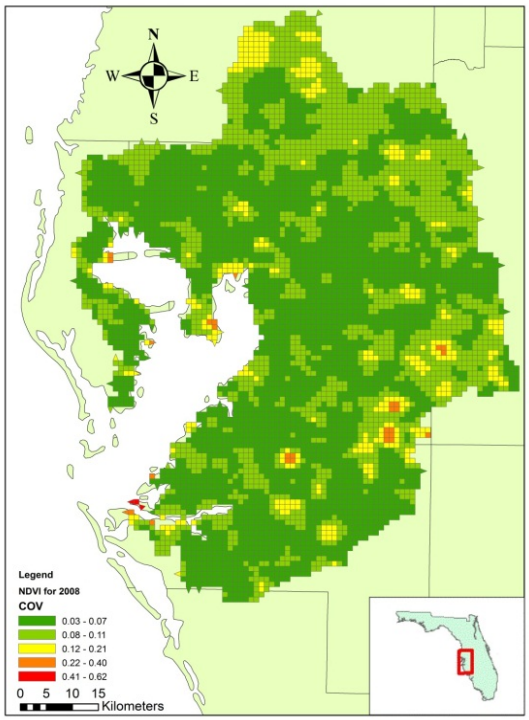

Figure 2.10 CoV analysis maps for NDVI (2005, 2007, and 2008).

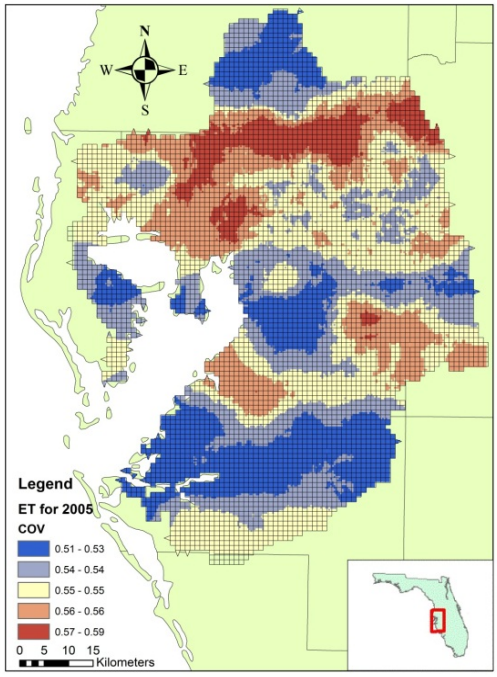
N
W
E
S
Legend
ET for 2005
COV
0.51 - 0.53
0.54 - 0.54
0.55 - 0.55
0.56 - 0.56
0.57 - 0.59
0 5 10 15
Kilometers

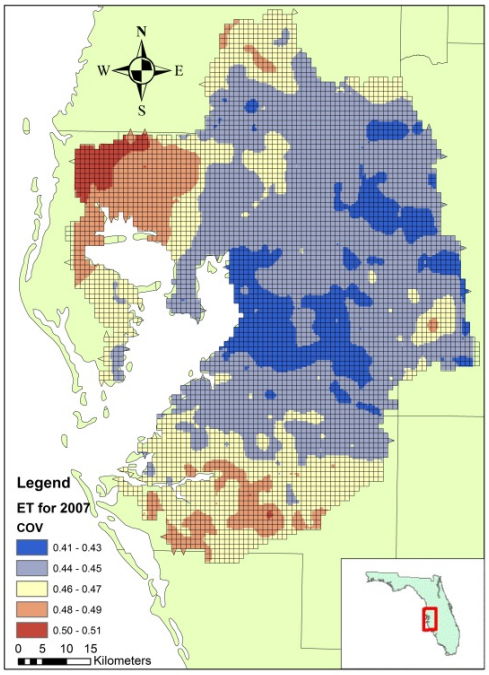
N
W
E
S
Legend
ET for 2007
COV
0.41 - 0.43
0.44 - 0.45
0.46 - 0.47
0.48 - 0.49
0.50 - 0.51
0 5 10 15
Kilometers

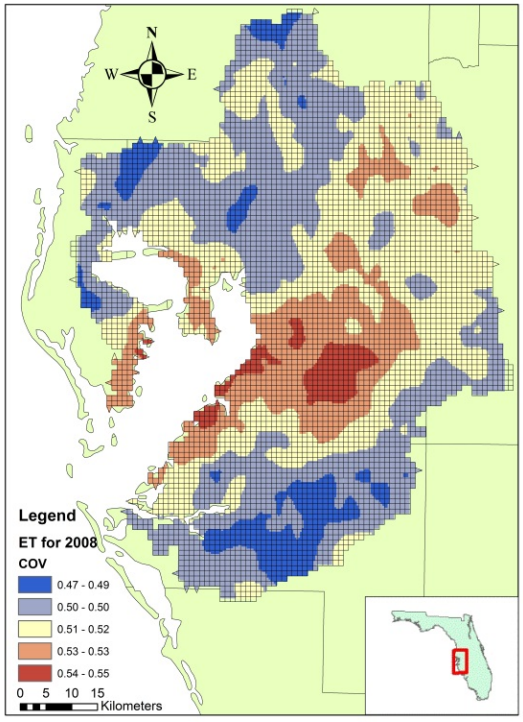

Figure 2.11 CoV analysis maps for ET (2005, 2007, and 2008).

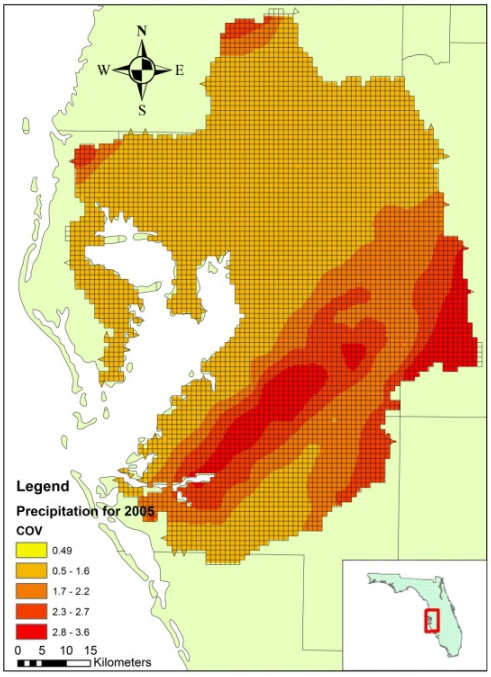
N
W
E
S
Legend
Precipitation for 2005
COV
0.49
0.5 - 1.6
1.7 - 2.2
2.3 - 2.7
2.8 - 3.6
0 5 10 15
Kilometers

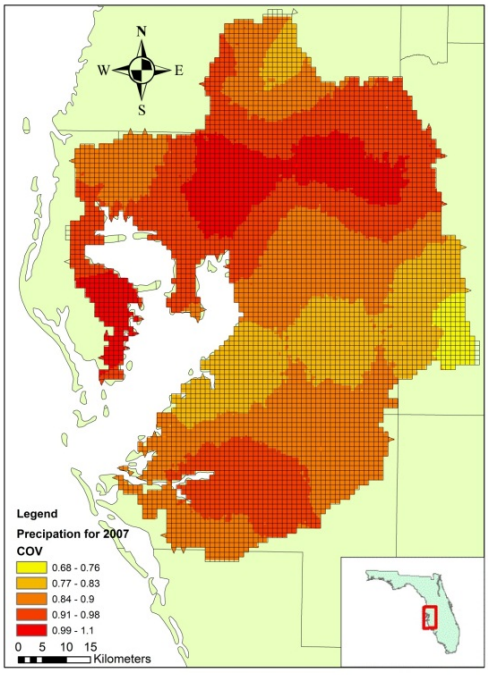
N
W
E
S
Legend
Precipation for 2007
COV
0.68 - 0.76
0.77 - 0.83
0.84 - 0.9
0.91 - 0.98
0.99 - 1.1
0 5 10 15
Kilometers

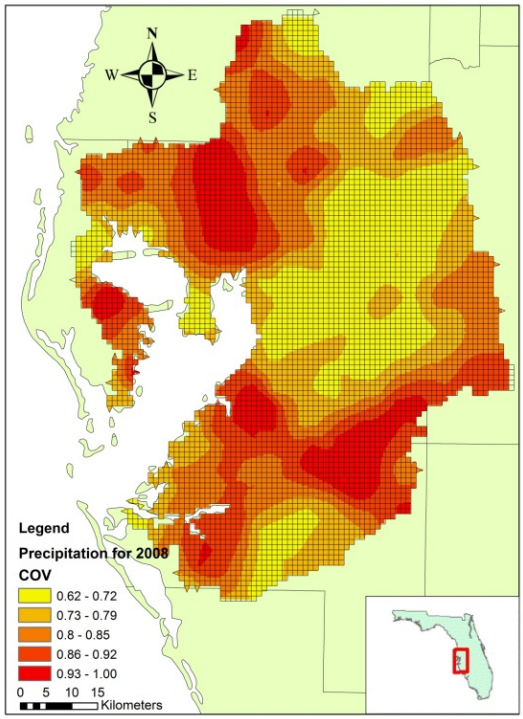

Figure 2.12 CoV analysis maps for precipitation (2005, 2007, and 2008).

2.3.3. Spatial Autocorrelation Analysis

The Moran's I spatial autocorrelation and z-score analysis was carried out via the Esri's ArcGIS software program. The calculations for distances are based on the squared Euclidean distance between data point centroids. The z-score is used to test the null hypothesis, "there exists no spatial clustering." In general, the z-score is determined to be statistically significant if compare it to the range of values for a particular confidence level. A positive z-score of Moran's I indicates that the particular field is more spatially focused than average and negative z-score indicates that a particular field is broader, or less focused. Locally, we can extract some information in terms of convergence and polarization. The four ecohydrologic parameters are

classified as having highly focused fields: both indices are highly positive in which imply highly focused spatial patterns (Table 2.3). This finding indicates that the echydrological spatial patterns for the parameters explored in this study are exceedingly positively autocorrelated in this coastal region. Therefore, the high z-score values indicate that the null hypothesis, "there exists no spatial clustering," can be rejected. NDVI and precipitation similar Moran's I coefficients while LST and ET have similar coefficients. NDVI and precipitation possess extremely high Moran's for all years; NDVI had the highest coefficient for all years and over all parameters investigated. The Moran's I coefficient and z-score for NDVI remained approximately constant during all years of the study. The maximum coefficient was 0.913 for NDVI, which occurred during the 2008 transition year and the minimum coefficient was 0.565 for LST, which occurred during the 2005 hurricane year. LST and Precipitation had a greater Moran's I coefficient and z-score during the 2007 drought year. The Moran's I coefficient for ET increased overtime for the years investigated.

Table 2.3 Summary table for Moran's I autocorrelation coefficient and z-score for LST, NDVI, ET, and precipitation.

		2005		
	NDVI	LST	ET	Precipitation
Moran's I	0.912	0.565	0.584	0.897
z-score	125.869	78.516	75.917	23.984
		2007		
	NDVI	LST	ET	Precipitation
Moran's I	0.911	0.707	0.679	0.907
z-score	125.719	97.798	96.182	24.251
		2008		
	NDVI	LST	ET	Precipitation
Moran's I	0.913	0.699	0.715	0.819
z-score	125.976	96.810	94.089	22.029

CHAPTER 3: IDENTIFICATION OF SPATIOTEMPORAL NUTRIENT PATTERNS IN A COASTAL BAY *VIA* AN INTEGRATED K-MEANS AND GRIVITY MODEL

3.1. Introduction

Nutrient over-enrichment, or eutrophication, alters competition among the dominant phytoplankton species for nutrients in coastal areas. About 65% of estuaries in the United States have moderate to high eutrophic conditions (Bricker et. al., 1999); the most eutrophic estuaries are in the Gulf of Mexico (National Oceanic and Atmospheric Administration, 2011). For more than 40 years, eutrophication of coastal water has been considered one of the major threats to the health status of marine ecosystems because of the various well-documented damaging impacts (Ryther and Dunstan, 1971; Cloern, 2001; Conley, et. al., 2002). Superfluous nutrients such as nitrogen (N) and phosphorus (P), which frequently occur in the forms of nitrite, nitrate, ammonia, and phosphate, are one of the major causes of cyanobacteria blooms (also known as blue-green algae) in water bodies; cyanobacteria blooms have been linked to human and animal illnesses around the world (Bobbin and Recknagel 2001; Wei et. al., 2001). During a national assessment, the consequences of coastal eutrophication symptoms over the years became more apparent, including loss of fish habitats, extensive submerged aquatic vegetation loss, worsening episodes of low dissolved oxygen (DO) in coastal systems, longer lasting or first-time nuisance and toxic algal blooms, commercially unproductive aquaculture, public health concerns, and loss of water resources (Bricker, et. al., 2007).

In Tampa Bay, Florida, the dominant phytoplankton species vary spatially and temporally, especially near river mouths (Steidinger). Phytoplankton species commonly found in Tampa Bay estuaries are *Skeletonema*, *Dactyliosolen*, *Pyrodinium bahamense* var *bahamense*, and *Pseudo-nitzschia*. Algal biomass is often expressed as chlorophyll *a* (Chl-*a*) concentration. Elevated Chl-*a* concentrations are indicative of advanced trophic state. Algal biomass affects light attenuation, which in turn affects water clarity and DO concentrations. Meanwhile, nutrient concentrations, water color, water temperature, and turbidity may alter the abundance of phytoplankton species, thereby changing the Chl-*a* concentrations throughout the bay as well. These characteristics of the bay change temporally and, to some extent, can reflect the amount of fresh water coming from rivers, which also carry run-off nutrients from uplands. Regionally, phytoplankton abundance and nutrient levels generally decreased with increasing salinity in the bay. Low N:P ratios in the Tampa Bay estuary systems throughout the years suggest nitrogen is more limiting than phosphorus and is also a contributor to phytoplankton production in coastal estuaries. In this regard, monitoring water quality of the bay is imperative to fight against water quality deterioration and to restore and protect ecosystems.

The traditional method for monitoring water quality of a coastal bay region is to evaluate long-term water quality on the basis of in-site measurements, collected and partitioned by a geographic classification system (i.e., bays). The long-term trends of Chl-*a* as well as total nitrogen (TN) and total phosphorus (TP) concentrations from 1974 to 1998 exhibit a decreasing trend throughout Tampa Bay (Janicki, Pribble, Janicki, and Winowitch). Although this method considers only one water quality aspect from the management point of view, an assortment of other parameters exists, such as the geographic characteristic of the system with sea–land

interactions, which should be also considered to understand a more sophisticated picture of the coupled bay and watershed system. Improved monitoring and assessment methods should be established to generate a more comprehensive and refined view of nutrient status and ecological implications. Some models have been formulated to address problems such as nutrient over-enrichment to develop strategies to control the size of dead zones and to minimize the impact of eutrophication. For instance, a tidal prism water quality model (TPWQM) was developed to simulate physical transport using the concept of tidal flushing for the representation of eutrophication processes in water column and benthic sediment (Kuo et. al., 2005). This model demonstrates interactions between water columns and sediment bed by considering molecular diffusion for dissolved nutrients and deposition for particulate nutrients. An integrated model, the Curvilinear-grid Hydrodynamics model in three-dimensions (CH3D), was generated to solve the time-dependent equations of motion for water level, three-dimensional velocities, and three-dimensional fields of temperature and salinity (Davis and Sheng, 2000). This model was used in summer 1991 to evaluate water quality in Tampa Bay (Yassuda and Sheng, 1998).

Due to the complexity of ecosystem dynamics in the bay, periodic point measurements in the bay may not be representative; samples of water taken at one period in time are displaced at another location or swept out into the ocean. Previous models did not attempt to improve the classification system of a coastal bay region by partitioning the bay into smaller areas based on water quality parameters and localized areas of concern for excess or limited nutrient levels. They also cannot reflect the mass transfer of nutrients from major river basins to areas located in the bay based on the mass production of one zone and mass attraction of another zone. To better demonstrate how the water quality of Tampa Bay transforms over the course of a year and how

watershed nutrient mass input locations affect the mass disbursement and nutrient levels throughout the bay, a novel, integrated k-means clustering and gravity model (IKCGM) was developed in this study to enrich the comprehensive assessment techniques for estimating and examining the impacts of major sources of watershed nutrient loading and the resultant locations of concern within a coastal bay.

3.2. Materials and methods

3.2.1. Study site

Tampa Bay, Florida, is the economic and environmental hub of a rapidly growing coastal region supporting almost three million people. It is Florida's largest open-water estuary, with a surface area of 1,031 km^2 and on average, 3.7 m deep. More than 100 tributaries flow into Tampa Bay, including dozens of meandering, brackish water creeks and four major rivers: Hillsborough River, Alafia River, Manatee River, and Little Manatee River (Greening, 2009). Currently, the bay is partitioned into four major sub-bay regions: Hillsborough Bay, Old Tampa Bay, Middle Tampa Bay, and Lower Tampa Bay (Figure 3.1). Tampa Bay is used for recreational activities (boating, fishing, and swimming) and as a source of drinking water for the greater Tampa Bay area inhabitants.

Figure 3.1 The location of Tampa Bay watershed and four main rivers.

3.2.2. Data collection

This study was conducted from January 1, 2008 to December 31, 2008; the Environmental Protection Commission of Hillsborough County (EPC) collected data on various water quality parameters from 55 individual sample stations throughout the bay on a monthly basis (Figure 3.2). The flow rates of three of the four major rivers basins (Hillsborough, Alafia, and Little Manatee) were collected on a monthly basis by the United States Geological Survey

(USGS) National Water Information System; the Manatee River was not included in this model because of insufficient data at the mouth of the river basin. Once the selected parameters were gathered, the data were divided temporally based on month and season. We believe that the differences in the composition of the data taken in the bay will be more evident across a seasonal temporal scale. Seasonal averages of all data collected were taken to ascertain the spatiotemporal patterns of water quality based on a seasonal time scale.

3.2.3. Variable selection

Input variables were selected by searching the preeminent available parameters measured by the EPC sample locations. The criterion to include or exclude a variable was based on the linkage of the major characteristics of a river mouth and the sample points in the bay as well as the importance of the parameter for water quality assessment. Chlorophyll content of phytoplankton cells is known to vary based on community composition, position in the water column, and seasons (Steidinger et. al., 2004; Felip and Catalan, 2000). The TN and TP characteristics were combined to derive the TN:TP ratio. This ratio was used to reduce the input variables because models with an excess of input parameters occasionally produce over-fitting and more representative characteristics than the individual concentrations alone at the sampling locations.

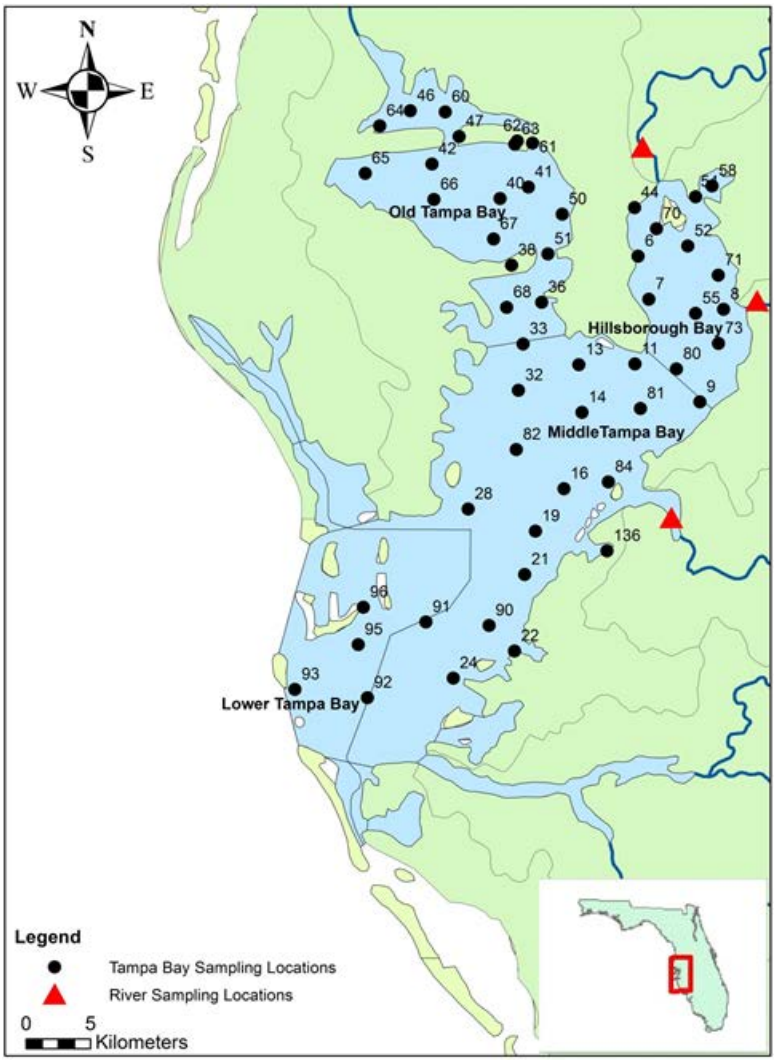

Figure 3.2 The location of the 55 sampling stations in Tampa bay.

Finally, eight variables were selected based on the presented criteria for the clustering analysis: latitude, longitude, TN:TP ratio, Chl-*a*, water color, water temperature, turbidity, and DO (Table 3.1). One problem associated with the study of a region like Tampa Bay is the large water volume fluctuation associated with each tide cycle. Samples of water taken at one location in time may soon be displaced at another location in the bay or even be swept out into the Gulf of Mexico. The dynamics of coastal bay water are complex. To help understand the effects of water motion, seabed topography and other effects not considered negligible may be lumped as

seasonal averages of all relevant parameters. Hence, the mixing effect of fresh water and seawater in an estuary provides changing water quality conditions associated with a range of salinities and other related properties (Ketchum, 1955), which can be postulated through our IKCGM analysis in this study.

To support the gravity segment of the gravity model, three additional parameters were collected: the flow rates (i.e., discharge rates) at the mouth of three of the four major rivers, Hillsborough, Alafia, and Little Manatee; the average depth of Tampa Bay; and the area of the clusters provided by the clustering analysis. The discharge rate was included in this model to particularly help weigh the nutrient input contribution from the rivers with larger flow rates more heavily than the rivers with minor flow rates. The area of the clusters and the average depth were included in this model to convert the concentration values of the clusters to mass values to aid in the characterization of gravity segment of the gravity model.

Table 3.1 Parameters used in the development of the IKCGM analysis

Parameter	Notation	Units
Latitude	lat	Degree
Longitude	long	Degree
Total Phosphorus	TP	$mg \cdot L^{-1}$
Total Nitrogen	TN	$mg \cdot L^{-1}$
Chlorophyll *a*	Chl-*a*	$\mu g \cdot L^{-1}$
Water Color	color	PCU
Temperature	temp	°C
Turbidity	turb	NTU
TN to TP Ratio	TN:TP	Unitless
Flow Rate	discharge	$m^3 \cdot s^{-1}$
Area	A	L^2
Average Depth	D	L
Dissolved Oxygen	DO	$mg \cdot L^{-1}$

3.2.4. Model development

The IKCGM is created by linking the k-means clustering analysis with a series gravity model; The k-means analysis was carried out to partition the accessible dataset into a user-specified number of subsets, called clusters, to discover as well as evaluate the spatiotemporal patterns of water quality in Tampa Bay based on parameters of similar qualities. The gravity model with segment structure was used to analyze the spatial propagation of nutrient fluxes in the bay and estimate the contribution of watershed nutrient input according to the classified clusters located throughout the bay. To estimate the inter-zonal transfer or spatial distribution from the watershed source to another location in the bay via gravity modeling, the bay needed to be divided into zones (i.e., segment structure or circular structure). Thus, the IKCGM algorithm would not be functional without the linkage between the k-means clustering analysis and the gravity model.

3.2.4.1. K-means Clustering Analysis.

The k-means clustering algorithm was discovered and used by many disciplines in early time (Lloyd, 1982; MacQueen, 1967). The k-means analysis is actually a data mining technique, which is a prototype-based partitioning technique, developed to identify a user-specified number of clusters (K) composed of a transformed dataset of (n) objects represented by their centroids (MacQueen, 1967). The user specifies the prescribed number of clusters to be generated in the analyses output with the limitation of $K < n$ (Thuraisingham, 1999). Techniques for selecting these initial seeds include sampling at random from the dataset, setting them as the solution of clustering a small subset of the data, or perturbing the global mean of the data *k* times (Thuraisingham, 1999). The k-means function is comprised of a two-step iterative process: step 1

assigns each data point to its closest centroid; step 2 relocates the cluster centroid until the distance between the centroid and the data points no longer change. The principle incorporated in the k-means clustering analysis is the Euclidean distance (in mathematics the distance between two points), which can be measured with a measuring device or found using the Pythagorean formula.

The basic K-mean function is expressed as follows:

$$C = \sum_{j=1}^{k} \sum_{i=1}^{n} \left\| x_i^{(j)} - c_j \right\|^2 \quad (1)$$

where $||x_i^{(j)} - c_j||$ is a chosen distance measured connecting a data point $x_i^{(j)}$ and the cluster center c_j (km); this gauges the distance of the (n) data points from their respective cluster.

There are a variety of advantages to using the k-means algorithm, such as its relatively simple implementation, ability to partition data into subsets based on the nonlinear relationships between the characteristics of the ecosystem, and its ability to work with relatively noisy or incomplete input data (Tang et. al., 2006). One disadvantage of using the k-means algorithm is that the number of clusters must be user-defined; therefore, several k-means models must be produced in sequence to retrieve the most representative model of the system. The k-means analysis was built using eight distinct parameters in this study, representing both physical and chemical properties of the ecosystem in the bay. IBM SPSS Modeler®, Version 14.1 was used with the aid of the module for k-means clustering analysis. The outputs of the k-means models partition the dataset into a series of subsets of sample points analogous to one another with respect to the eight selected parameters. For each of the k-means models produced, the input data were divided into two series, namely training series and test series, for promoting the model credibility. All collected data available to generate these k-means models were homogeneously

distributed within a year. We decided to separate the yearly time series based on season, dividing this annual period of time into four series and taking seasonal averages of the data, and to construct four k-means clustering models with 6, 8, 10, and 12 clusters, respectively, to determine the best fitted k-means model before conducting the gravity modeling analysis. The best fitted k-means model was selected based on the cluster quality (silhouette of cohesion and separation) and minimal standard deviation between sample parameters within each cluster, in addition to the model with the minimal clusters containing less than three sample points.

3.2.4.2. Gravity Model.

The gravity model is based on Newton's law of gravitation where the force of attraction between two bodies is directly proportional to the product of the masses of the two bodies and inversely proportional to the square of the distance between them:

$$F = G\left(\frac{m_1 m_2}{r^2}\right) \quad (2)$$

where, m_1 is the first mass, m_2 is the second mass, G is the gravitational constant, and r is the distance between the masses.

The gravity model is applied frequently in various disciplines to estimate the inter-zonal transfer or spatial distribution of an entity from one place to another. For example, in transportation the gravity model is applied to the problem of estimating the number of automobile trips between points or "zones" of a highway network given the number of trips concomitant with arrival and departure from each of the points (Wu et. al., 2008). The gravity model is formulated in this study to represent the transfer of nutrient mass from the mouth of each major river connected with terrestrial watersheds and the zones identified by the selected clustering analysis. We decided to square the impact of the functional distance in the model to

reflect the perception that the movement of nutrients is discouraged with increasing distance between the two zones. An additional inter-zonal adjustment factor (i.e., a set of inter-zonal adjustment factors) was also included in the model to aid operation of the model and represent other effects not taken into consideration. The computations for the gravity model from and calibration to validation were made with the aid of Microsoft ® Excel, and the formulation of gravity model in this study is tailored as follows:

$$Q_{IJ} = P_I \left(\frac{A_J F_{IJ} K_{IJ}}{\sum_x A_x F_{Ix} K_{Ix}}\right) = P_I p_{IJ} \quad (3)$$

where, Q_{ij} = interchange between a nutrient production zone i and a nutrient-attraction zone j (tones/period); P_i = magnitude of the nutrient production of zone i (tones/period); A_j = magnitude of nutrient attraction of zone j (tones/period); F_{ij} = travel friction factor, which is also equal to W_{ij}^{-1} (km^{-2}), where W_{ij} is the function of the impedance between the two zones (km^2); and K_{ij} = a set of inter-zonal adjustment factors to capture other residual effects.

3.2.4.3. Holistic Algorithm for the IKCGM.

Within the IKCGM algorithm, 20 steps can be summarized:

1. Determine the number of (K) clusters to be created.

2. Place (K) points into the space represented by the objects, which are to be clustered; these points represent initial group centroid.

3. Assign each object to the group in which has the closest centroid.

4. When all objects have been assigned to the closest centroid, recalculate the positions of the K centroids using Euclidean distance (Eq.1).

5. Repeat Steps 3 and 4 until the centroids no longer move. This produces a separation of the objects into groups from which the metric to be minimized can be calculated.

6. Determine if the current clusters are efficient to continue; if it is decided the clusters are not efficient to continue, repeat steps 1 through 6.

7. Set up the gravity model by first assuming the given area is split into zones 1 through K.

8. Denote the production P_I from the *i*th zone and arrival A_J in the *j*th zone.

$$\sum_j Q_{ij} = P_I \tag{4a}$$

$$\sum_i Q_{ij} = A_J \tag{4b}$$

9. Assume the interchange volume Q_{IJ} between the two zones is the product of three factors: one dependent on I alone, one dependent on J alone, and one dependent on I and J mutually.

$$Q_{IJ} = (\alpha_I)(\beta_J)(W_{ij}) \tag{5}$$

10. Using the equations (4a), (4b), and (5) yields:

$$\alpha_I \sum_j (\beta_J)(W_{IJ}) = P_I \tag{6a}$$

$$\beta_J \sum_i (\alpha_I)(W_{IJ}) = A_J \tag{6b}$$

11. Eliminating α_I from 6a produces:

$$\beta_j \sum_i \left[\frac{(P_i)(W_{ij})}{\sum_j \beta_j W_{ij}}\right] = A_J \tag{7}$$

12. Next, solve equations (7) for the α_J's and use the α_J's to compute the Q_{IJ}'s from the formula:

$$Q_{ij} = \beta_j W_{ij} \left(\frac{P_i}{\sum_j \beta_j W_{ij}} \right) \tag{8}$$

13. Denote the left-hand side of (8) as $f(\alpha)$ and rewrite in the form

$$\alpha_j = \frac{\alpha_J P_I}{f_I(\alpha^{k-1})} \tag{9}$$

14. Using equation (9), compute α_J, where,

$$\alpha^k = \left(\alpha_1^k, \alpha_2^k, \ldots, \alpha_N^k\right) \tag{10}$$

is the *k*th iteration to the solution.

15. Now, let K be the number of zones in the network.

16. For each zone *i*, use the values of W_{i1}, …, W_{iN}; P_1, …, P_N; and α_1^{k-1}, …, α_N^{k-1} in order to calculate

$$\beta_i^{k-1} = \frac{P_I}{\sum_j \alpha_J^{k-1} W_{IJ}} \tag{11a}$$

Obtained from,

$$Q_{IJ}^{k-1} = \beta_I^{k-1} \alpha_J^{k-1} W_{IJ}, \quad \text{where } (j = 1, \ldots, N) \tag{11b}$$

17. Add the calculated Q_{IJ}^{k-1} to the N partial sums where the totals are equal to

$$f_J(\alpha^{k-1}) = \sum_i Q_{IJ}^{k-1} \tag{12}$$

18. Once completing the computations for each zone, calculate new estimates for the α_J's through the utilization of formula (12).

19. Repeat until convergence of Q_{IJ}^{k}.

20. End.

Note: There is no surety of the convergence of the gravity model. The criterion for stopping the iterations should be based on the convergence of the generated Q_{IJ}^{k} and the actual Q_{IJ}^{k} (Wu et. al., 2008).

3.2.5. Verification and Validation of IKCGM.

To verify and validate the IKCGM, an algorithm based on an additional two years of data from 2005 and 2007 was applied to gauge performance and accuracy. Because the calibration of the IKCGM was based on 2008, a transition year between a drought period and a high precipitation period may be selected for model verification and validation (Figure 3.3). We completed the verification effort for a high precipitation year, 2005 and the validation effort for a drought year, 2007. In addition, 2005 also encompassed one hurricane event, Hurricane Wilma, which made landfall in south Florida on October 24, 2005. Within both verification and validation stages, the k-mean clustering analysis was carried out with respect to the cluster quality (i.e., silhouette of cohesion and separation) and standard deviation between sample parameters within each cluster. To verify and validate the gravity model segment of IKCGM, the gravity modeling analysis was conducted for 2005 and 2007 using the model developed for 2008. The model's performance was gauged on the agreement primarily related to satisfying the

convergence of the predicted production values of TN and TP with the actual production values from each river. Such rigorous verification and validation efforts ensure that the IKCGM does not favor one situation over another, given that the algorithm was intensively tested based on a situation of overall heterogeneous parameters as well as a period of high or low variations in water quality and discharge characteristics in the bay as a result of changing runoff volumes. This philosophy can be further confirmed by the hydrograph (Figure 3.3).

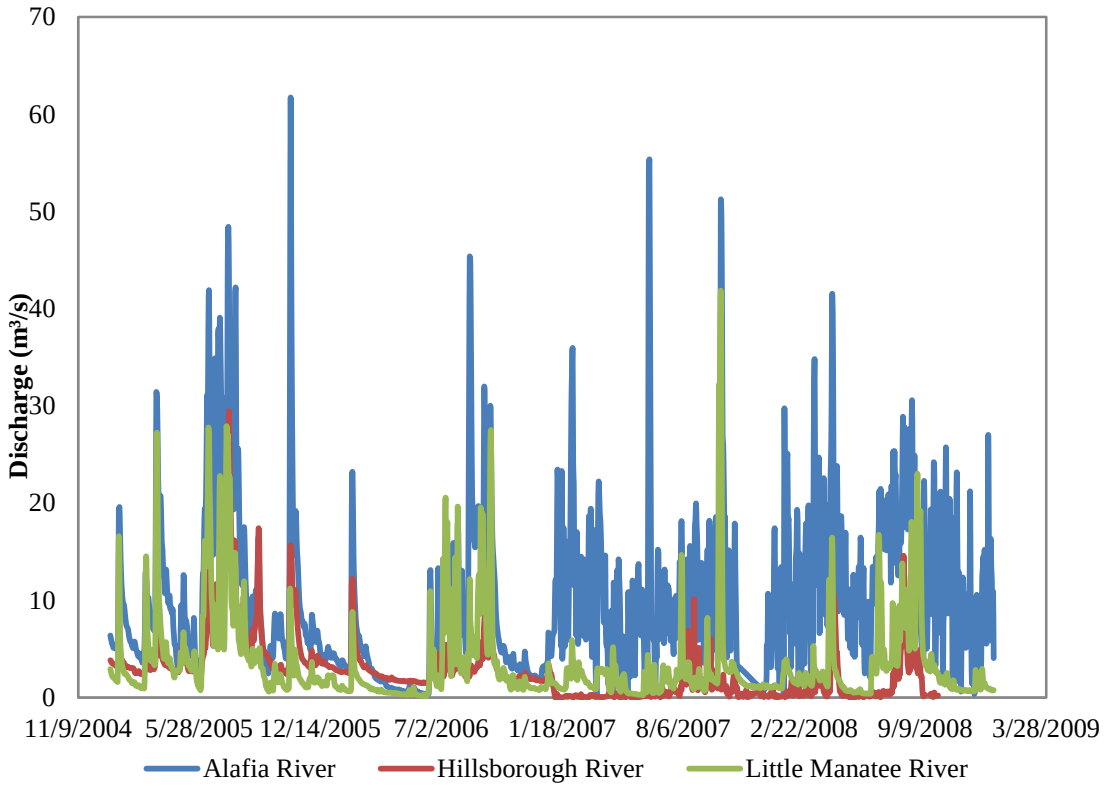

Figure 3.3 Daily hydrograph in m^3/s into Tampa Bay from the Alafia River, Hillsborough River, and Little Manatee River.

The verification and validation years were used to provide an indication of overall performance of IKCGM algorithm based on four statistical indices, including 1) square of the Pearson product moment correlation coefficient (RSQ), 2) root mean square error (RSME), 3)

ratio of standard deviation of predicted to observed values (CO), and 4) mean of percent error (PE),. In principle, a respectable model should offer the least differences between the predicted values and the observed values. These four statistical measures as applied to this case study are described below.

3.2.5.1. Square of the Pearson product moment correlation coefficient.

The RSQ indicates a better model as it approaches 1:

$$RSQ\ (r^2) = \left[\frac{\sum_{i=1}^{N}(y_{pi-}\bar{y}_{pi})(y_{oi-}\bar{y}_{oi})}{\sqrt{\sum_{i=1}^{N}(y_{pi-}\bar{y}_{pi})^2 \sum_{i=1}^{N}(y_{oi-}\bar{y}_{oi})^2}}\right]^2 \quad (13)$$

where, y_{pi} is the predicted value and y_{oi} is the observed value.

3.2.5.2. Root mean square error.

The RMSE indicates a better model as the value approaches zero:

$$RMSE = \sqrt{\frac{\sum_{i=1}^{N} y_{pi-}\, y_{oi}}{N}} \quad (14)$$

where, y_{pi} is the *i*th predicted value and y_{oi} is the *i*th observed value. Here the sum of square errors (SE) is the square root of sum of square of the difference between predicted value and observed value divided by *N*, the total number of data points involved.

3.2.5.3. Ratio of standard deviation of predicted to observed values.

The CO gives the ratio of the standard deviations of predicted value to observed value, which indicates a better model as this ratio approaches 1:

$$CO = \sqrt{\frac{\sum_{i=1}^{N}(y_{pi-}\bar{y}_{pi})^2}{\sum_{i=1}^{N}(y_{oi-}\bar{y}_{oi})^2}} \quad (15)$$

where, y_{pi} is the predicted value; $\bar{y}_{pi}$ is the mean of the *i*th predicted value; y_{oi} is the observed value; and $\bar{y}_{oi}$ is the mean of the observed value. The bar above each parameter indicates the arithmetic mean.

3.2.5.4. Mean of percent error.

The mean of PE indicates a better model when its value approaches zero:

$$PE = \frac{\sum_{i=1}^{N}\left(\frac{y_{pi}- y_{oi}}{y_{oi}}\right)x\ 100\%}{N}. \quad (16)$$

3.3. Results and discussion

The derivation, verification, validation, and application of IKCGM were systematically carried out for Tampa Bay, Florida. Nevertheless, the ever-changing dynamics of coastal bay water makes the distribution of nutrients exceptionally complex. To clarify the application potential, this section is composed of first, the k-means analysis and second, the gravity model analysis in sequence prior to the integrated assessment.

3.3.1. Results of k-means clustering analysis

3.3.1.1 k-mean Clustering.

Four clustering practices were organized and tested for screening to determine the optimal number of clusters in the bay that reflects the spatial patterns over time in support of the gravity modeling analysis to the maximum extent. Each practice with differing settings of clusters produces a progressively refined picture of the structure of spatiotemporal patterns of water quality in the bay (Figure 3.4). The optimal number of clusters was finally selected based on the three collective criteria: cluster quality (i.e., silhouette of cohesion and separation),

minimal standard deviation between sample parameters within each cluster, and the model with the minimal clusters containing less than three sample points (Table 3.2).

A plausible assumption would be that as the number of distinct clusters increased, the standard deviation values would decrease across the parameters of water quality in each modeling practice. Based on the three criteria above, the modeling practice with eight clusters was deemed the most suitable for subsequent gravity modeling analysis. An interesting finding was that the model with eight clusters had lower standard deviation values than the model with ten clusters. Both the clustering models with eight or twelve clusters produced the maximum silhouette of cohesion and separation value of 0.418. Yet, the model with twelve clusters was ruled out based on the last criterion because there were two clusters with less than three samples compared to the counterparts. Finally, four seasonal models with eight clusters, namely one model for each season, were produced and inspected to determine if there was a significant change in the composition of the spatiotemporal patterns in the bay. We found no significant change across the seasons in 2008. This observation aids in final screening and selection as described below.

3.3.1.2. Water quality assessment associated with spring cluster.

The results of the k-means clustering analysis for the spring season (Table 3.3) show that cluster 2 had a TP concentration of 0.35 $mg \cdot L^{-1}$, which is the highest concentration of TP, while clusters 3 and 6 presented the lowest concentration of TP, 0.11 $mg \cdot L^{-1}$. Cluster 5 had the greatest value of water color with a value of 16.13 PCU as well as the greatest TN concentration at 0.80 $mg \cdot L^{-1}$, suggesting an excess of TN. Cluster 2 had the smallest value of TN with a concentration of 0.22 $mg \cdot L^{-1}$; because cluster 2 had the lowest TN concentration and the maximum value of

TP, it also had the lowest TN:TP ratio, suggesting TN is limited in comparison to TP. Cluster 8 had the highest Chl-*a* concentration of 25.84 $\mu g \cdot L^{-1}$, the highest temperature value of 23.22 ºC, and the highest turbidity value of 5.15 NTU.

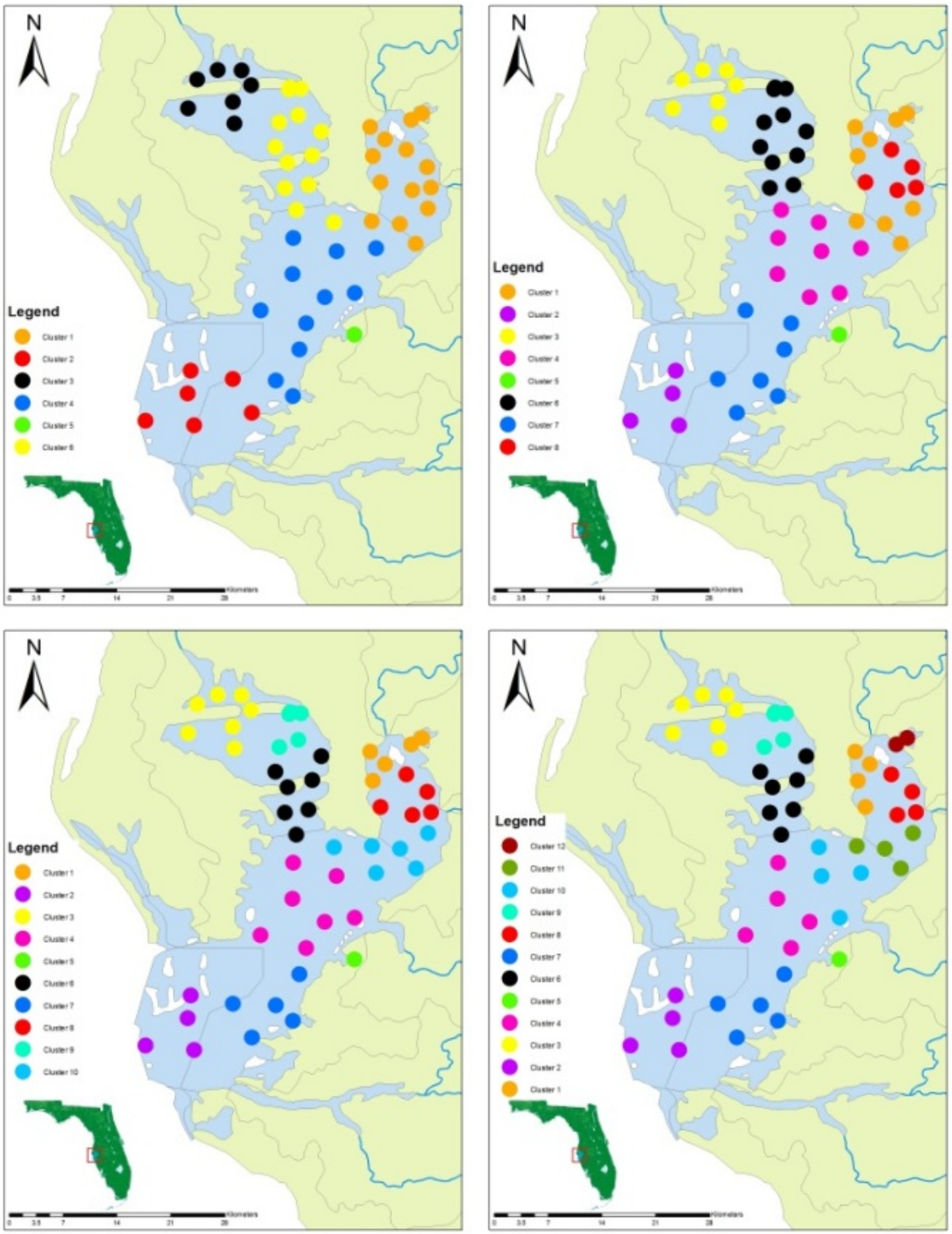

Figure 3.4 The four clustering models generated by the k-means clustering analysis: 6, 8, 10, and 12 defined clusters.

Table 3.2 The results for the determination of the optimal number of clusters based on the collective criteria of cluster quality.

Model	Silhouette	Cluster	Latitude	Longitude	Chlorophyll a (µg/L)	Color (PCU)	Temperature (Deg C)	Turbidity (NTU)	TN:TP
1	0.376	cluster-1	0.049	0.026	1.167	0.422	0.666	0.571	0.341
		cluster-2	0.027	0.044	0.412	0.616	0.214	0.398	0.743
		cluster-3	0.024	0.027	1.818	0.766	0.721	1.116	0.629
		cluster-4	0.063	0.039	0.506	0.706	0.236	1.674	0.741
		cluster-5	0.000	0.000	0.000	0.000	0.000	0.000	0.000
		cluster-6	0.054	0.020	0.931	1.083	0.473	0.270	0.790
2	0.418	cluster-1	0.060	0.027	0.983	0.404	0.770	0.594	0.380
		cluster-2	0.030	0.027	0.285	0.539	0.269	0.358	0.932
		cluster-3	0.024	0.027	1.818	0.766	0.721	1.116	0.629
		cluster-4	0.037	0.036	0.555	0.447	0.225	1.717	0.448
		cluster-5	0.000	0.000	0.000	0.000	0.000	0.000	0.000
		cluster-6	0.043	0.017	0.930	1.096	0.507	0.227	0.817
		cluster-7	0.045	0.032	0.506	0.671	0.105	0.494	0.590
		cluster-8	0.020	0.024	1.247	0.388	0.486	0.394	0.243
3	0.393	cluster-1	0.020	0.027	1.093	0.395	0.488	0.502	0.357
		cluster-2	0.030	0.027	0.285	0.539	0.269	0.358	0.932
		cluster-3	0.024	0.027	1.818	0.766	0.721	1.116	0.629
		cluster-4	0.036	0.037	0.552	0.627	0.220	1.887	0.613
		cluster-5	0.000	0.000	0.000	0.000	0.000	0.000	0.000
		cluster-6	0.032	0.019	0.326	0.240	0.331	0.197	0.728
		cluster-7	0.027	0.033	0.554	0.820	0.096	0.524	0.572
		cluster-8	0.020	0.024	1.247	0.388	0.486	0.394	0.243
		cluster-9	0.020	0.010	1.195	1.484	0.688	0.290	0.630
		cluster-10	0.018	0.040	1.051	0.374	0.795	0.742	0.398
4	0.418	cluster-1	0.028	0.008	0.349	0.152	0.334	0.463	0.199
		cluster-2	0.030	0.027	0.285	0.539	0.269	0.358	0.932
		cluster-3	0.024	0.027	1.818	0.766	0.721	1.116	0.629
		cluster-4	0.039	0.028	0.659	0.552	0.169	0.355	0.624
		cluster-5	0.000	0.000	0.000	0.000	0.000	0.000	0.000
		cluster-6	0.032	0.019	0.326	0.240	0.331	0.197	0.728
		cluster-7	0.027	0.033	0.554	0.820	0.096	0.524	0.572
		cluster-8	0.022	0.014	1.061	0.335	0.491	0.208	0.150
		cluster-9	0.020	0.010	1.195	1.484	0.688	0.290	0.630
		cluster-10	0.034	0.023	0.238	0.347	0.308	2.212	0.366
		cluster-11	0.057	0.025	0.858	0.282	0.861	0.781	0.491
		cluster-12	0.000	0.000	0.000	0.000	0.000	0.000	0.000

3.3.1.3. Water quality assessment associated with summer cluster.

The results of the k-means clustering analysis for the summer season (Table 3.4) show that the majority of the TN and TP concentrations for the clusters in the bay for 2008 were at

their maximum value. Cluster 5 had the highest TN concentration of 0.68 $mg \cdot L^{-1}$ as well as the highest water color value at 23.77 PCU. Cluster 8 had the maximum concentration of TP at 0.27 $mg \cdot L^{-1}$ and turbidity value of 6.12 NTU. Cluster 3 had a significantly higher Chl-*a* concentration at 29.01 $\mu g \cdot L^{-1}$, a value approximately twice that of the next highest Chl-*a* concentration cluster. Cluster 5 had the greatest value of water color, 16.13 PCU, as well as the greatest TN concentration, 0.80 $mg \cdot L^{-1}$; these high values suggest an excess of TN. During the summer season, the data suggest an abnormal increase in the nutrient input, which corresponds with the increase in precipitation in this region. Most likely, the increase in nutrient concentrations is due to the increase in discharge into the bay transmitted from watershed input (Figure 3.5).

Table 3.3 k-means clustering analysis for the spring season based on the eight clusters.

Cluster Centroid			Water Quality Parameter							
Cluster	Latitude	Longitude	TP ($mg \cdot L^{-1}$)	TN ($mg \cdot L^{-1}$)	Chl-*a* ($\mu g \cdot L^{-1}$)	Color (PCU)	Temp (°C)	Turb (NTU)	TN:TP	DO ($mg \cdot L^{-1}$)
1	27.8701	-82.4487	0.19	0.39	12.13	7.10	22.99	4.42	2.10	6.94
2	27.6004	-82.7042	0.35*	0.22**	2.35**	2.64**	22.84	2.38	0.62**	7.20
3	27.9655	-82.6529	0.10**	0.50	5.46	6.70	22.76	3.14	4.67*	7.44
4	27.7743	-82.5325	0.15	0.38	4.03	5.12	22.83	2.30	2.99	7.28
5	27.6800	-82.4992	0.23	0.80*	7.07	16.13*	20.50**	4.67	3.48	5.59**
6	27.9156	-82.5686	0.11	0.43	4.77	5.87	22.70	3.28	3.86	7.44*
7	27.6450	-82.5932	0.17	0.31	2.67	3.86	22.80	1.79**	2.80	7.25
8	27.8668	-82.4323	0.22	0.46	25.84*	9.23	23.22*	5.15*	2.15	7.18

Note: * indicates maximum values and ** indicates minimum values for the season

Table 3.4 k-means clustering analysis for the summer season based on the eight clusters.

Cluster Centroid			Water Quality Parameter							
Cluster	Latitude	Longitude	TP ($mg \cdot L^{-1}$)	TN ($mg \cdot L^{-1}$)	Chl-*a* ($\mu g \cdot L^{-1}$)	Color (PCU)	Temp (°C)	Turb (NTU)	TN:TP	DO ($mg \cdot L^{-1}$)
1	27.8701	-82.4487	0.23	0.45	12.84	10.11	29.67	4.27	1.96	5.91
2	27.6004	-82.7042	0.07**	0.31**	3.81**	3.34**	30.26*	2.07	4.43	6.09
3	27.9655	-82.6529	0.15	0.66	29.01*	11.06	29.32	4.04	4.50*	6.35
4	27.7743	-82.5325	0.14	0.51	7.10	6.92	29.53	2.02	3.58	6.48**
5	27.6800	-82.4992	0.23	0.68*	14.10	23.77*	29.55	4.50	2.96	5.38*
6	27.9156	-82.5686	0.15	0.50	13.41	8.16	29.31**	2.60	3.55	6.20
7	27.6450	-82.5932	0.12	0.40	4.60	5.43	29.88	1.99**	3.46	6.02
8	27.8668	-82.4323	0.27*	0.49	25.84	11.33	30.00	6.12*	1.85**	6.45

Note: * indicates maximum values and ** indicates minimum values for the season

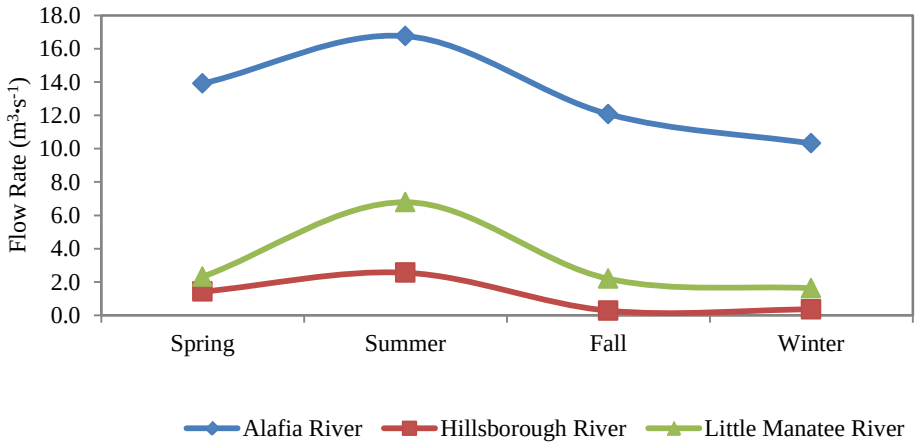

Figure 3.5 Seasonal flow rate values for the Alafia River, Hillsborough River, and Little Manatee River.

3.3.1.4. Water quality assessment associated with fall cluster.

The results of the k-means clustering analysis for the fall season (Table 3.5) show that the TP concentration was at its maximum value for 2008 in cluster 8 with a concentration of 0.33 $mg \cdot L^{-1}$. The maximum TN concentration of 0.84 $mg \cdot L^{-1}$ occurred in cluster 5 as well as the highest water color value at 23.77 PCU. During the fall season, the DO concentration for cluster 5 was at it minimum value at 2.59 $mg \cdot L^{-1}$ for 2008. Cluster 1 had a significantly low TN:TP ratio at 1.78 in addition to a drastically higher turbidity value of 6.46 NTU in comparison to the other clusters.

Table 3.5 k-means clustering analysis for the fall season based on the eight clusters.

Cluster Centroid			Water Quality Parameter							
Cluster	Latitude	Longitude	TP ($mg \cdot L^{-1}$)	TN ($mg \cdot L^{-1}$)	Chl-*a* ($\mu g \cdot L^{-1}$)	Color (PCU)	Temp (°C)	Turb (NTU)	TN:TP	DO ($mg \cdot L^{-1}$)
1	27.8701	-82.4487	0.32	0.56	11.56	7.69	25.43	6.46*	1.78**	4.27
2	27.6004	-82.7042	0.08**	0.22**	3.05**	3.61**	21.44**	2.88	2.62	5.82
3	27.9655	-82.6529	0.20	0.60	14.15*	9.96	25.25	3.00	2.94	5.99*
4	27.7743	-82.5325	0.19	0.42	5.57	6.15	24.91	2.93	2.26	5.53
5	27.6800	-82.4992	0.27	0.84*	13.77	18*	23.34	5.77	3.11*	2.59**
6	27.9156	-82.5686	0.19	0.56	10.32	9.04	25.40	2.15**	2.90	5.33
7	27.6450	-82.5932	0.13	0.29	3.57	5.05	21.97	2.55	2.23	5.43
8	27.8668	-82.4323	0.33*	0.62	11.87	7.56	25.51*	5.49	2.11	4.95

Note: * indicates maximum values and ** indicates minimum values for the season

3.3.1.5. Water quality assessment associated with winter cluster.

The results of the k-means clustering analysis for the winter season (Table 3.6) show that the majority of the water quality parameters for the clusters in the bay were at their minimal values. The lowest concentration value for Chl-*a* concentration in winter season was 1.53 $\mu g \cdot L^{-1}$, which suggests a decrease in the growth of phytoplankton during this season. During the winter season, the data suggest an abnormal decrease in the nutrient input, which corresponds with the decrease in precipitation in this region (Figure 3.5). Most likely, the decrease in nutrient concentrations is due to the decrease in discharge into the bay transmitted from watershed input. These changes in the composition of water nutrients can directly affect the production of various algal species, which may rely on these nutrients for survival (D'Esopo and Lefkowitz, 1963; Hu et. al., 2004).

Table 3.6 k-means clustering analysis for the winter season based on the eight clusters.

Cluster Centroid			Water Quality Parameter							
Cluster	Latitude	Longitude	TP ($mg \cdot L^{-1}$)	TN ($mg \cdot L^{-1}$)	Chl-*a* ($\mu g \cdot L^{-1}$)	Color (PCU)	Temp (°C)	Turb (NTU)	TN:TP	DO ($mg \cdot L^{-1}$)
1	27.8701	-82.4487	0.20	0.46	4.16	5.54	17.86	3.11	2.40	5.27
2	27.6004	-82.7042	0.09**	0.23**	1.53**	2.65**	17.54	2.32	2.88	6.51*
3	27.9655	-82.6529	0.12	0.44	4.44	7.02	17.83	2.28	3.64*	6.48
4	27.7743	-82.5325	0.13	0.34	2.33	4.61	17.72	2.45	2.68	6.3
5	27.6800	-82.4992	0.17	0.60*	7.80*	15.67*	19.02*	5.83*	3.53	4.6**
6	27.9156	-82.5686	0.14	0.38	3.60	5.87	17.46**	1.58**	3.02	6.09
7	27.6450	-82.5932	0.09	0.32	1.93	3.45	17.53	1.76	3.50	6.35
8	27.8668	-82.4323	0.22*	0.47	5.24	5.89	18.03	3.61	2.21**	5.86

Note: * indicates maximum values and ** indicates minimum values for the season

3.3.1.6. Cluster analysis anomalies.

In every clustering practice generated by the k-means algorithm, sampling station #136, which corresponds to Bishop Harbor, was continuously classified as cluster 5. Cluster 5 was formed because of its distinct characteristics unlike other points in its proximity, and it is the

only cluster with only one sample point. In all seasons, it had the maximum TN concentrations and the maximum water color value. In the winter season, it had the maximum TN concentration, Chl-*a* concentration, water color value, temperature value, and turbidity value. The water color value in cluster 5 was exceptionally greater, approximately three times the value of any of the other generated clusters across every season. The elevated TN concentration, water color value, and Chl-*a* concentration suggests that there also exists a high colored dissolved organic matter (CDOM) value in this vicinity; CDOM is transported by water runoff from watersheds into the bay (Strickland, *1960;* Branco and Kremer, 2005). These prominent high values suggest deteriorated water quality and some obvious water quality management problems in this area. Given that CDOM strongly absorbs light, it affects the light transparency, which influences the production of phytoplankton and seaweed in ecosystems, in particular ultra-violet light (Strickland, *1960;* Branco and Kremer, 2005). This anomaly most likely occurred as a result of an accumulation of nutrients in this sub-bay carried by stormwater runoff from the watershed, which causes high temperatures in this shallow water with little circulation from the bay.

Another anomaly encountered during the clustering analysis was that cluster 2 had the minimum values of TN concentration, Chl-*a* concentration, and water color value for every season as well as the minimum concentration value for TP for three consecutive seasons: summer, fall, and winter. This information reveals an area of limited nutrient for most of the year affecting the ratio between nitrogen and phosphorus concentrations. The ratio between nitrogen and phosphorus concentrations in an aquatic ecosystem, however, can often be associated with cyanobacteria species dominance, which can influence total phytoplankton productivity (Branco and Kremer, 2005; Takamura et. al., 1992; The Cadmus Group, Inc., 2009).

3.3.2. Results of the gravity modeling analysis

The second part of the IKCGM analysis is the gravity modeling analysis. The primary focus of the gravity model is to conduct a spatial distribution analysis and estimate and interpret the impacts of watershed nutrient input based on the generated clusters. Through the formulation of the gravity model presented, we examined the inherent linkage between the mass of one location in the bay and the major contribution of terrestrial nutrient mass. To support the gravity model, an additional parameter, the water discharge rate, was gathered for three of the four major rivers: Hillsborough, Alafia, and Little Manatee. The water discharge rate was one of the predominate variables considered for determining the impact of the nutrient input based on the clusters in the bay. The results presented by the gravity model represent an estimation of the impacts of the nutrient input transported from the major watershed outlets based on the selected clusters throughout the bay.

3.3.2.1 Gravity model assessment.

The results of the gravity modeling analysis for TP and TN (Tables 3.7 and 3.8) suggest that the Alafia River is the major contributor of nutrients in Tampa Bay and is significantly higher than the other primary contributors. Although the data show that Hillsborough River has a high concentration of TN and TP, the discharge rate into the bay is significantly lower in comparison to the other rivers, resulting in a lower nutrient input for the year. Although the Hillsborough River has a larger drainage basin area than the Little Manatee River, approximately 983 km^2 compared to 633 km^2, the Hillsborough River has a manmade dam, which inhibits the discharge into Hillsborough Bay. For the fall season, the model shows that the Alafia River is the primary contributor of TP for all clusters in the bay (see Figures 3.6 and 3.7). In the spring

season, the Little Manatee River was the primary contributor of TP for cluster 3 and cluster 5. In summer, the Alafia River was the major contributor of TP as well as TN for all clusters; this can be easily explained by the large flow rate from this river during the summer season as well as being in close proximity to the cluster centroid. In the spring and winter seasons, the Little Manatee River was the primary contributor of TN for cluster 5, which was still the case for clusters 5 and 7 during the summer and fall seasons. Further investigation revealed that the Alafia River, at its maximum value, contributes to approximately 0.864 tonnes of TP per day and 1.486 tonnes of TN per day during the summer season.

Table 3.7 Gravity model analysis for TP mass value in tonnes for each season based on the eight clusters.

Total Phosphorus								
Spring								
Origin	Destination (Cluster)							
	1	2	3	4	5	6	7	8
Alafia River	13.079*	2.397*	0.830	6.265*	0.332	2.255*	2.460*	25.692*
Hillsborough River	0.641	0.090	0.076	0.212	0.009	0.252	0.082	0.412
Little Manatee River	0.499	0.499	0.93*	0.091	0.879*	0.203	1.526	0.340
Summer								
Origin	Destination (Cluster)							
	1	2	3	4	5	6	7	8
Alafia River	20.459*	0.637*	1.447*	7.57*	0.425	3.832*	2.192	40.509*
Hillsborough River	1.704	0.041	0.225	0.434	0.019	0.727	0.124	1.105
Little Manatee River	1.715	0.542	0.347	5.959	2.475*	0.756	2.987*	1.177
Fall								
Origin	Destination (Cluster)							
	1	2	3	4	5	6	7	8
Alafia River	10.554*	0.393*	1.132*	4.009*	1.309*	1.411*	1.368*	22.126*
Hillsborough River	0.286	0.006	0.052	0.049	0.041	0.022	0.047	0.068
Little Manatee River	0.385	0.150	0.091	2.701	0.028	0.490	0.145	0.312
Winter								
Origin	Destination (Cluster)							
	1	2	3	4	5	6	7	8
Alafia River	8.692*	0.392*	0.607*	3.45*	0.306	1.796*	0.858*	16.63*
Hillsborough River	0.174	0.006	0.023	0.048	0.002	0.082	0.012	0.109
Little Manatee River	0.240	0.110	0.048	0.893	0.306*	0.117	0.384	0.159

Note: * indicate the maximum values corresponding to the primary contributor to the mass value

Table 3.8 Gravity modeling analysis for TN mass value in tonnes for each season based on the eight clusters

Total Nitrogen								
Spring								
Origin	Destination (Cluster)							
	1	2	3	4	5	6	7	8
Alafia River	18.421*	1.025*	2.650*	10.941*	0.794	5.955*	3.07*	37.314*
Hillsborough River	1.907	0.081	0.511	0.780	0.044	1.404	0.216	1.265
Little Manatee River	1.121	0.634	0.461	6.255	3.355*	0.853	3.038	0.787
Summer								
Origin	Destination (Cluster)							
	1	2	3	4	5	6	7	8
Alafia River	30.629*	2.097*	5.066*	20.976*	0.976	10.054*	5.872	57.953*
Hillsborough River	2.974	0.156	0.916	1.403	0.050	2.223	0.387	1.842
Little Manatee River	2.891	2.010	1.367	18.599	6.397*	2.234	9.011*	1.896
Fall								
Origin	Destination (Cluster)							
	1	2	3	4	5	6	7	8
Alafia River	11.455*	0.451*	1.409*	5.277*	0.366	3.439*	1.267	22.169*
Hillsborough River	0.530	0.016	0.121	0.168	0.009	0.362	0.040	0.336
Little Manatee River	0.908	0.363	0.319	3.928	2.016*	0.642	1.633*	0.609
Winter								
Origin	Destination (Cluster)							
	1	2	3	4	5	6	7	8
Alafia River	13.512*	0.659*	1.443*	5.999*	0.370	3.268*	1.97*	23.784*
Hillsborough River	0.510	0.019	0.101	0.156	0.007	0.281	0.050	0.294
Little Manatee River	0.719	0.356	0.219	2.997	1.366*	0.409	1.703	0.438

Note: * indicate the maximum values corresponding to the primary contributor to the mass value

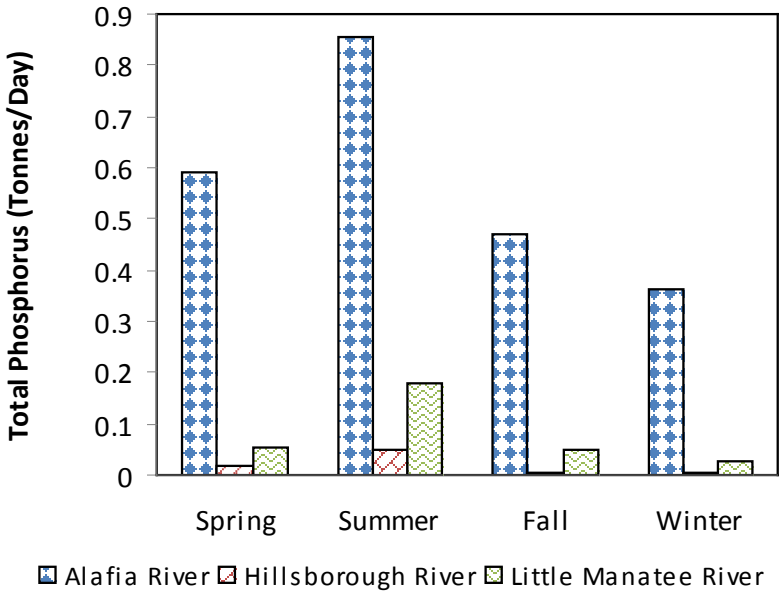

Figure 3.6 Seasonal TP input in tonnes·day^{-1} into Tampa Bay from the Alafia River, Hillsborough River, and Little Manatee River.

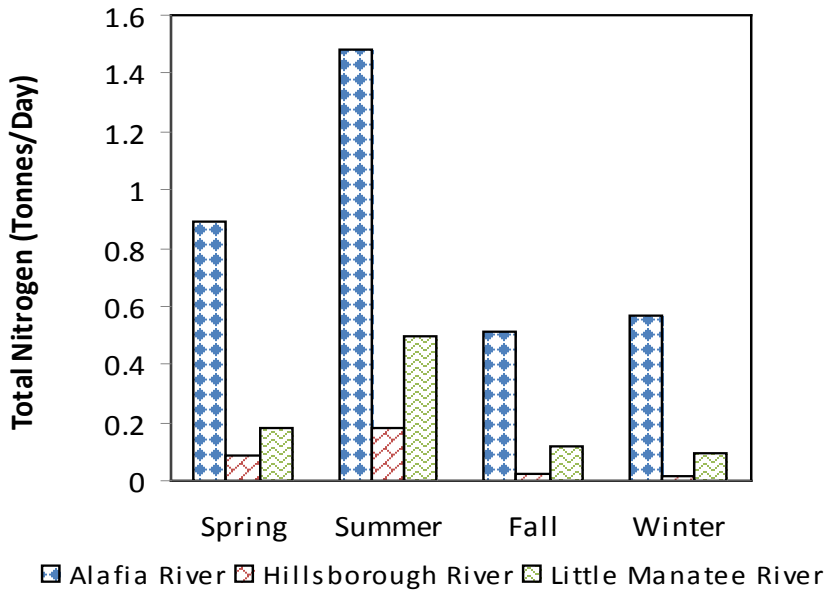

Figure 3.7 Seasonal TN input in tonnes·day^{-1} into Tampa Bay from the Alafia River, Hillsborough River, and Little Manatee River.

3.3.3. Ecological impact assessment: DO vs. nutrients

Globally, the number and size of anoxic and hypoxic areas (also known as “dead zones”) have developed dramatically in recent years (Diaz and Rosenberg, 2008). Although hypoxia can occur via natural processes, the prevalence of hypoxia is believed to be increasing due to increased eutrophication (NRC, 2000). Various studies have found that two-thirds of the coastal estuaries in the United States are degraded as a result of nutrient over-enrichment, which can be directly associated with dissolved oxygen depletion (Diaz and Rosenberg, 2008; NRC, 2000; Howarth, Chan, Conley et. al., 2011; Boynton and Kemp, 1985). Hypoxic (DO concentration below 2.0-3.0 $mg \cdot L^{-1}$) and anoxic (lack of oxygen) water in coastal estuaries are known to be one of the causes of various major environmental problems, mainly created as planktonic algae die and add to the flow of organic matter to the seabed to fuel microbial respiration (Diaz and Rosenberg, 2008). The development of coastal hypoxia is most easily seen along eastern boundary currents, where winds moving toward the equator drive the surge of oxygen-poor and nutrient-enhanced water from the ocean interior into coastal waters (Howarth et. al., 2011). Clusters 1, 3, 4, 5, 6, and 8 (Figure 3.8) all display the inverse relationship between DO concentration and nutrient (TN and TP) concentration levels. These clusters are located away from the mouth of the bay (Figure 3.4), where the tidal effect is trivial and the nutrient loading is relatively large. In cluster 5, the DO concentration dropped below the 3 $mg \cdot L^{-1}$ level during the fall season where the cluster can be classified as hypoxic. Currently, the DO levels in most clusters, other than cluster 5, are about two times larger than the hypoxia threshold, but hypoxic conditions can still be reached. Although high nutrient inputs are required to drive a weakly stratified ecosystem to the point of hypoxia, even moderate increases in nutrient loading and

eutrophication could lead to hypoxic conditions in a strongly stratified water body (NRC, 2000; Howarth et. al., 2011; Boynton and Kemp, 1985).

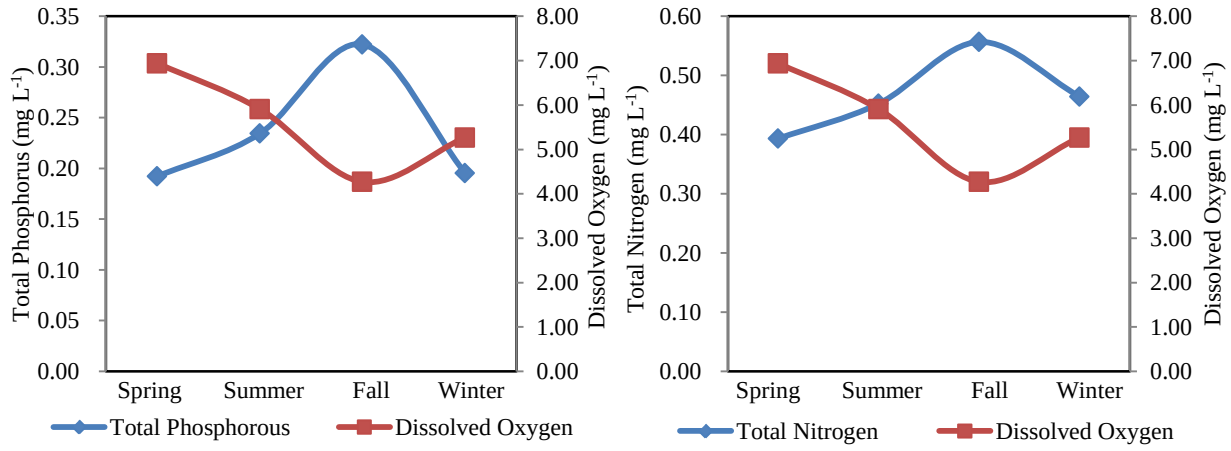

(a) Cluster 1

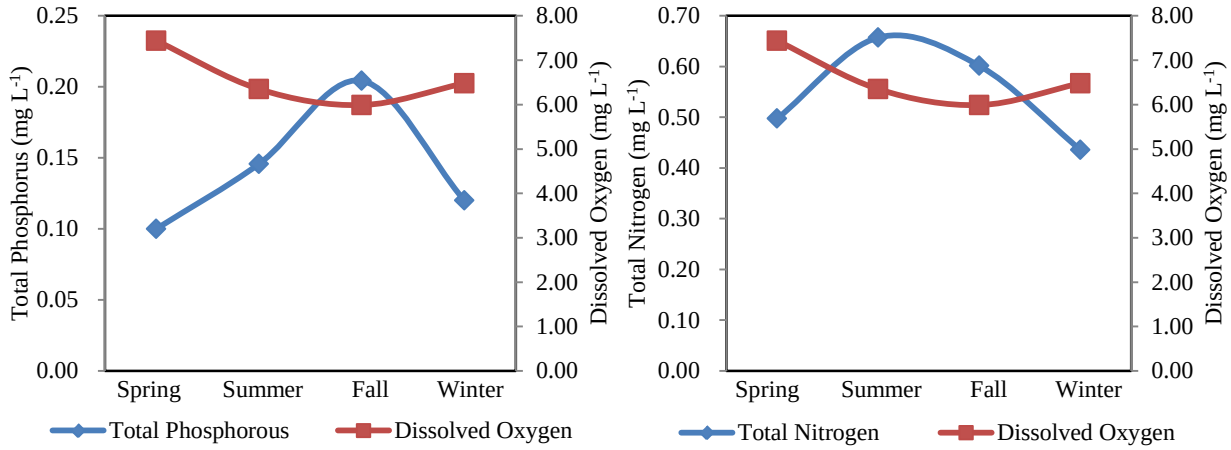

(b) Cluster 3

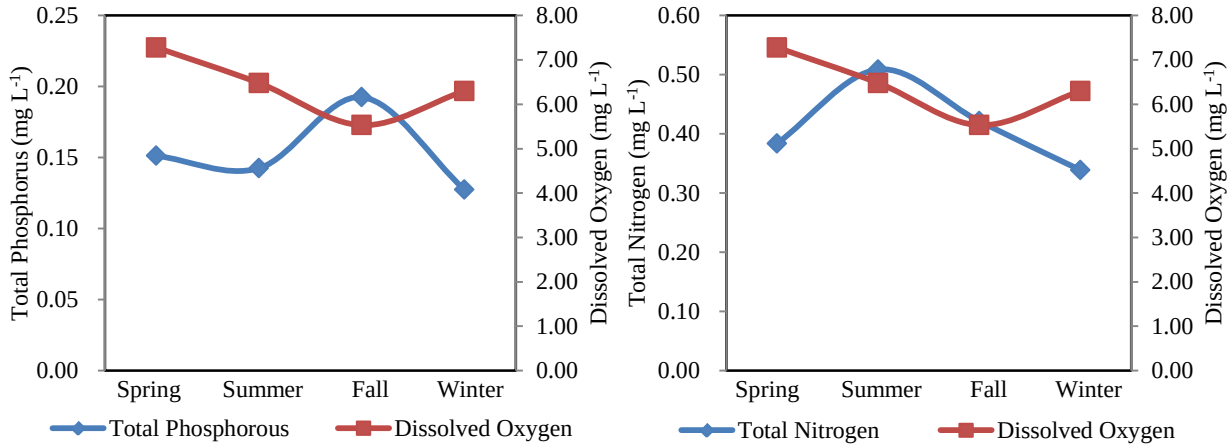

(c) Cluster 4

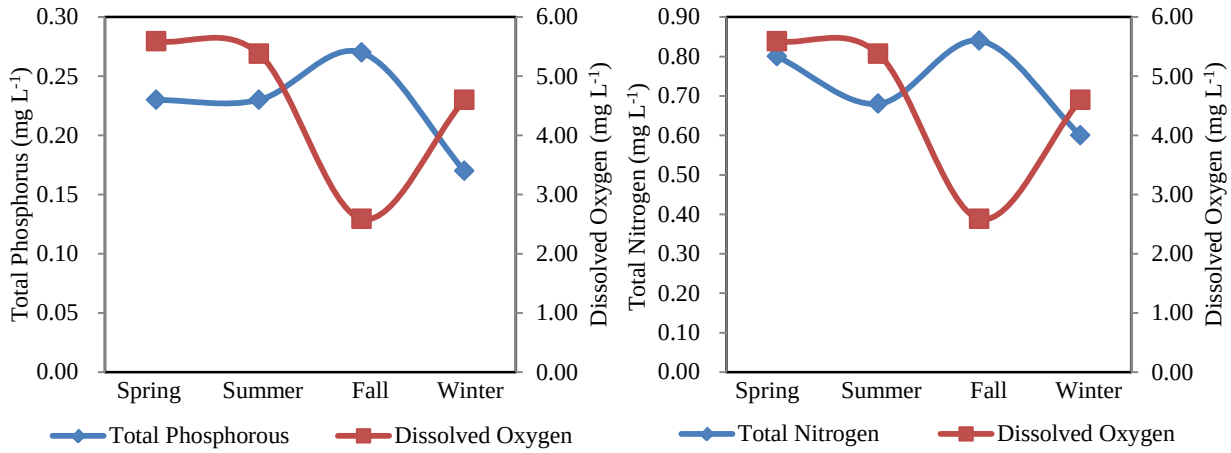

(d) Cluster 5

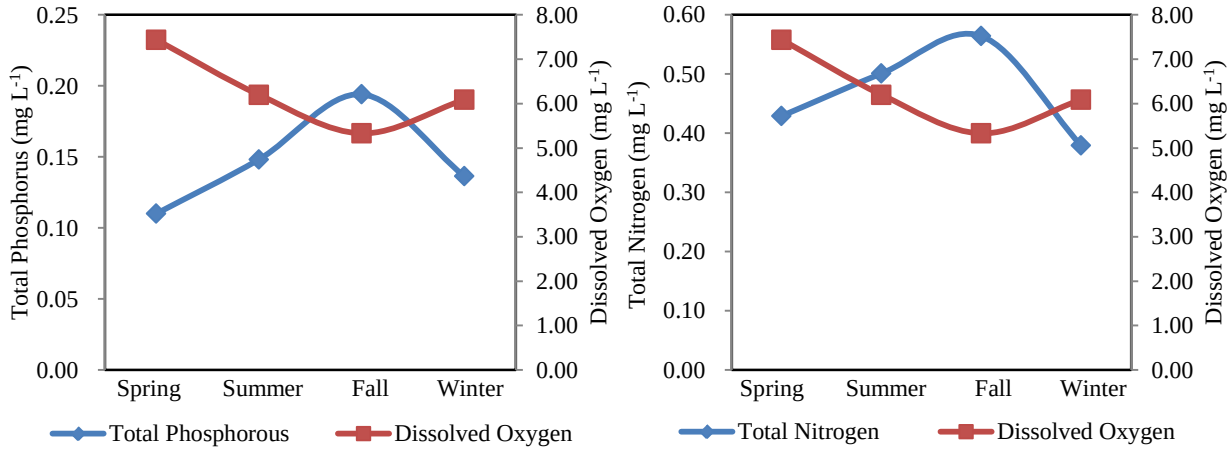

(e) Cluster 6

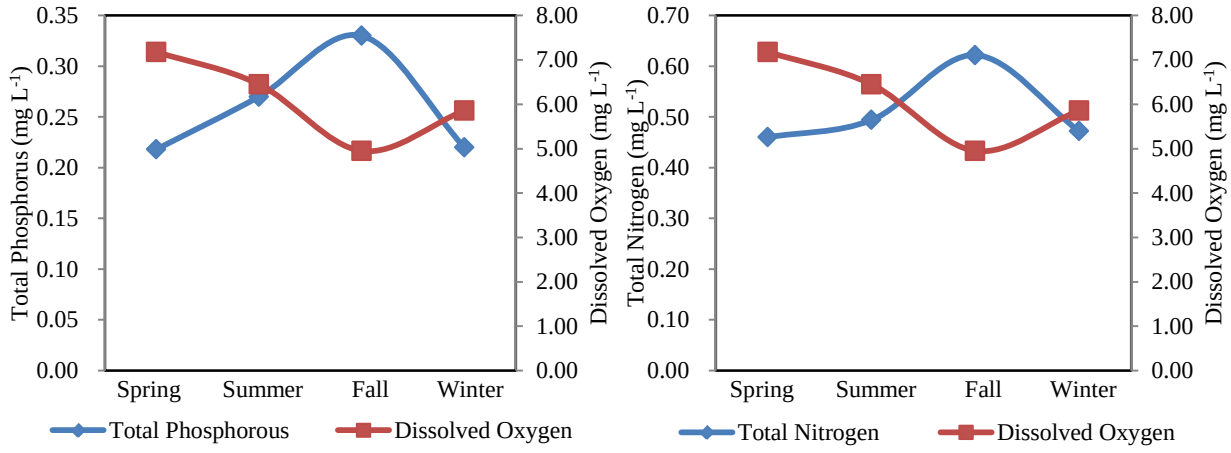

(f) Cluster 8

Figure 3.8 Seasonal plots of nutrient and dissolved oxygen concentration: (a) Cluster 1, (b) Cluster 3, (c) Cluster 4, (d) Cluster 5, (e) Cluster 6, (f) Cluster 8.

3.3.4. Verification and validation of IKCGM

The cluster quality and standard deviation of parameters within each cluster of the k-means clustering analysis for the calibration study in Tampa Bay in 2008 were determined (Table 3.2). Following the same context of the IKCGM algorithm, the results obtained for 2005 in verification and 2007 in validation displayed the same partition strategies of clusters with similar cluster quality and minimal standard deviation between sample parameters within each cluster. It would be beneficial to summarize the calibration (for 2008), verification (for 2005), and validation (for 2007) of the gravity model as a whole. The comparative evaluation was conducted based on four statistical indices including the square of the Pearson product moment correlation coefficient, ratio of standard deviation of predicted to observed values, mean of percent error (PE), and root mean square error (RMSE) of predicted production of TP and TN and actual production of the nutrients for each of the rivers (Table 3.9). The predicted production of TN and TP were compared against the actual production of the TN and TP for each of the

major rivers across selected years for verification and validation (Figure 3.9). The performance of the IKCGM displays a general good agreement primarily related to satisfying the convergence of the predicted production values of TN and TP and the actual production of TN and TP values from each river, confirming that the well-calibrated gravity model for 2008 does perform well continuously in verification for 2005 and in validation for 2007.

Table 3.9 Statistical assessments of the gravity model for TN and TP mass loading value in tonnes for each season.

Total Phosphorus									
	Alafia River			Hillsborough River			Little Manatee River		
Index	Validation		Calibration	Validation		Calibration	Validation		Calibration
	2005	2007	2008	2005	2007	2008	2005	2007	2008
RSQ	0.991	0.911	0.973	0.994	0.949	0.999	0.998	0.998	0.999
RMSE	1.470	1.682	1.824	1.708	0.459	0.558	2.370	1.092	1.014
CO	1.143	0.932	0.998	1.098	1.019	0.994	1.394	1.293	0.997
PE	-1.040	-0.529	-0.044	-0.089	-0.831	-1.036	-0.024	-0.071	-0.177

Total Nitrogen									
	Alafia River			Hillsborough River			Little Manatee River		
Index	Validation		Calibration	Validation		Calibration	Validation		Calibration
	2005	2007	2008	2005	2007	2008	2005	2007	2008
RSQ	0.987	0.982	0.993	0.985	0.994	0.999	0.999	0.992	0.998
RMSE	2.537	1.921	2.511	1.980	0.769	0.850	3.125	1.509	1.685
CO	1.088	0.932	1.001	1.053	0.956	1.001	1.328	0.917	1.001
PE	-0.467	-0.463	-0.538	-0.111	-0.732	-0.049	-0.008	-0.030	0.001

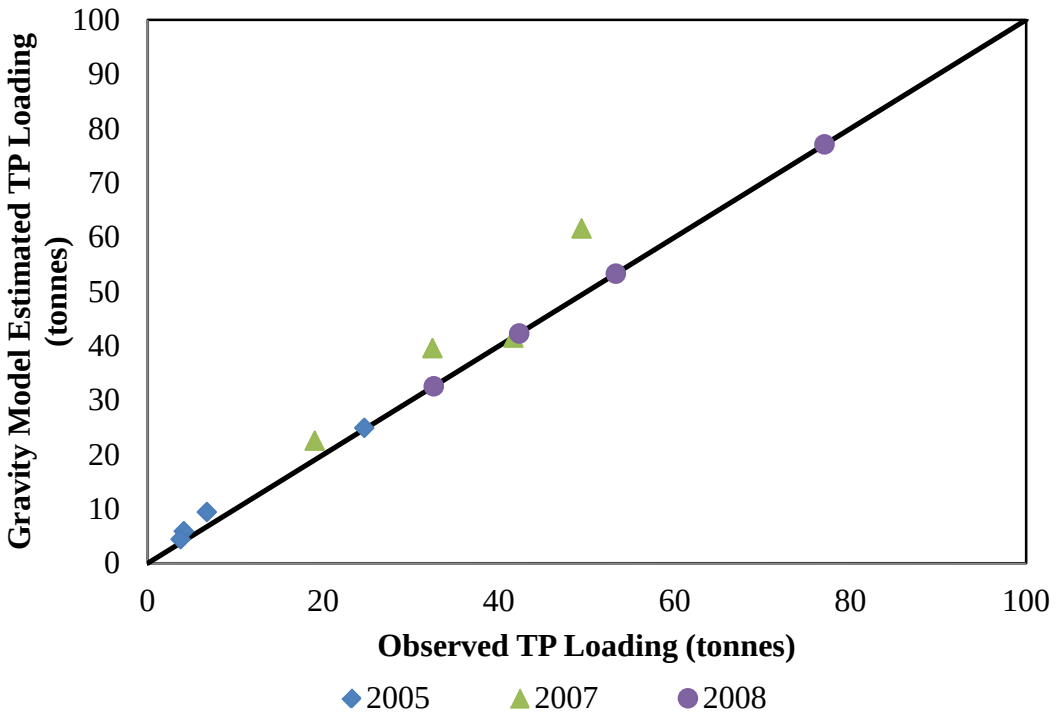

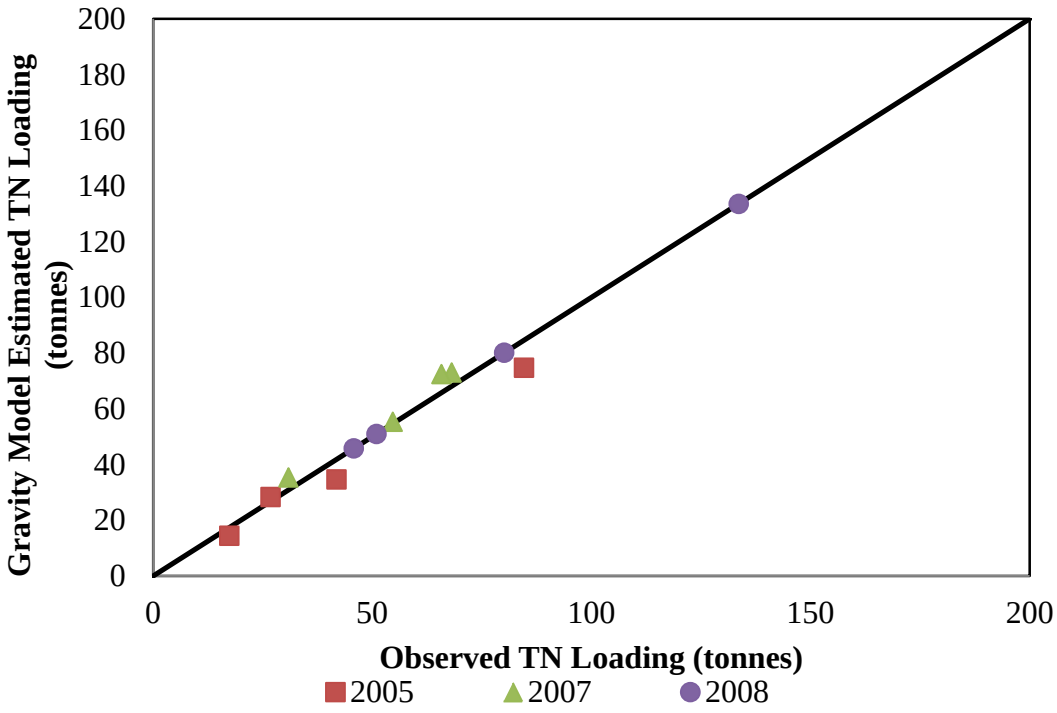

(a) Alafia River

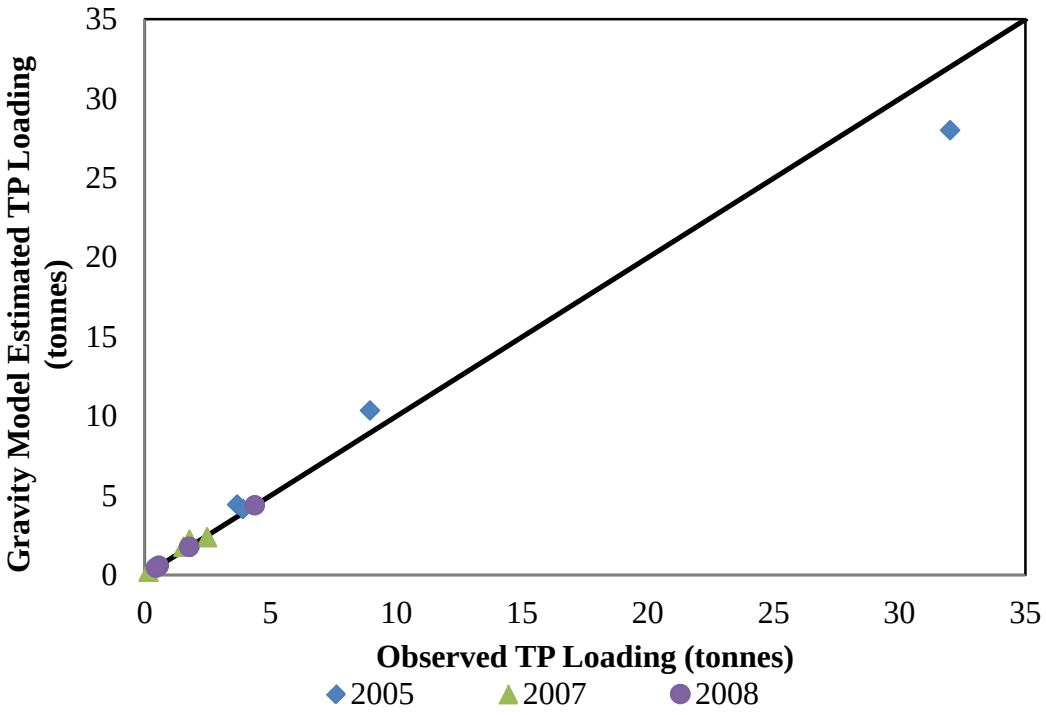

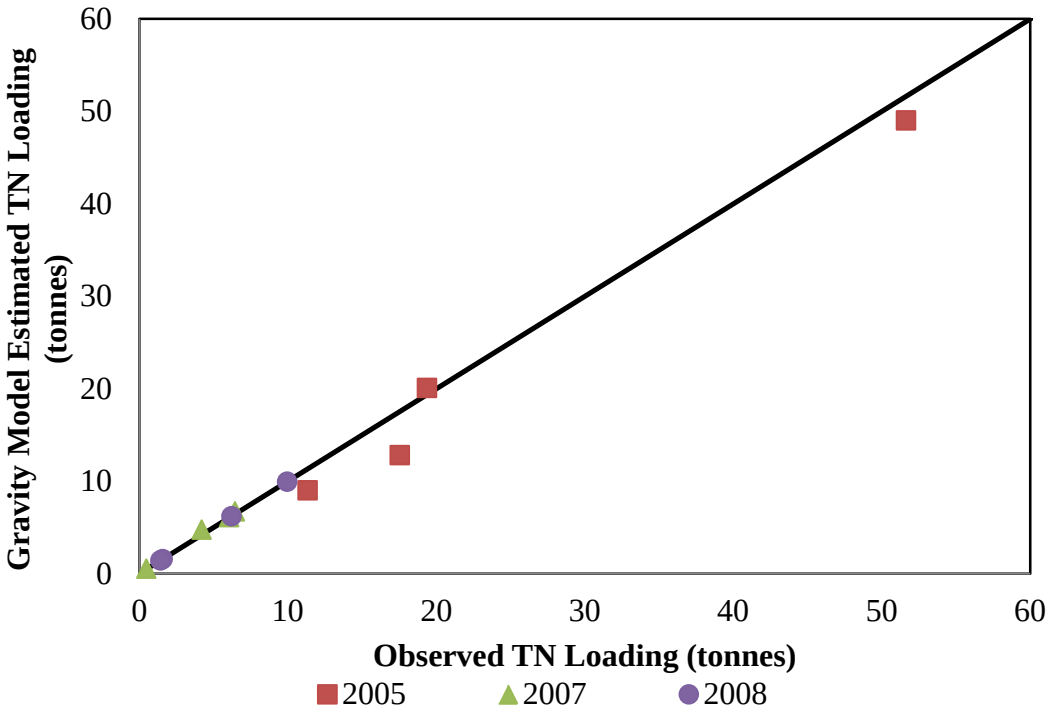

(b) Hillsborough River

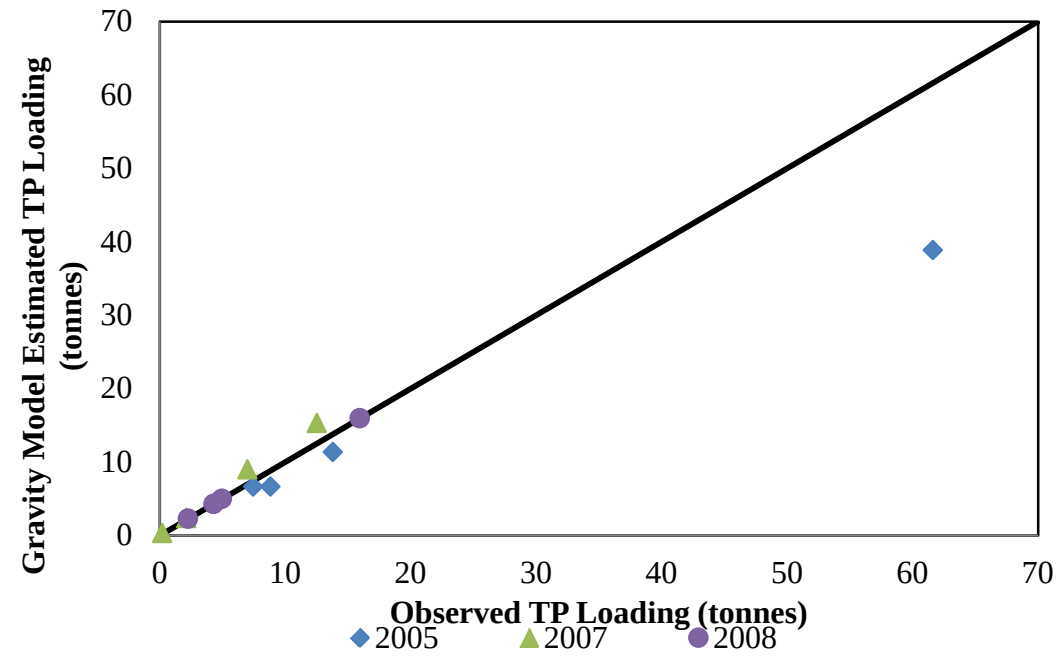

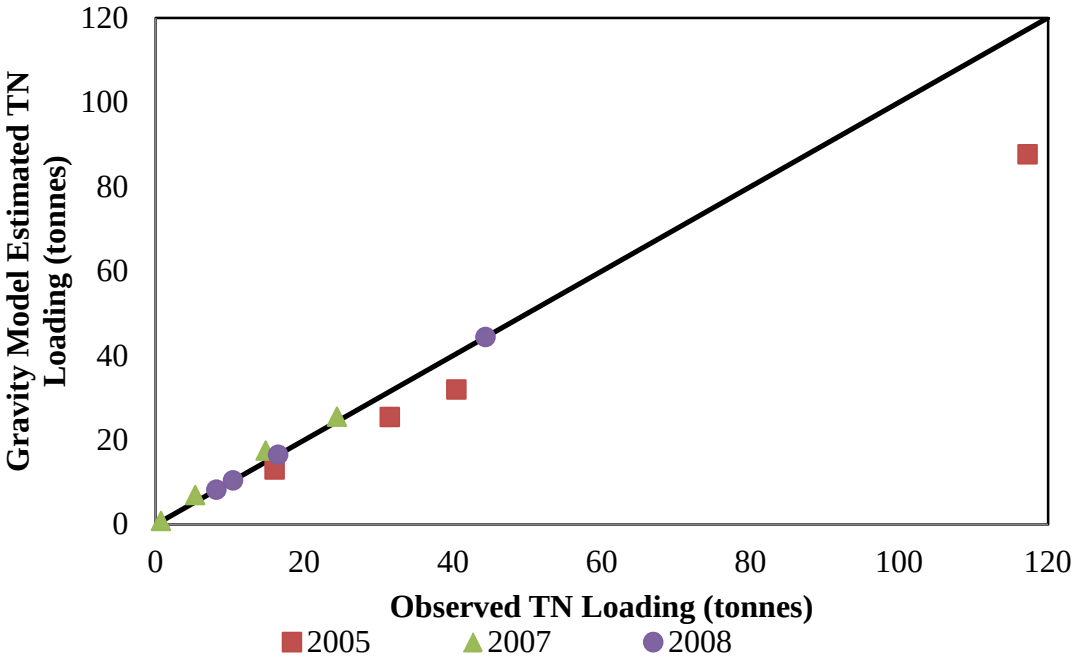

(c) Little Manatee River

Figure 3.9 Gravity model correlation between estimated production values of Total Nitrogen and Total Phosphorus and the actual production nutrient values: (a) Alafia River, (b) Hillsborough River, and (c) Little Manatee River. The Line is the 1:1 linear trend.

Overall assessment of the IKCGM algorithm reveals lower RMSE in both verification and validation stages that would indicate no overfitting issue, whereas higher R^2 values in both verification and validation stages confirm a better agreement. Furthermore, this finding also supports that the IKCGM provides accurate estimation over space without losing the temporal pattern. Yet, a decrease in the performance of the IKCGM was noticed for 2005, the year selected as a period of high variation in water quality and discharge characteristics in the bay as a result of high volumes of runoff. In any circumstance, these efforts show the ability of the IKCGM to accurately quantify the impacts of watershed nutrient input on a coastal bay with a set of spatiotemporal distributions of water quality based on a user-specified number of subsets composed of related objects in clusters. Such a technical setting leads to improved monitoring and evaluation for coastal water quality management and ecosystem restoration to be established via controlling terrestrial nutrient contribution.

CHAPTER 4: CONCLUSIONS

4.1. Spatiotemporal Variability of Ecohydrological Patterns in the Tampa Bay Watershed, Florida under the Impacts of Hurricanes and Droughts

In this study the different facets of potential spatiotemporal variability and polarization of ecohydrological patterns and the impact of land use land cover in the Tampa Bay Watershed, Florida under major climatic events, in particular, hurricanes and droughts was thoroughly investigated. The methodology presented in this study can be applied in any geographical region and its primary limitations are related to data availability. Based on the ecohydrological parameters explored comprised of ET data, precipitation data provided by NEXRAD, NDVI and LST, data provided by remote sensing products derived from the MODIS images this study carried out a spatiotemporal analysis via the use of a GIS platform. This unique ecohydrological analysis based on remote sensing shows that the culminating effect among influential factors, namely extreme climatic events, LULC and associated UHI effect, on ecohydrological parameters is phenomenal.

The similarities in trends, patterns, and variations in the ecohydrologic variables at select locations imply that the trends in ecohydrologic variables are highly linked to the interactions between LULC and extreme climatic events. Spatial and temporal variations were noted in the occurrence and the direction of trends implying trends that might arise as a result of extreme climatic events. There were several ecohydrologic variables in which were noted to have predominantly strong associations. During October 2005 hurricane event, a drop in the LST value was observed while in 2007 and 2008 there is generally a crest in LST temporal trend in

which suggests that during a hurricane event there is a general decrease in LST. This phenomenon could possibly be a result of an increase in precipitation across a large portion of the watershed area. NDVI shows a flat receding tail for the September crest in 2005 while the years of 2007 and 2008 demonstrated an exponential drop after a crest in the curve signifying that the hurricane event in October dampened the severity of the winter dry season in which alludes to relative system memory. An interesting abnormality occurred during the 2008 transition year between dry and wet seasons occurring in the middle of the year. The onset of drought lags the first crest of the ET curve during a year by approximately one month every year of drought. During the transition, ET appears to start to shift back into the analogous temporal pattern as the 2005 wet year. A similar behavior as the ET curve was also observed for precipitation where the maximum crest in the precipitation curve is lagged between 2005 and 2007 by approximately two months and then demonstrates a sudden swift transition back to the similar temporal pattern as a typical wet year in 2008. These fascinating irregularities display some of the key ecohydrological implications of an extreme drought event.

An association between high variations in rainfall and LST; where high variations in rainfall exists, there also exists high variations in LST was observed and after inspection of the spatial distribution for the LST CoV revealed that significant variation is found in areas where the LULC classification is considered to be “developed” areas of varying intensity. This continuous trend on a long-term basis may partially support the influence of urban heat island effect in respect to the possible reason causing the variations in vegetation cover and precipitation in which reflects UVI’s direct influence on the variations in the coastal region to a significant extent. During the drought year, comparing LST, NDVI, and precipitation shows that

they all have a similar spatial pattern. During 2007 and 2008, higher variations in precipitation were observed in areas considered to possess "developed" feature in LULC classification with varying intensities, in particular, 2007; this observation suggests that drought events may in fact increase rainfall events in urbanized regions compared to years considered to be wet years.

By employing the Moran's I coefficient we attempted to capture the autocorrelation aspect of spatial patterns. The four ecohydrologic parameters are classified as having highly focused fields: both indices are highly positive in which imply highly focused spatial patterns. This finding indicates that the echydrological spatial patterns for the parameters explored in this study are exceedingly positively autocorrelated in this coastal region. Therefore, the high z-score values indicate that the null hypothesis, "there exists no spatial clustering," can be rejected.

The results indicate that the temporal patterns in certain variables have not been uniform and that the ecohydrologic variables may accentuate trends and patterns that exist in the external variables that act as inputs to the variations in the hydrologic, ecologic, and thermal cycles. At present, it is not appropriate to state that the observed trends have occurred as a direct result of climatic change. Rather, the LUCC may possibly play some of the pivotal role to some extent.

4.2. Identification of Spatiotemporal Nutrient Patterns in a Coastal Bay *via* an Integrated K-means and Gravity Model

Several types of k-mean clustering practices were carried out in this study to partition a set of data into a user-specified number of subsets composed of related objects in clusters. These efforts reveal spatiotemporal patterns of water quality in Tampa Bay, Florida. Note that the selection of variables in the model are based on the linkage of the major characteristics of a river

basin and the sample points in the bay with respect to the importance of the parameter for water quality evaluation. The exclusion of variables does not mean that those parameters are not important to monitoring and evaluation of water quality, but that the data may be present in other considered parameters; we used variables that were independent from one another to avoid overlap of input data, although interdependencies possibly exist.

The optimal number of clusters in the modeling analysis was screened and selected based on the criteria of cluster quality (i.e., silhouette of cohesion and separation), minimal standard deviation between sample parameters within each cluster, and the model with the minimal clusters containing less than three sample points collectively. Based on these three criteria, the model with 8 clusters was selected. The 8-cluster model and the 12-cluster model produced the maximum silhouette of cohesion and separation value of 0.418, resulting in the removal of the models with 6 and 10 defined clusters. The exclusion of the model with 12 clusters was based on the last criterion, which reveals the model was inefficient because it contained two clusters with less than three sample points compared to the model with 8 clusters, which produced only one similar case.

In addition, it is imperative to note that the gravity model results represent an estimate of the impacts of the nutrient input transported from the major watershed input locations on the clusters partitioned throughout Tampa Bay. The interface between the k-mean clustering analysis and the gravity model has been smoothed out in our IKCGM algorithm in which the application potential has been holistically confirmed in this study. The results of the application provided by the Tampa Bay case study were conducted to show satisfactory agreement in terms of statistical indexes. Through this refined classification system, the bay can be partitioned into zones based

on water quality associated with some localize concerns for high or limited nutrient levels as they change during the course of a year. This analysis of IKCGM may be used to finally realize the impacts of watershed nutrient input on a coastal bay with a set of spatiotemporal distributions of water quality based on a user-specified number of subsets composed of related objects in clusters.

The methodology presented in this study can be applied in any geographical coastal region, and its main limitations are related to data availability. This IKCGM may further improve monitoring and evaluation methods for water quality management and coastal ecosystem restoration to be established via controlling terrestrial nutrient contribution. Nevertheless, the integrated approach should be continuously fed with new data every year to better update the changing spatiotemporal patterns and reflect the unpredictable dynamics of natural and anthropogenic stressors present across these intimately linked sea-land interactions.

4.2. Future Work

This two part study has eventually enabled the knowledge discovery of the spatiotemporal patterns of ecohydrologic parameters to capture the inherent linkages of hydrodynamic and ecological features to advance our understanding of sea–land interactions of a coastal bay region. Future work will encompass the issue of trend attribution and computational modeling in order to establish a linkage between climatic change and the observed ecohydrologic trends as well as the sea-land interactions linked with LUCC. The ultimate goal will be to utilize the ecohydrological parameters explored in segment one to predict the nutrient loading from the major river basins in segments two via a neural network model.

APPENDIX A: TAMPA BAY WATERSHED ECOHYDROLOGICAL PATTERNS

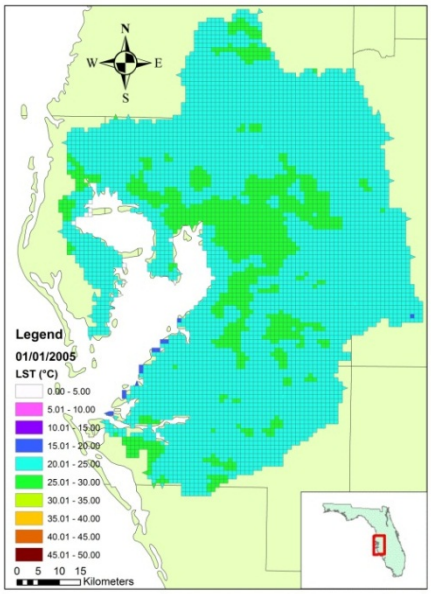
N
W
E
S
Legend
01/01/2005
LST (°C)
0.00 - 5.00
5.01 - 10.00
10.01 - 15.00
15.01 - 20.00
20.01 - 25.00
25.01 - 30.00
30.01 - 35.00
35.01 - 40.00
40.01 - 45.00
45.01 - 50.00
0 5 10 15
Kilometers

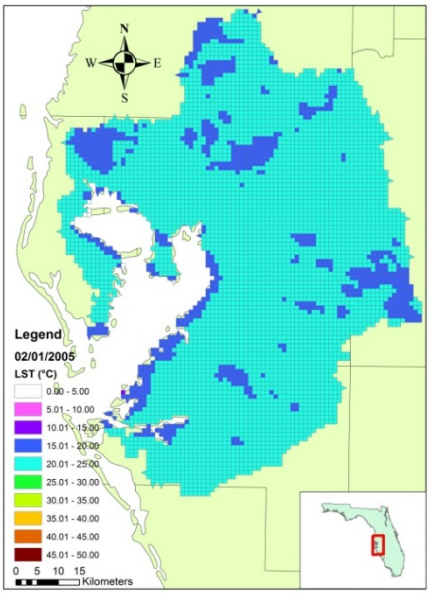
N
W
E
S
Legend
02/01/2005
LST (°C)
0.00 - 5.00
5.01 - 10.00
10.01 - 15.00
15.01 - 20.00
20.01 - 25.00
25.01 - 30.00
30.01 - 35.00
35.01 - 40.00
40.01 - 45.00
45.01 - 50.00
0 5 10 15
Kilometers

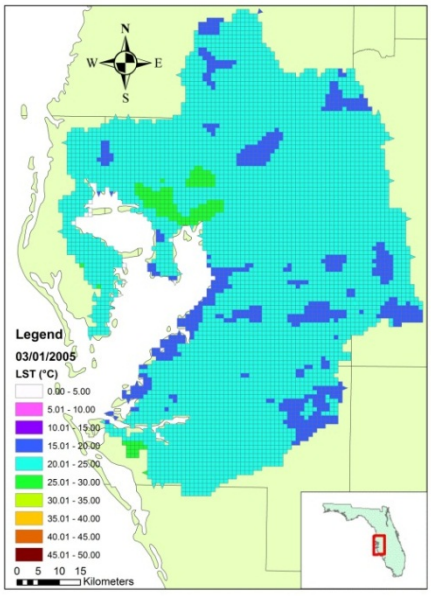
N
W
E
S
Legend
03/01/2005
LST (°C)
0.00 - 5.00
5.01 - 10.00
10.01 - 15.00
15.01 - 20.00
20.01 - 25.00
25.01 - 30.00
30.01 - 35.00
35.01 - 40.00
40.01 - 45.00
45.01 - 50.00
0 5 10 15
Kilometers

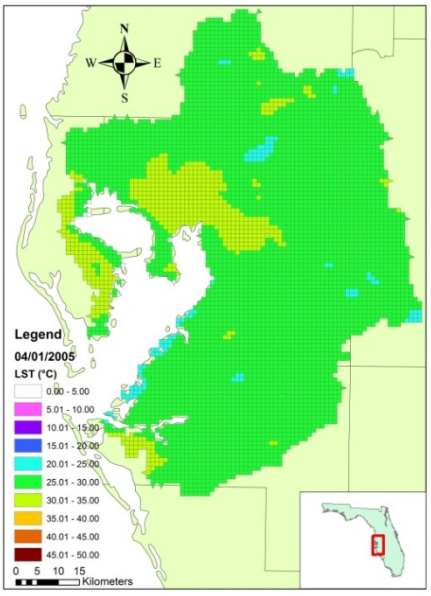
N
W
E
S
Legend
04/01/2005
LST (°C)
0.00 - 5.00
5.01 - 10.00
10.01 - 15.00
15.01 - 20.00
20.01 - 25.00
25.01 - 30.00
30.01 - 35.00
35.01 - 40.00
40.01 - 45.00
45.01 - 50.00
0 5 10 15
Kilometers

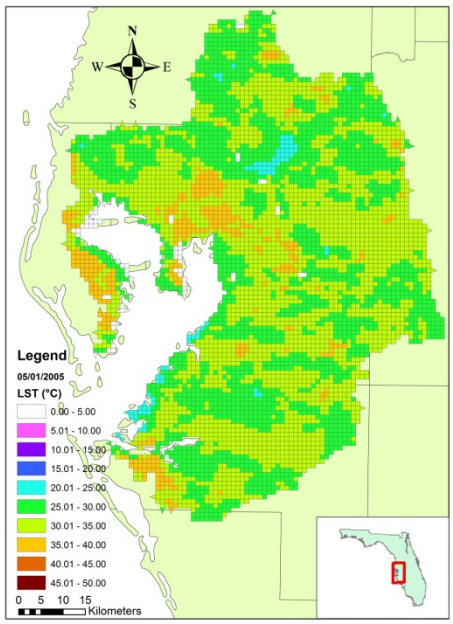
N
W
E
S
Legend
05/01/2005
LST (°C)
0.00 - 5.00
5.01 - 10.00
10.01 - 15.00
15.01 - 20.00
20.01 - 25.00
25.01 - 30.00
30.01 - 35.00
35.01 - 40.00
40.01 - 45.00
45.01 - 50.00
0 5 10 15
Kilometers

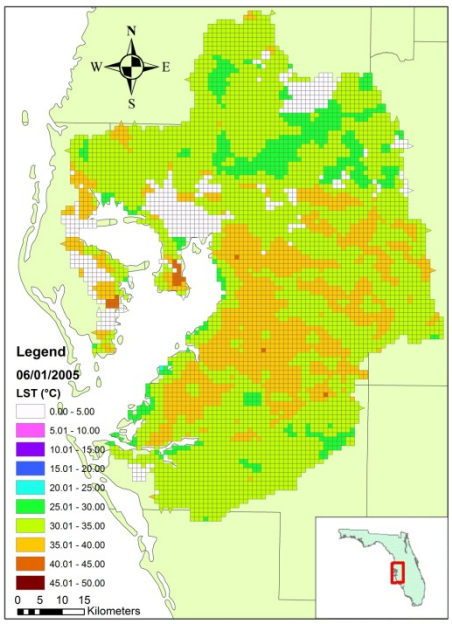
N
W
E
S
Legend
06/01/2005
LST (°C)
0.00 - 5.00
5.01 - 10.00
10.01 - 15.00
15.01 - 20.00
20.01 - 25.00
25.01 - 30.00
30.01 - 35.00
35.01 - 40.00
40.01 - 45.00
45.01 - 50.00
0 5 10 15
Kilometers

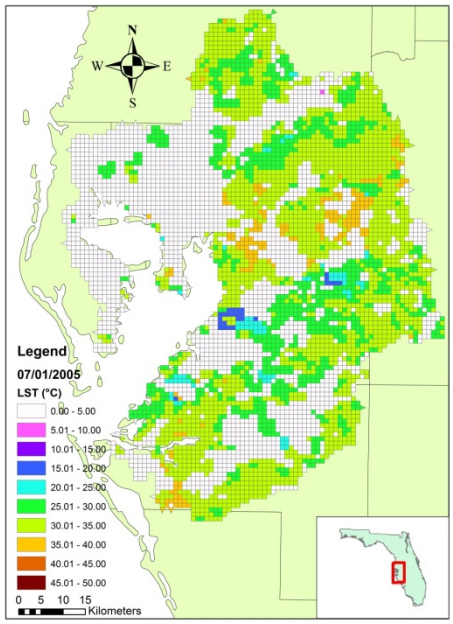
N
W
E
S
Legend
07/01/2005
LST (°C)
0.00 - 5.00
5.01 - 10.00
10.01 - 15.00
15.01 - 20.00
20.01 - 25.00
25.01 - 30.00
30.01 - 35.00
35.01 - 40.00
40.01 - 45.00
45.01 - 50.00
0 5 10 15
Kilometers

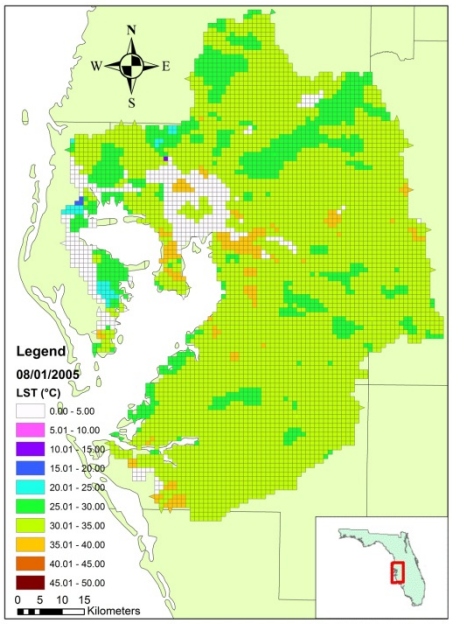
N
W
E
S
Legend
08/01/2005
LST (°C)
0.00 - 5.00
5.01 - 10.00
10.01 - 15.00
15.01 - 20.00
20.01 - 25.00
25.01 - 30.00
30.01 - 35.00
35.01 - 40.00
40.01 - 45.00
45.01 - 50.00
0 5 10 15
Kilometers

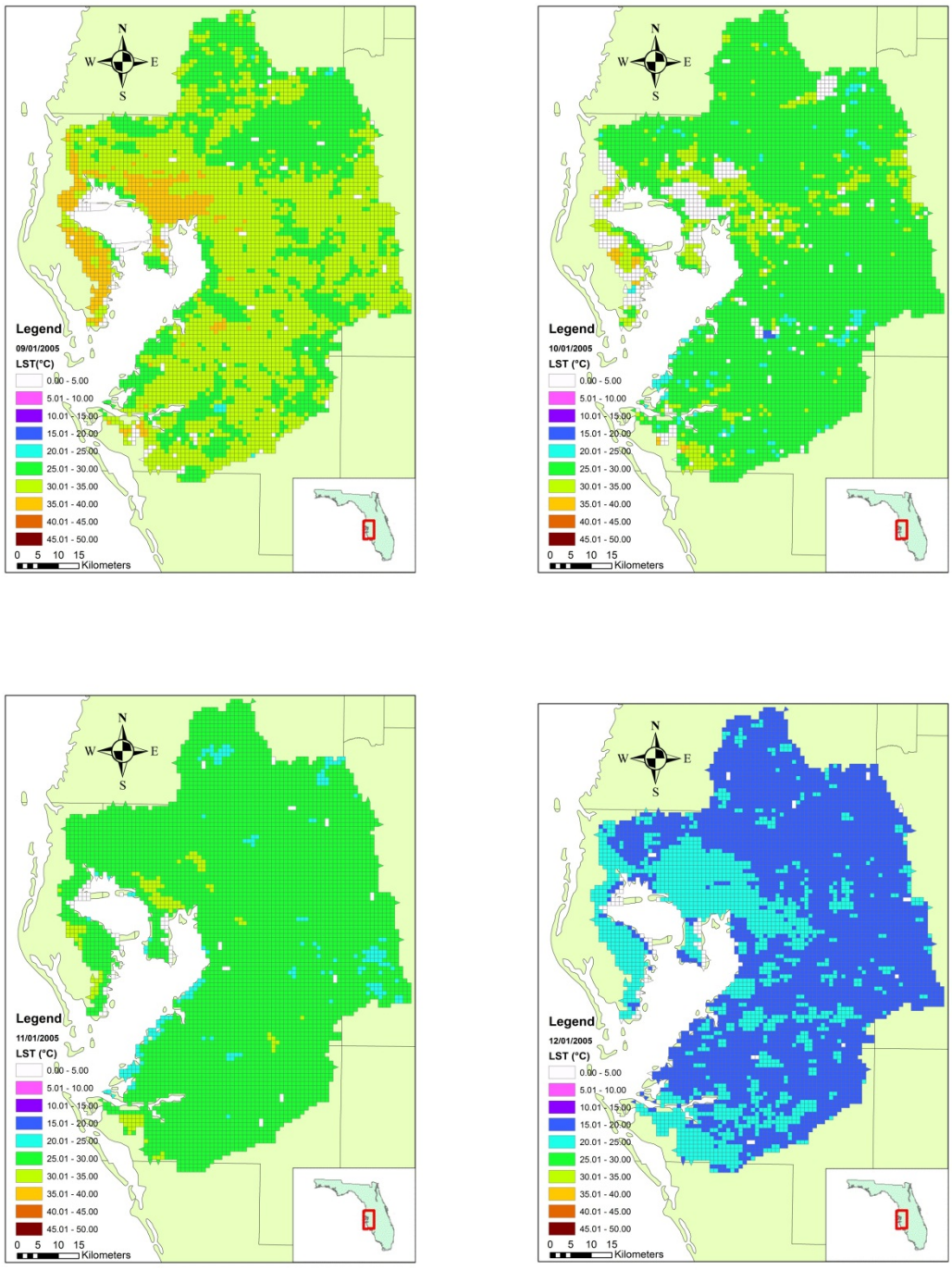

Figure A.1 8-day LST (°C) maps for the Tampa Bay watershed for 2005.

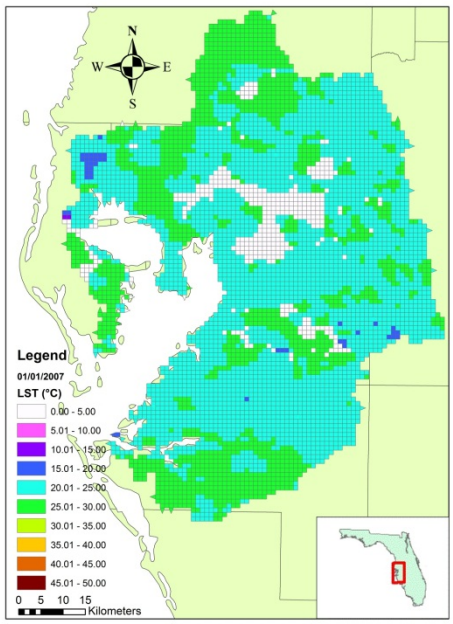
N
W
E
S
Legend
01/01/2007
LST (°C)
0.00 - 5.00
5.01 - 10.00
10.01 - 15.00
15.01 - 20.00
20.01 - 25.00
25.01 - 30.00
30.01 - 35.00
35.01 - 40.00
40.01 - 45.00
45.01 - 50.00
0 5 10 15
Kilometers

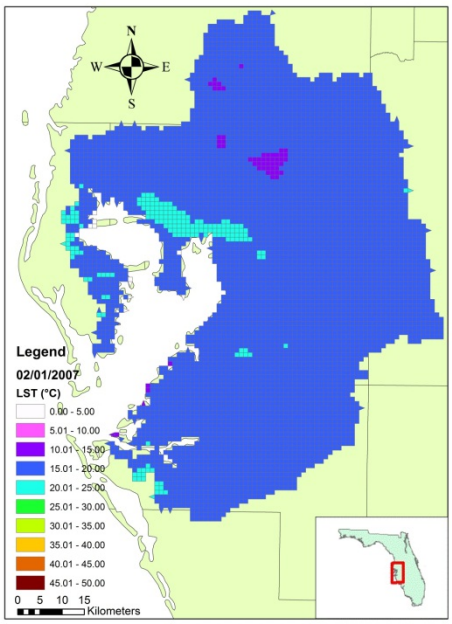
N
W
E
S
Legend
02/01/2007
LST (°C)
0.00 - 5.00
5.01 - 10.00
10.01 - 15.00
15.01 - 20.00
20.01 - 25.00
25.01 - 30.00
30.01 - 35.00
35.01 - 40.00
40.01 - 45.00
45.01 - 50.00
0 5 10 15
Kilometers

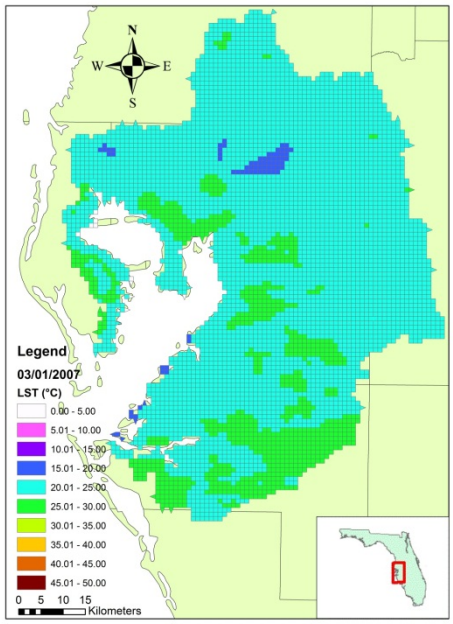
N
W
E
S
Legend
03/01/2007
LST (°C)
0.00 - 5.00
5.01 - 10.00
10.01 - 15.00
15.01 - 20.00
20.01 - 25.00
25.01 - 30.00
30.01 - 35.00
35.01 - 40.00
40.01 - 45.00
45.01 - 50.00
0 5 10 15
Kilometers

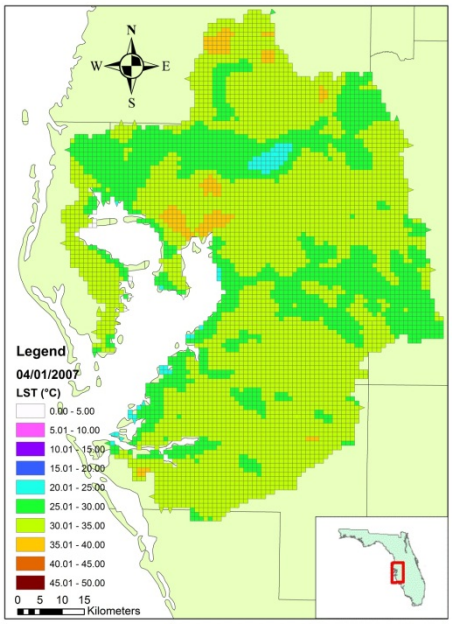
N
W
E
S
Legend
04/01/2007
LST (°C)
0.00 - 5.00
5.01 - 10.00
10.01 - 15.00
15.01 - 20.00
20.01 - 25.00
25.01 - 30.00
30.01 - 35.00
35.01 - 40.00
40.01 - 45.00
45.01 - 50.00
0 5 10 15
Kilometers

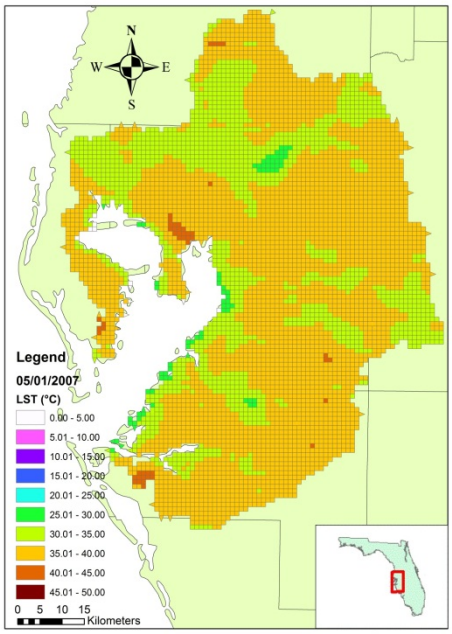
N
W
E
S
Legend
05/01/2007
LST (°C)
0.00 - 5.00
5.01 - 10.00
10.01 - 15.00
15.01 - 20.00
20.01 - 25.00
25.01 - 30.00
30.01 - 35.00
35.01 - 40.00
40.01 - 45.00
45.01 - 50.00
0 5 10 15
Kilometers

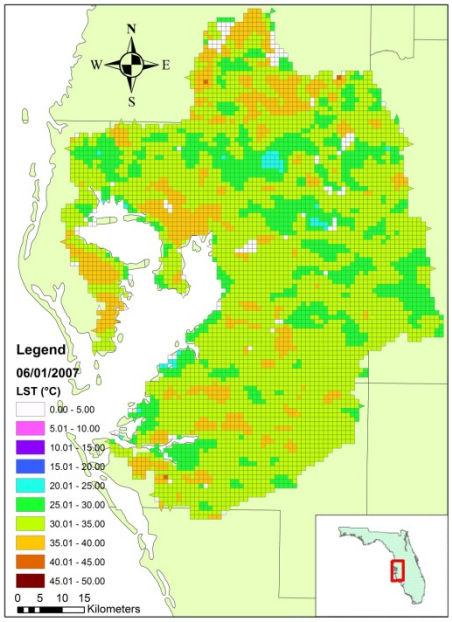
N
W
E
S
Legend
06/01/2007
LST (°C)
0.00 - 5.00
5.01 - 10.00
10.01 - 15.00
15.01 - 20.00
20.01 - 25.00
25.01 - 30.00
30.01 - 35.00
35.01 - 40.00
40.01 - 45.00
45.01 - 50.00
0 5 10 15
Kilometers

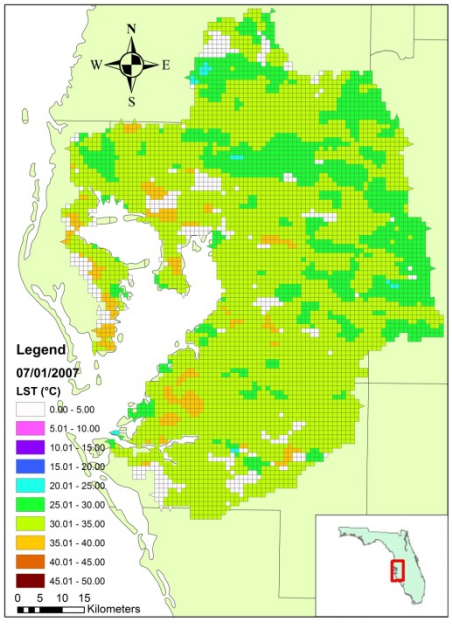
N
W
E
S
Legend
07/01/2007
LST (°C)
0.00 - 5.00
5.01 - 10.00
10.01 - 15.00
15.01 - 20.00
20.01 - 25.00
25.01 - 30.00
30.01 - 35.00
35.01 - 40.00
40.01 - 45.00
45.01 - 50.00
0 5 10 15
Kilometers

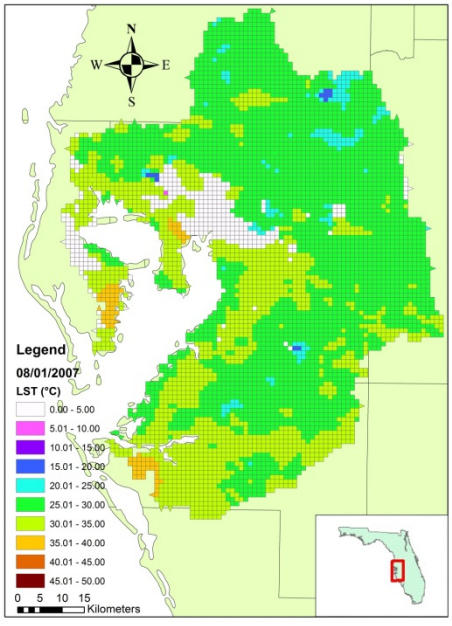
N
W
E
S
Legend
08/01/2007
LST (°C)
0.00 - 5.00
5.01 - 10.00
10.01 - 15.00
15.01 - 20.00
20.01 - 25.00
25.01 - 30.00
30.01 - 35.00
35.01 - 40.00
40.01 - 45.00
45.01 - 50.00
0 5 10 15
Kilometers

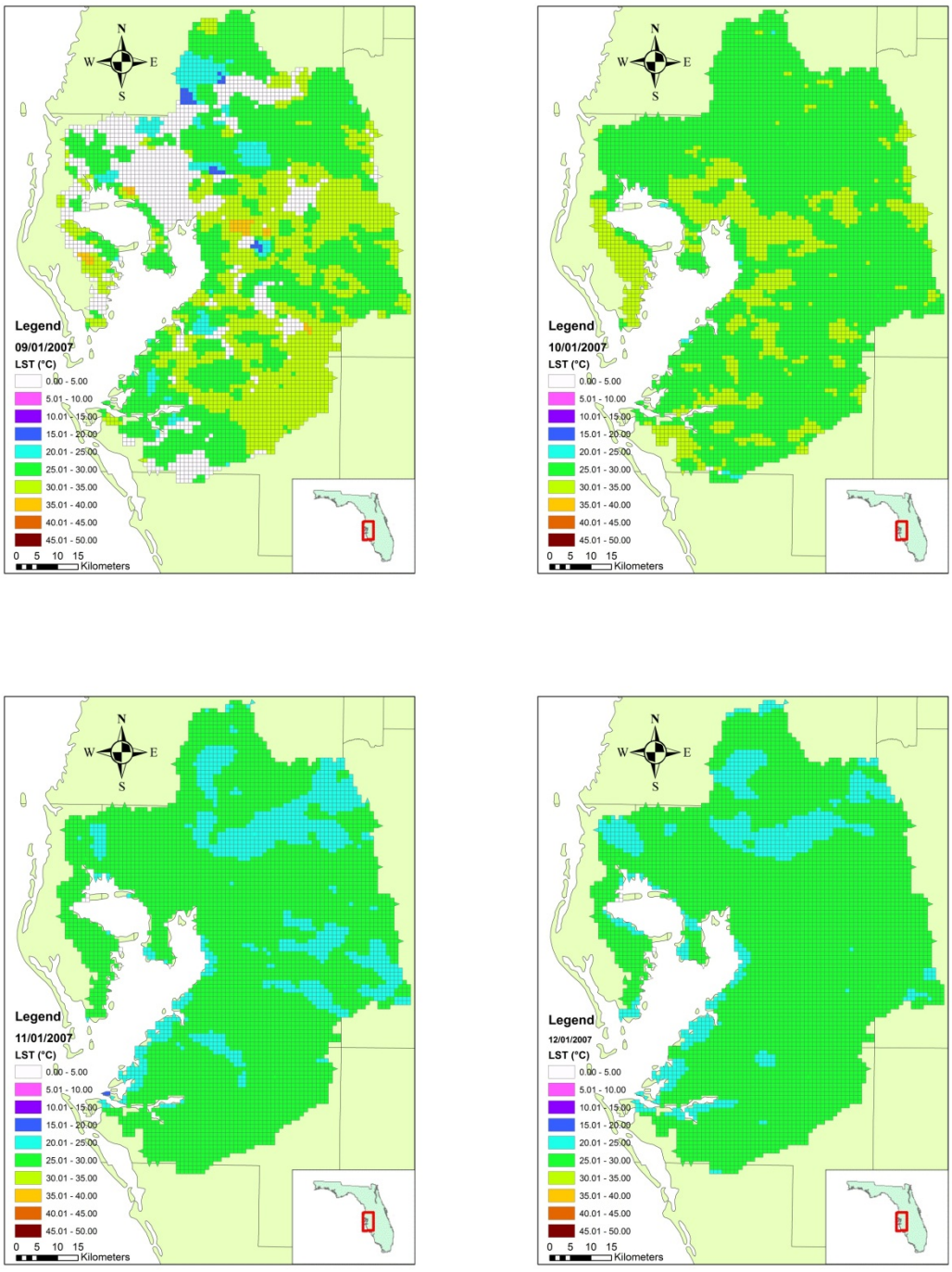

Figure A.2 8-day LST (°C) maps for the Tampa Bay watershed for 2007.

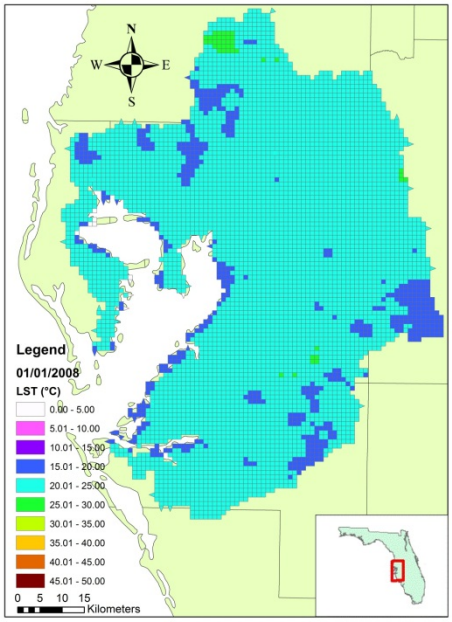
N
W
E
S
Legend
01/01/2008
LST (°C)
0.00 - 5.00
5.01 - 10.00
10.01 - 15.00
15.01 - 20.00
20.01 - 25.00
25.01 - 30.00
30.01 - 35.00
35.01 - 40.00
40.01 - 45.00
45.01 - 50.00
0 5 10 15
Kilometers

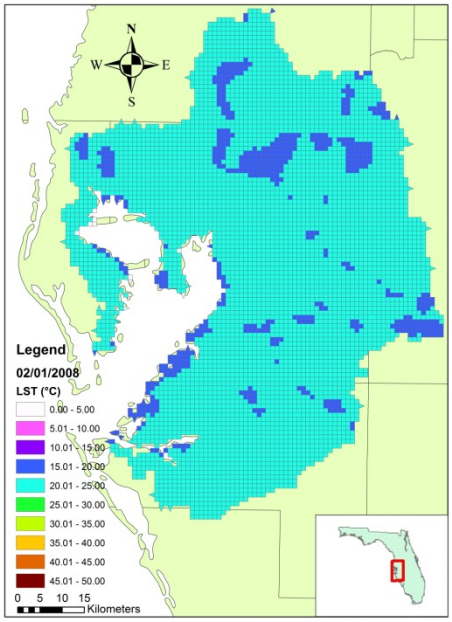
N
W
E
S
Legend
02/01/2008
LST (°C)
0.00 - 5.00
5.01 - 10.00
10.01 - 15.00
15.01 - 20.00
20.01 - 25.00
25.01 - 30.00
30.01 - 35.00
35.01 - 40.00
40.01 - 45.00
45.01 - 50.00
0 5 10 15
Kilometers

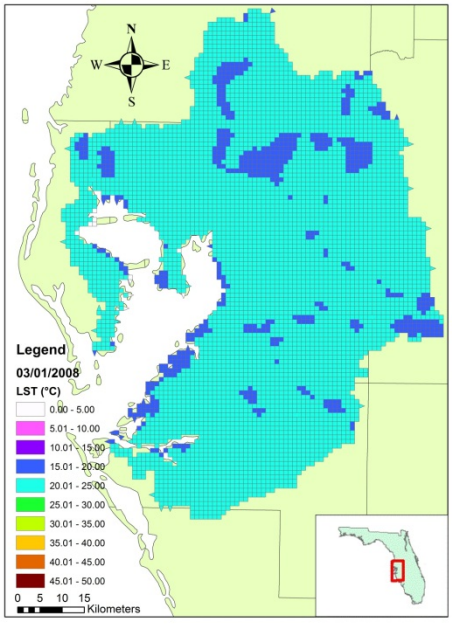
N
W
E
S
Legend
03/01/2008
LST (°C)
0.00 - 5.00
5.01 - 10.00
10.01 - 15.00
15.01 - 20.00
20.01 - 25.00
25.01 - 30.00
30.01 - 35.00
35.01 - 40.00
40.01 - 45.00
45.01 - 50.00
0 5 10 15
Kilometers

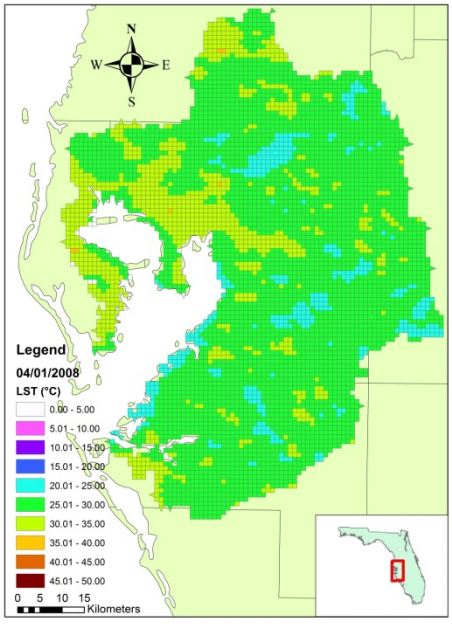
N
W
E
S
Legend
04/01/2008
LST (°C)
0.00 - 5.00
5.01 - 10.00
10.01 - 15.00
15.01 - 20.00
20.01 - 25.00
25.01 - 30.00
30.01 - 35.00
35.01 - 40.00
40.01 - 45.00
45.01 - 50.00
0 5 10 15
Kilometers

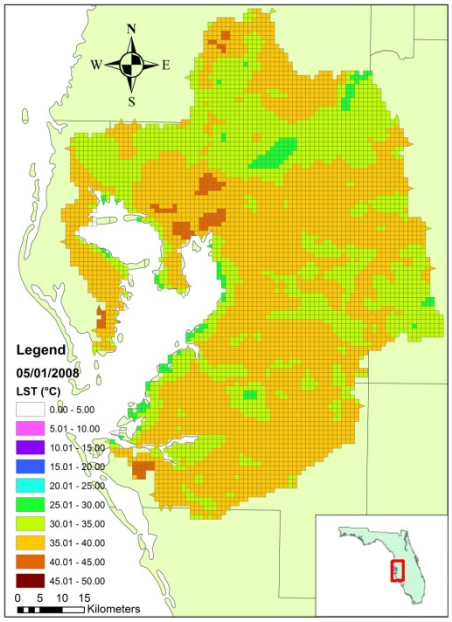
N
W
E
S
Legend
05/01/2008
LST (°C)
0.00 - 5.00
5.01 - 10.00
10.01 - 15.00
15.01 - 20.00
20.01 - 25.00
25.01 - 30.00
30.01 - 35.00
35.01 - 40.00
40.01 - 45.00
45.01 - 50.00
0 5 10 15
Kilometers

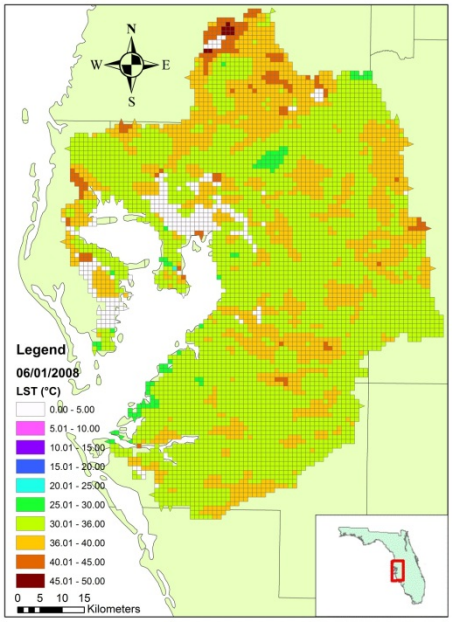
N
W
E
S
Legend
06/01/2008
LST (°C)
0.00 - 5.00
5.01 - 10.00
10.01 - 15.00
15.01 - 20.00
20.01 - 25.00
25.01 - 30.00
30.01 - 36.00
36.01 - 40.00
40.01 - 45.00
45.01 - 50.00
0 5 10 15
Kilometers

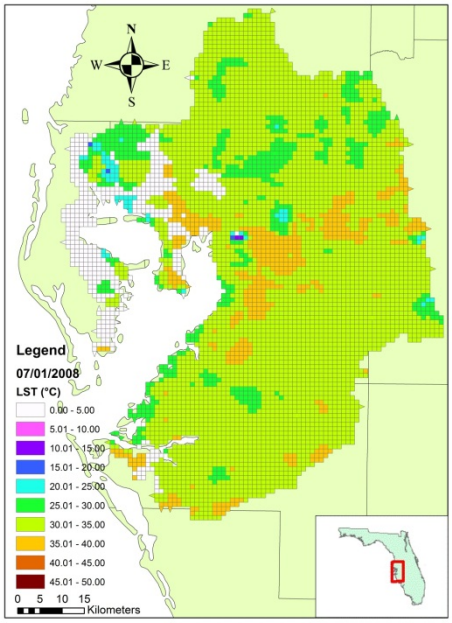
N
W
E
S
Legend
07/01/2008
LST (°C)
0.00 - 5.00
5.01 - 10.00
10.01 - 15.00
15.01 - 20.00
20.01 - 25.00
25.01 - 30.00
30.01 - 35.00
35.01 - 40.00
40.01 - 45.00
45.01 - 50.00
0 5 10 15
Kilometers

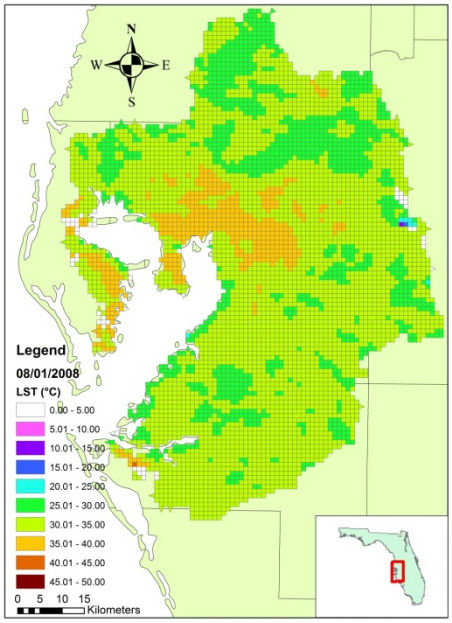
N
W
E
S
Legend
08/01/2008
LST (°C)
0.00 - 5.00
5.01 - 10.00
10.01 - 15.00
15.01 - 20.00
20.01 - 25.00
25.01 - 30.00
30.01 - 35.00
35.01 - 40.00
40.01 - 45.00
45.01 - 50.00
0 5 10 15
Kilometers

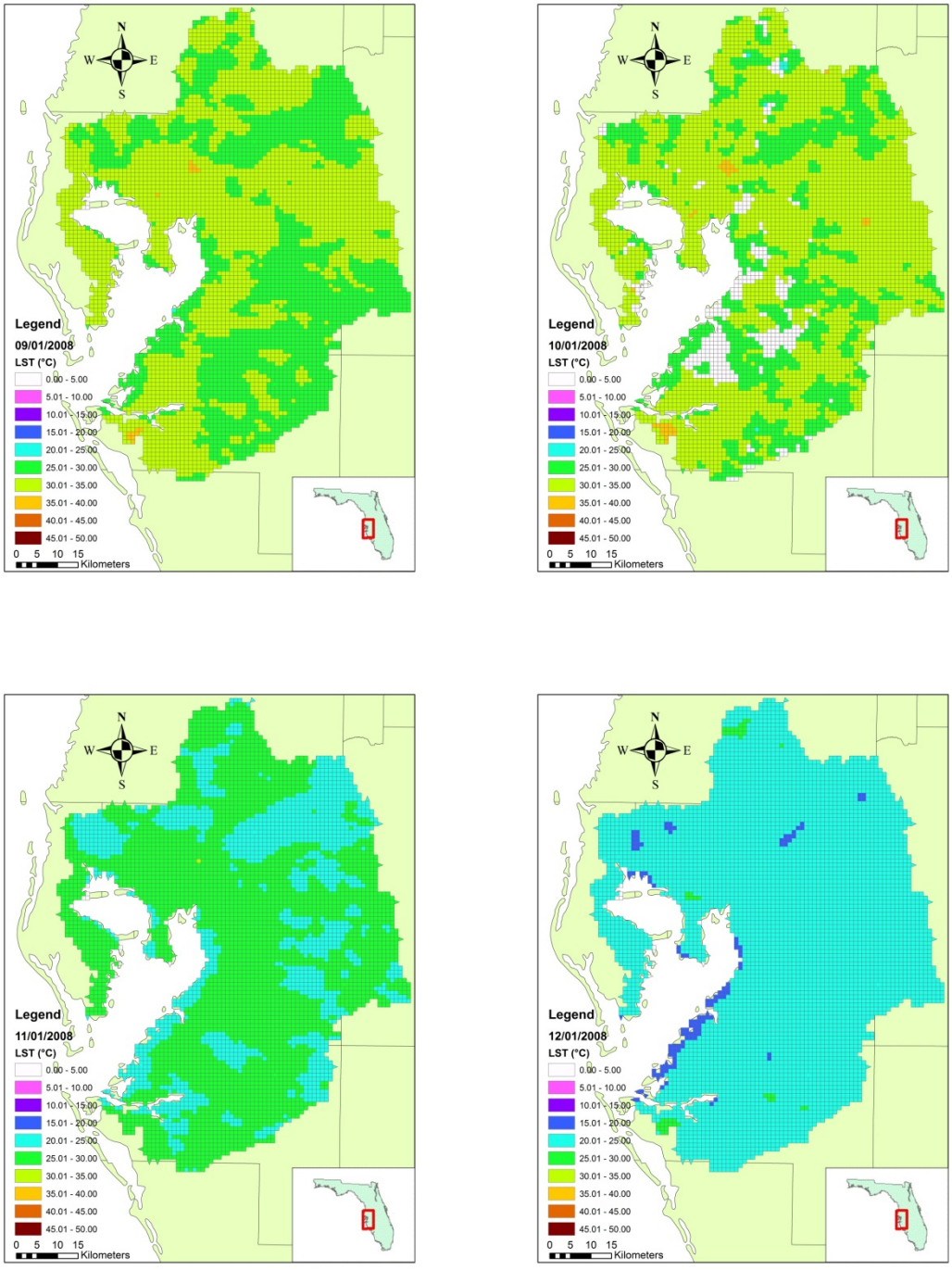

Figure A.3 8-day LST (°C) maps for the Tampa Bay watershed for 2008.

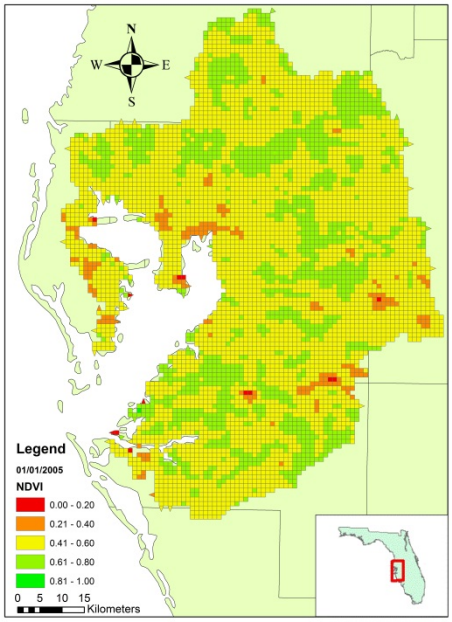
N
W
E
S
Legend
01/01/2005
NDVI
0.00 - 0.20
0.21 - 0.40
0.41 - 0.60
0.61 - 0.80
0.81 - 1.00
0 5 10 15
Kilometers

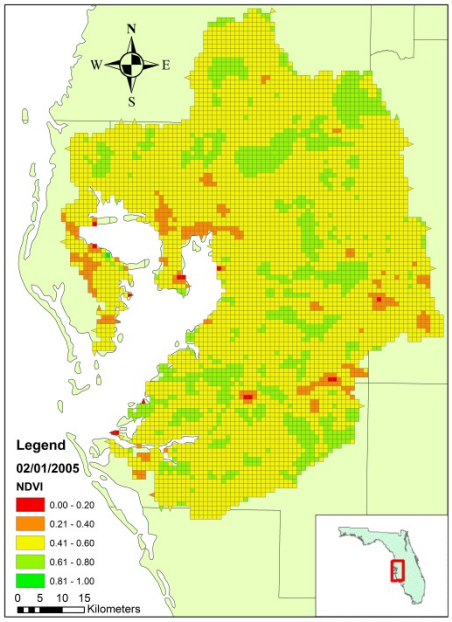
N
W
E
S
Legend
02/01/2005
NDVI
0.00 - 0.20
0.21 - 0.40
0.41 - 0.60
0.61 - 0.80
0.81 - 1.00
0 5 10 15
Kilometers

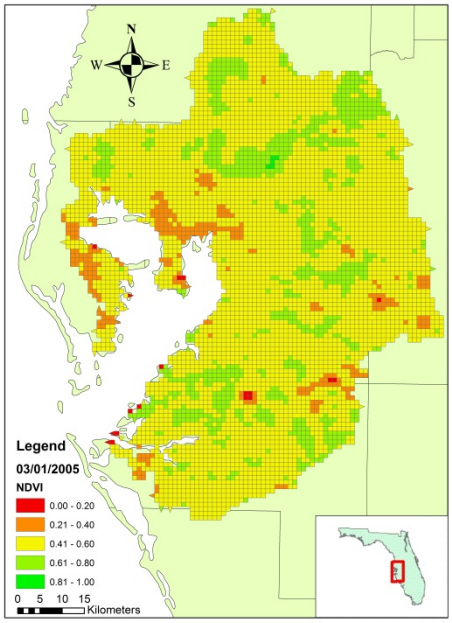
N
W
E
S
Legend
03/01/2005
NDVI
0.00 - 0.20
0.21 - 0.40
0.41 - 0.60
0.61 - 0.80
0.81 - 1.00
0 5 10 15
Kilometers

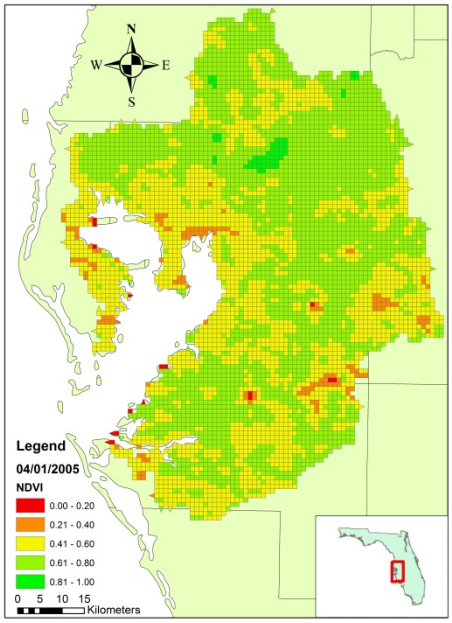
N
W
E
S
Legend
04/01/2005
NDVI
0.00 - 0.20
0.21 - 0.40
0.41 - 0.60
0.61 - 0.80
0.81 - 1.00
0 5 10 15
Kilometers

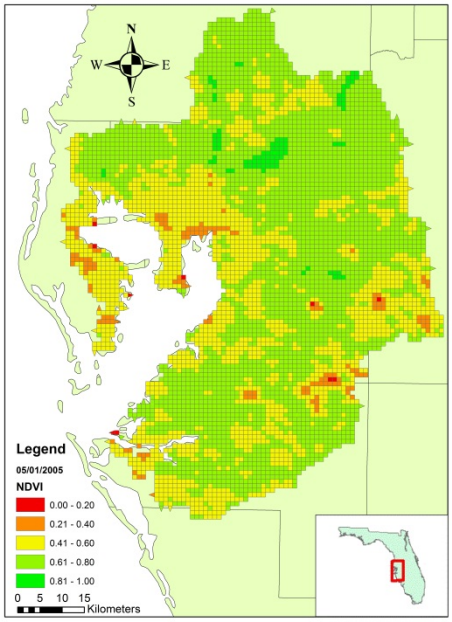
N
W
E
S
Legend
05/01/2005
NDVI
0.00 - 0.20
0.21 - 0.40
0.41 - 0.60
0.61 - 0.80
0.81 - 1.00
0 5 10 15
Kilometers

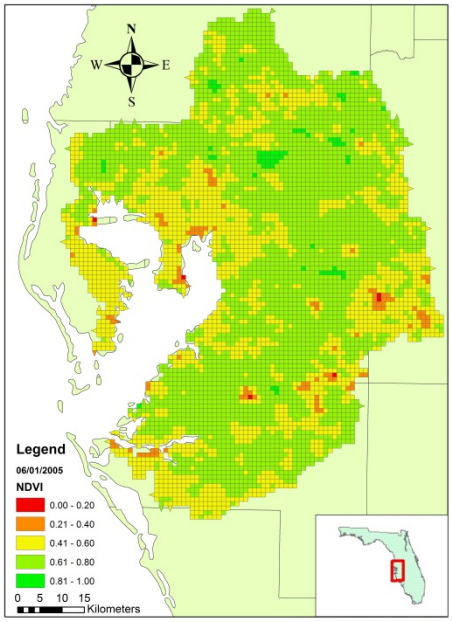
N
W
E
S
Legend
06/01/2005
NDVI
0.00 - 0.20
0.21 - 0.40
0.41 - 0.60
0.61 - 0.80
0.81 - 1.00
0 5 10 15
Kilometers

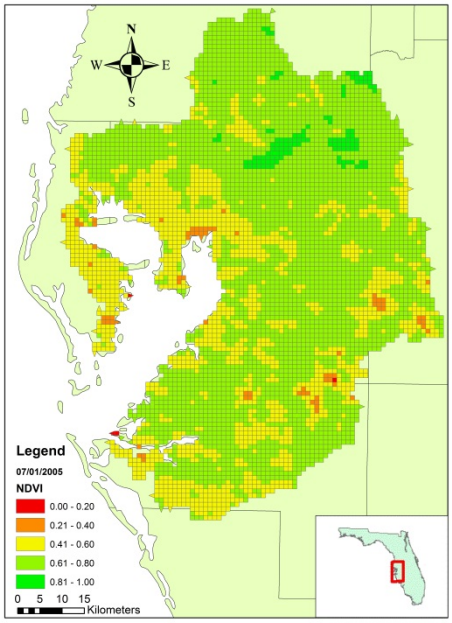
N
W
E
S
Legend
07/01/2005
NDVI
0.00 - 0.20
0.21 - 0.40
0.41 - 0.60
0.61 - 0.80
0.81 - 1.00
0 5 10 15
Kilometers

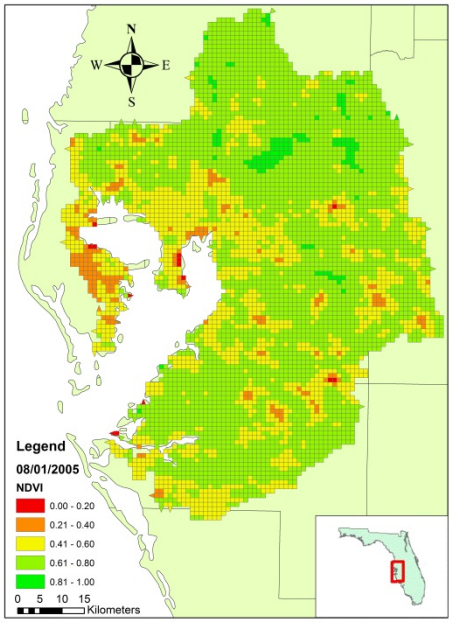
N
W
E
S
Legend
08/01/2005
NDVI
0.00 - 0.20
0.21 - 0.40
0.41 - 0.60
0.61 - 0.80
0.81 - 1.00
0 5 10 15
Kilometers

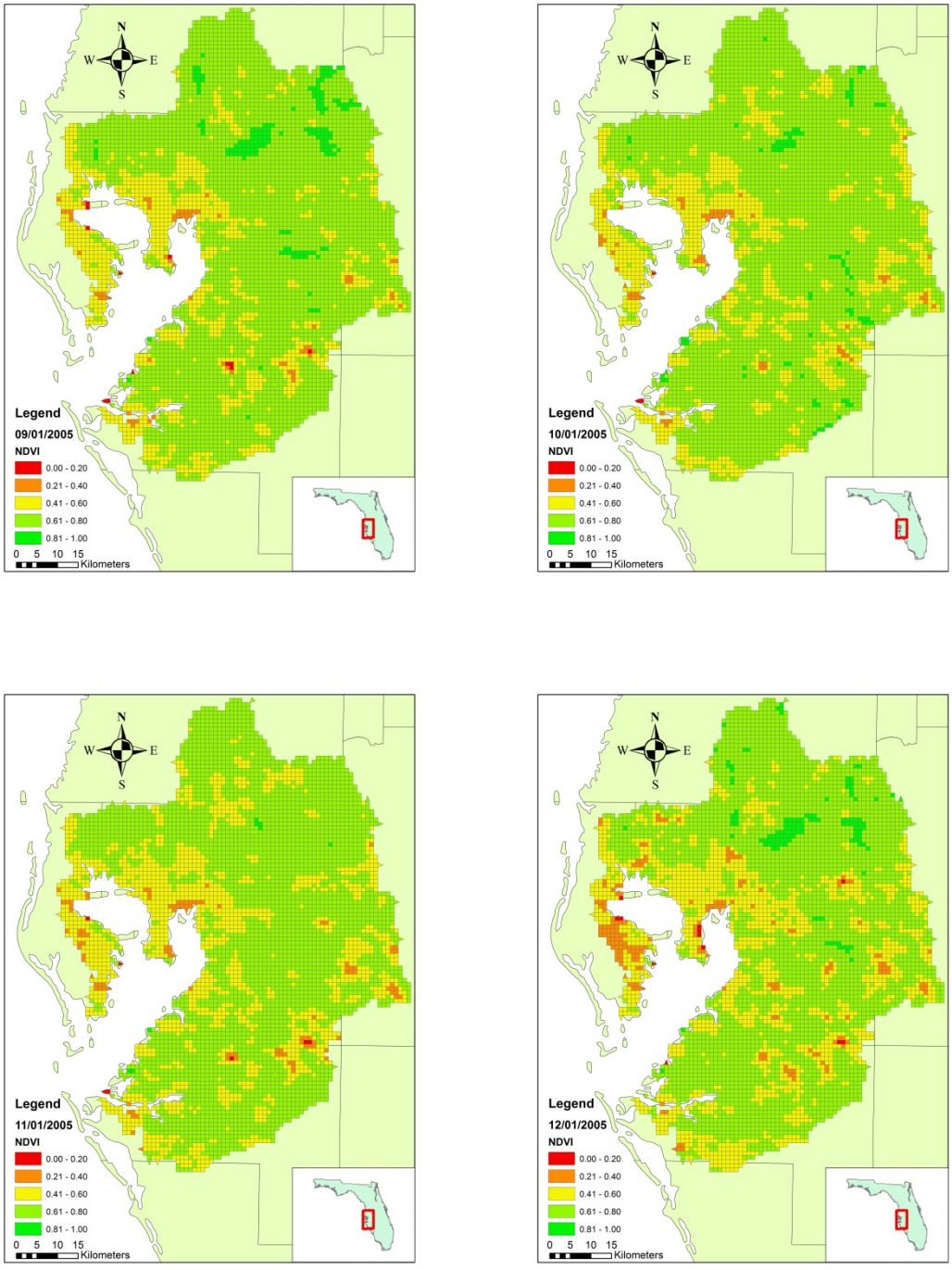

Figure A.4 16-day NDVI maps for the Tampa Bay watershed for 2005.

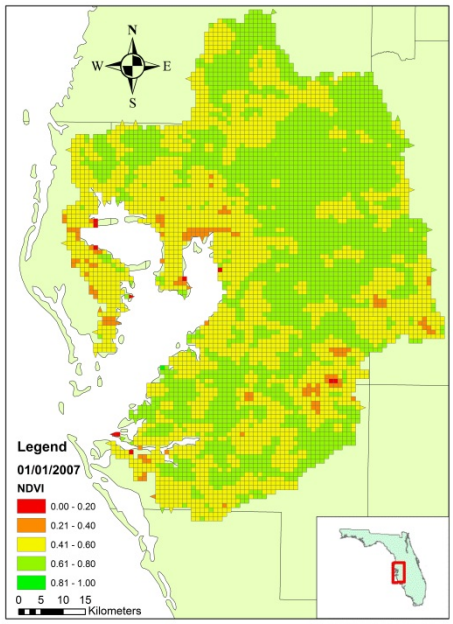
N
W
E
S
Legend
01/01/2007
NDVI
0.00 - 0.20
0.21 - 0.40
0.41 - 0.60
0.61 - 0.80
0.81 - 1.00
0 5 10 15
Kilometers

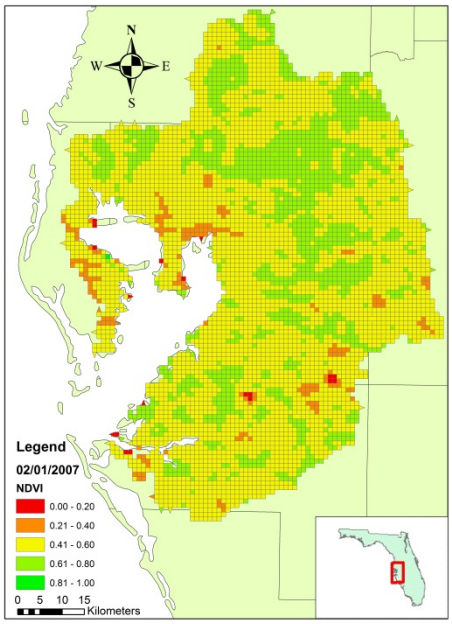
N
W
E
S
Legend
02/01/2007
NDVI
0.00 - 0.20
0.21 - 0.40
0.41 - 0.60
0.61 - 0.80
0.81 - 1.00
0 5 10 15
Kilometers

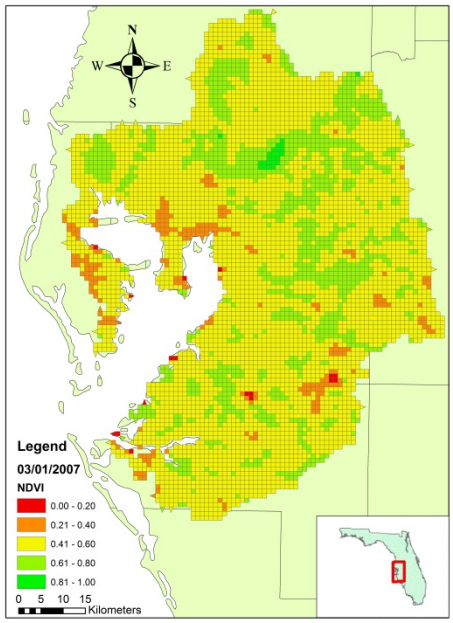
N
W
E
S
Legend
03/01/2007
NDVI
0.00 - 0.20
0.21 - 0.40
0.41 - 0.60
0.61 - 0.80
0.81 - 1.00
0 5 10 15
Kilometers

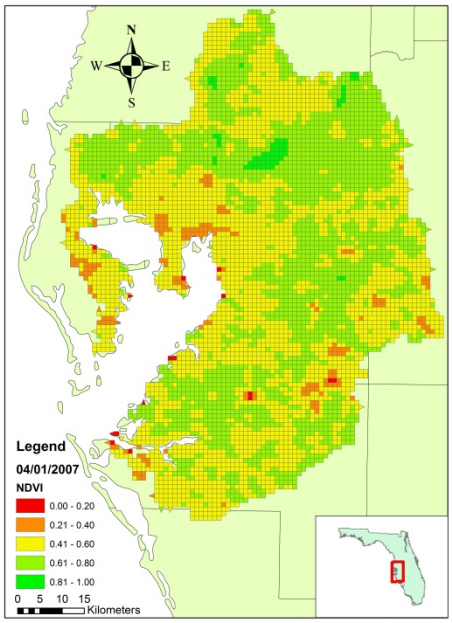
N
W
E
S
Legend
04/01/2007
NDVI
0.00 - 0.20
0.21 - 0.40
0.41 - 0.60
0.61 - 0.80
0.81 - 1.00
0 5 10 15
Kilometers

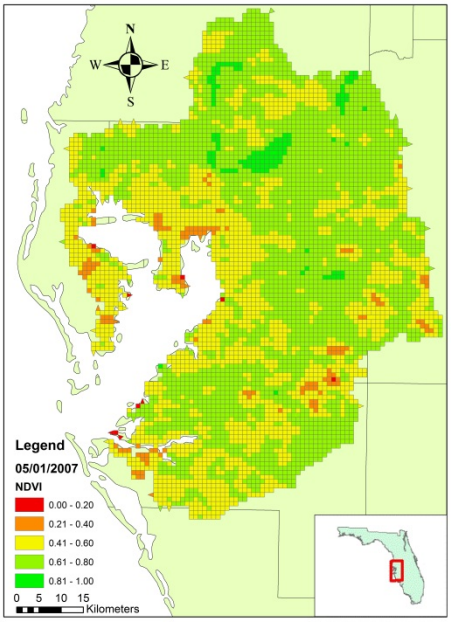
N
W
E
S
Legend
05/01/2007
NDVI
0.00 - 0.20
0.21 - 0.40
0.41 - 0.60
0.61 - 0.80
0.81 - 1.00
0 5 10 15
Kilometers

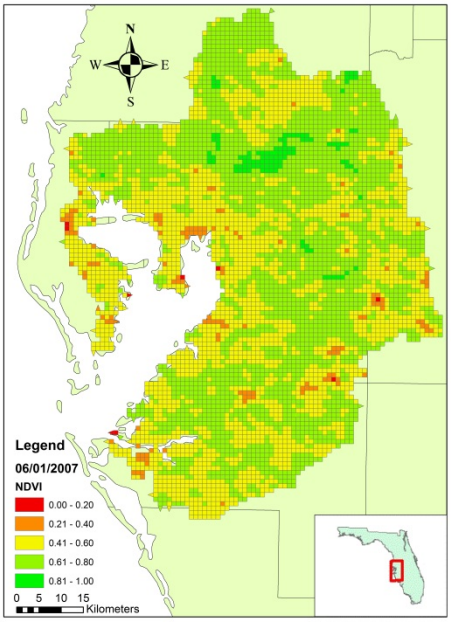
N
W
E
S
Legend
06/01/2007
NDVI
0.00 - 0.20
0.21 - 0.40
0.41 - 0.60
0.61 - 0.80
0.81 - 1.00
0 5 10 15
Kilometers

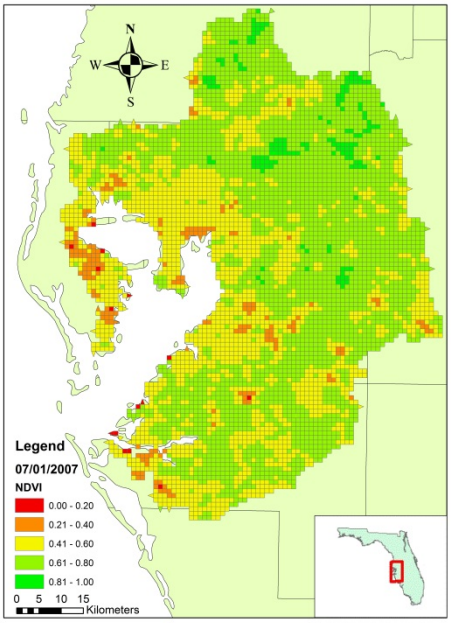
N
W
E
S
Legend
07/01/2007
NDVI
0.00 - 0.20
0.21 - 0.40
0.41 - 0.60
0.61 - 0.80
0.81 - 1.00
0 5 10 15
Kilometers

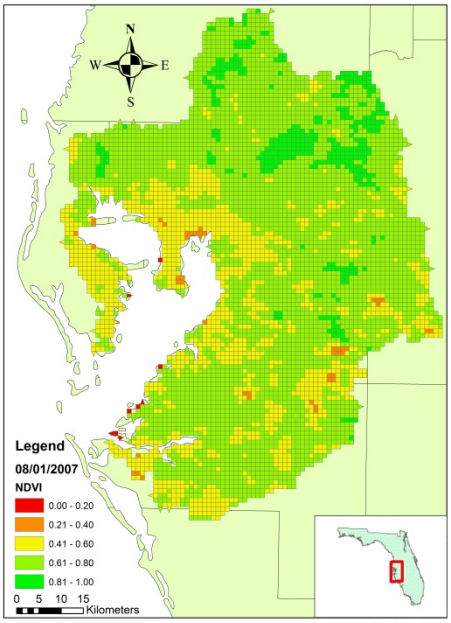
N
W
E
S
Legend
08/01/2007
NDVI
0.00 - 0.20
0.21 - 0.40
0.41 - 0.60
0.61 - 0.80
0.81 - 1.00
0 5 10 15
Kilometers

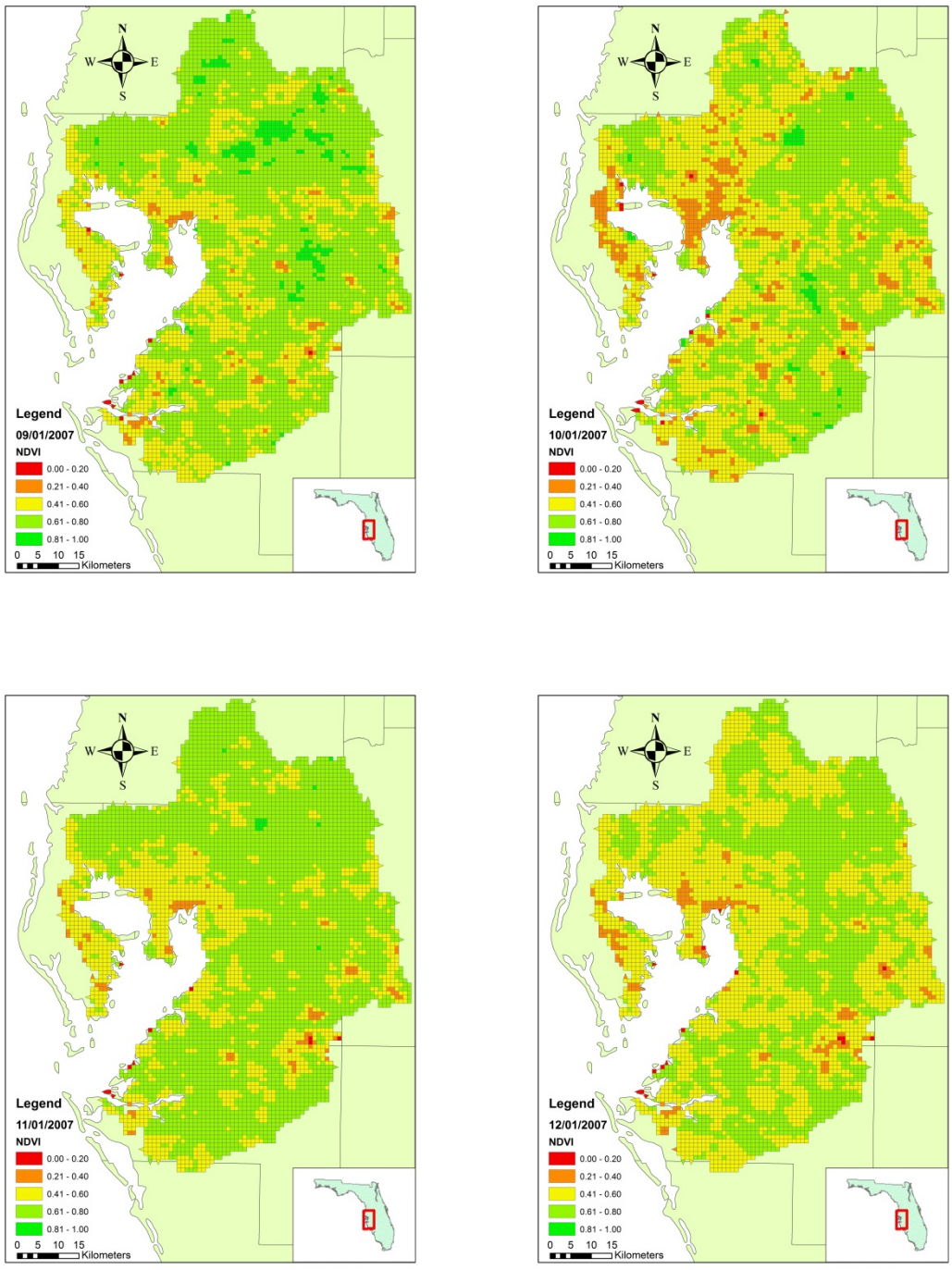

Figure A.5 16-day NDVI maps for the Tampa Bay watershed for 2007.

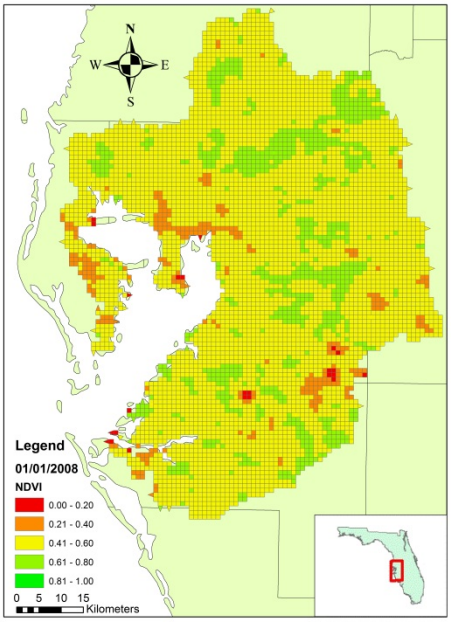
N
W
E
S
Legend
01/01/2008
NDVI
0.00 - 0.20
0.21 - 0.40
0.41 - 0.60
0.61 - 0.80
0.81 - 1.00
0 5 10 15
Kilometers

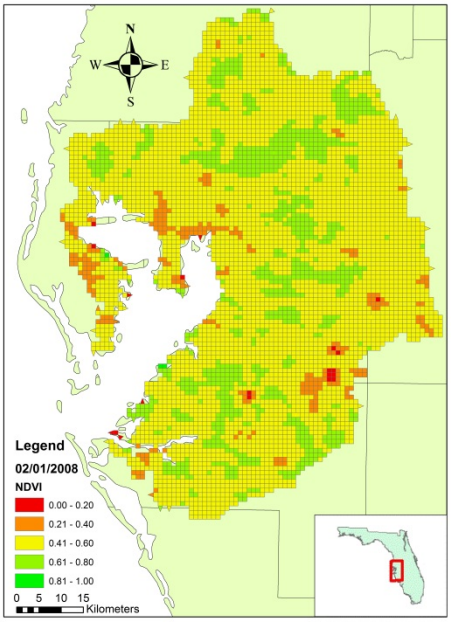
N
W
E
S
Legend
02/01/2008
NDVI
0.00 - 0.20
0.21 - 0.40
0.41 - 0.60
0.61 - 0.80
0.81 - 1.00
0 5 10 15
Kilometers

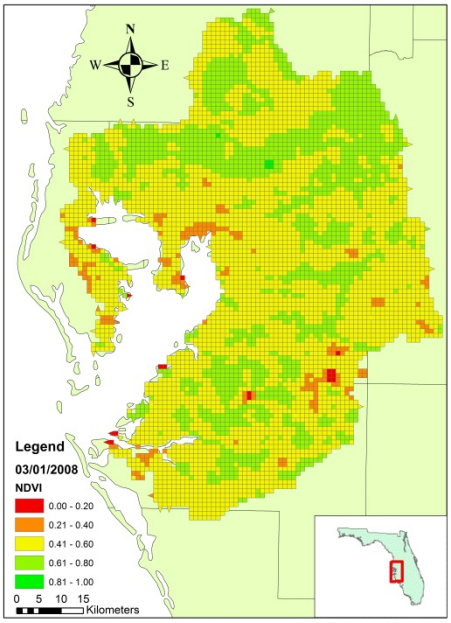
N
W
E
S
Legend
03/01/2008
NDVI
0.00 - 0.20
0.21 - 0.40
0.41 - 0.60
0.61 - 0.80
0.81 - 1.00
0 5 10 15
Kilometers

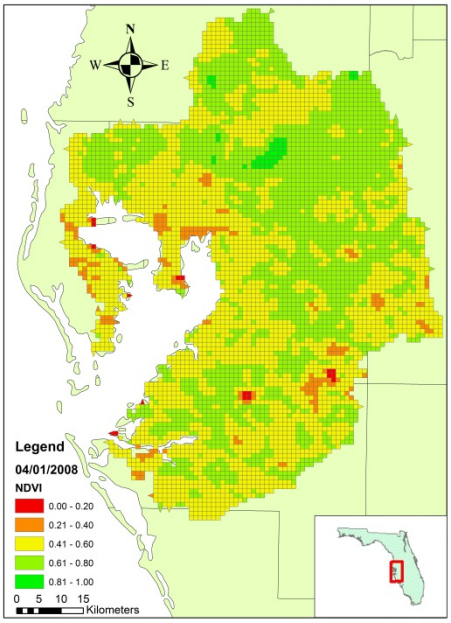
N
W
E
S
Legend
04/01/2008
NDVI
0.00 - 0.20
0.21 - 0.40
0.41 - 0.60
0.61 - 0.80
0.81 - 1.00
0 5 10 15
Kilometers

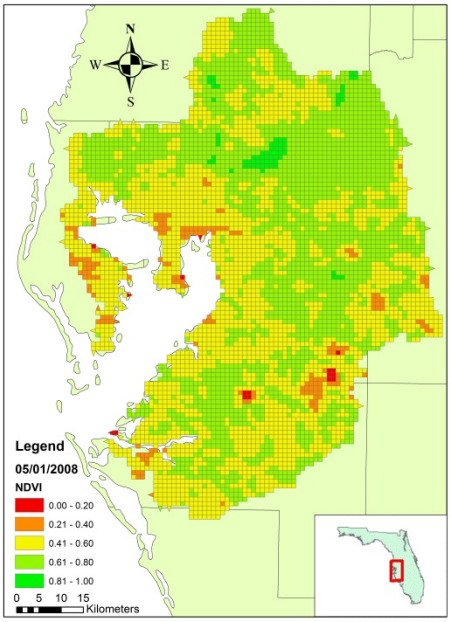
N
W
E
S
Legend
05/01/2008
NDVI
0.00 - 0.20
0.21 - 0.40
0.41 - 0.60
0.61 - 0.80
0.81 - 1.00
0 5 10 15
Kilometers

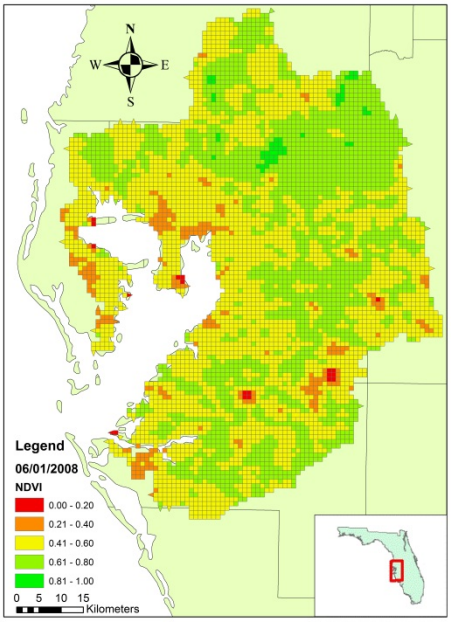
N
W
E
S
Legend
06/01/2008
NDVI
0.00 - 0.20
0.21 - 0.40
0.41 - 0.60
0.61 - 0.80
0.81 - 1.00
0 5 10 15
Kilometers

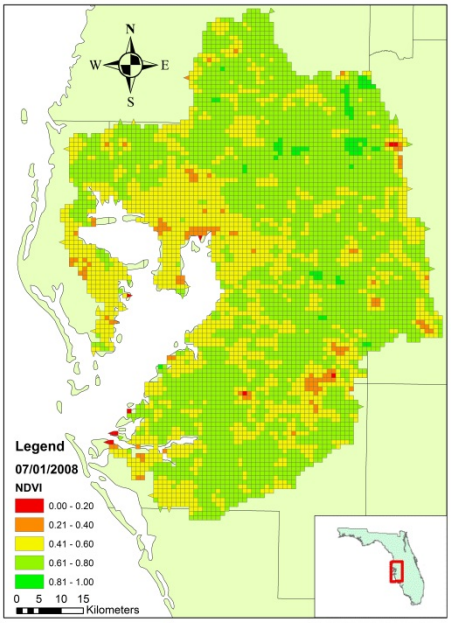
N
W
E
S
Legend
07/01/2008
NDVI
0.00 - 0.20
0.21 - 0.40
0.41 - 0.60
0.61 - 0.80
0.81 - 1.00
0 5 10 15
Kilometers

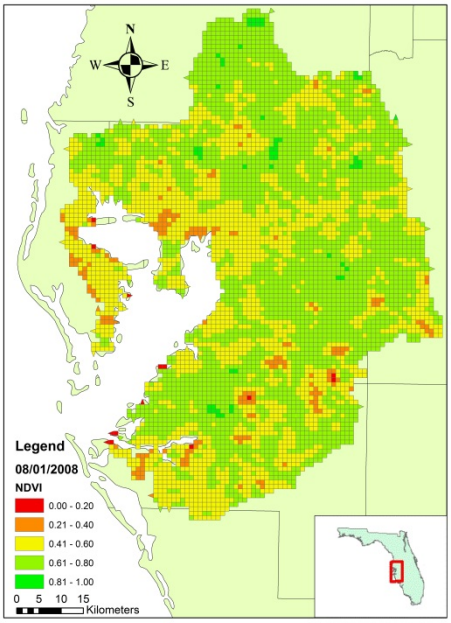
N
W
E
S
Legend
08/01/2008
NDVI
0.00 - 0.20
0.21 - 0.40
0.41 - 0.60
0.61 - 0.80
0.81 - 1.00
0 5 10 15
Kilometers

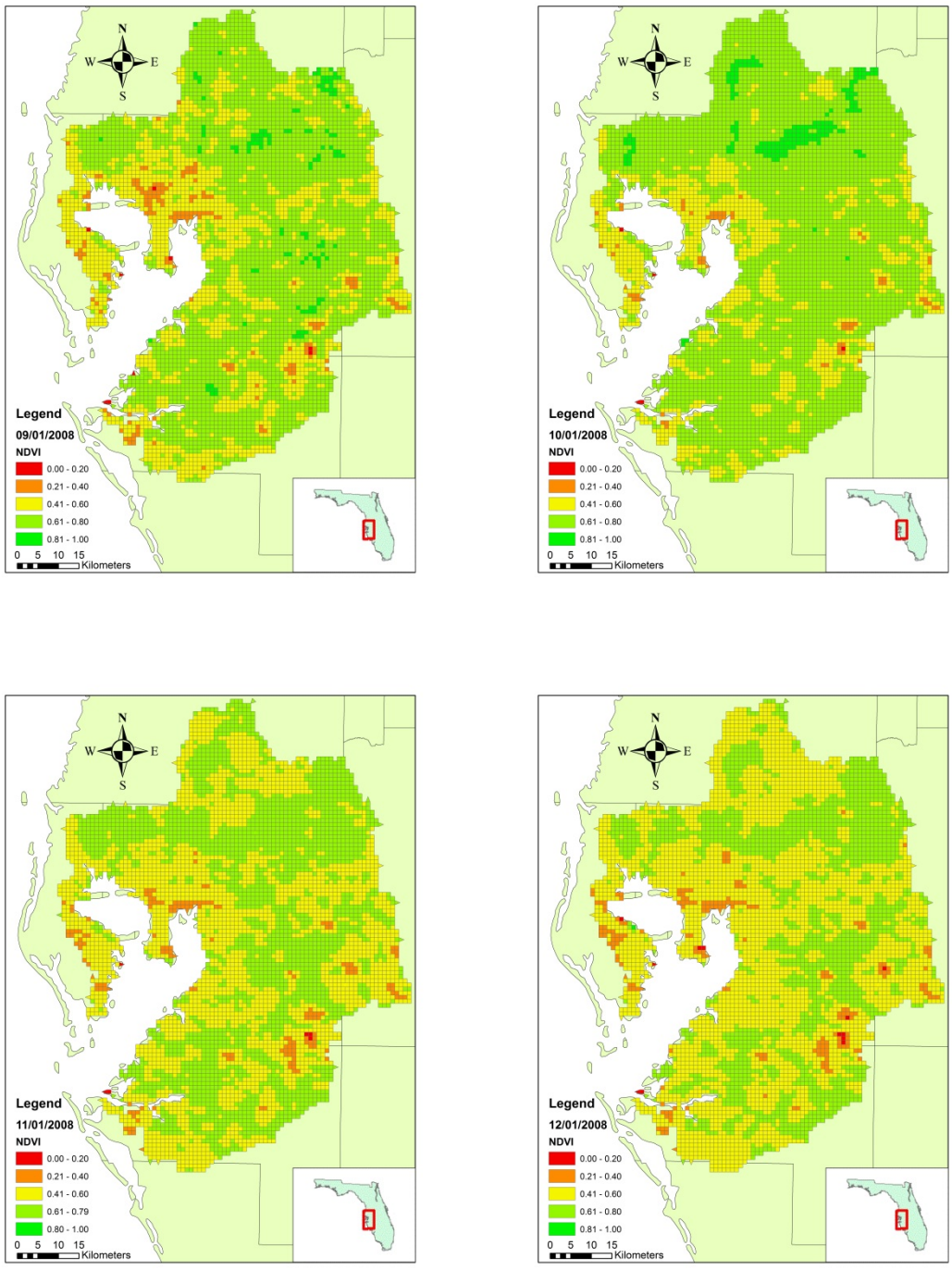

Figure A.6 16-day NDVI maps for the Tampa Bay watershed for 2008.

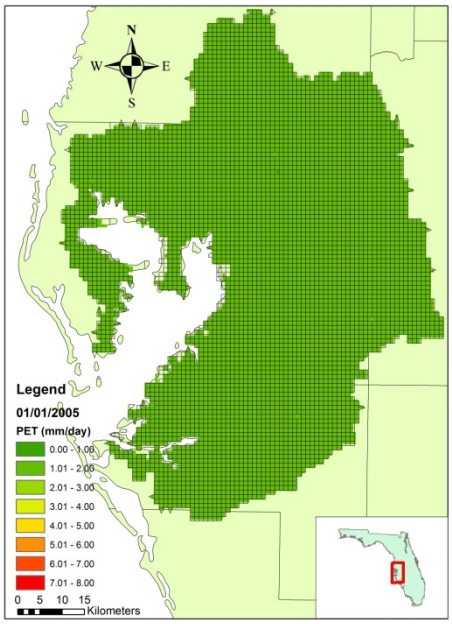
N
W
E
S
Legend
01/01/2005
PET (mm/day)
0.00 - 1.00
1.01 - 2.00
2.01 - 3.00
3.01 - 4.00
4.01 - 5.00
5.01 - 6.00
6.01 - 7.00
7.01 - 8.00
0 5 10 15
Kilometers

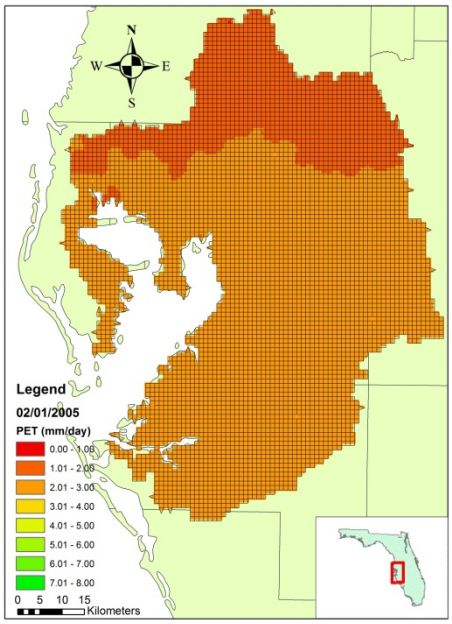
N
W
E
S
Legend
02/01/2005
PET (mm/day)
0.00 - 1.00
1.01 - 2.00
2.01 - 3.00
3.01 - 4.00
4.01 - 5.00
5.01 - 6.00
6.01 - 7.00
7.01 - 8.00
0 5 10 15
Kilometers

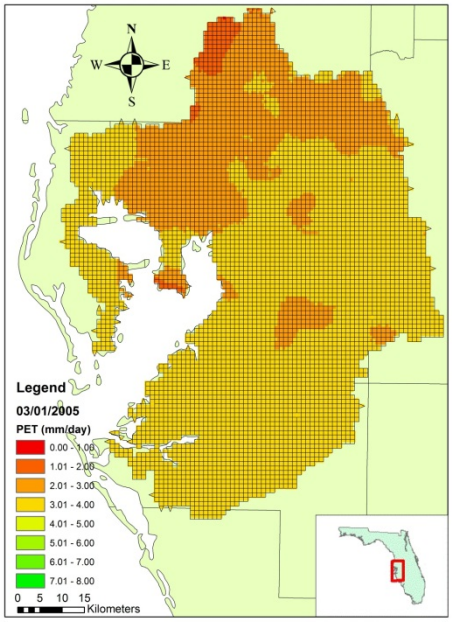
N
W
E
S
Legend
03/01/2005
PET (mm/day)
0.00 - 1.00
1.01 - 2.00
2.01 - 3.00
3.01 - 4.00
4.01 - 5.00
5.01 - 6.00
6.01 - 7.00
7.01 - 8.00
0 5 10 15
Kilometers

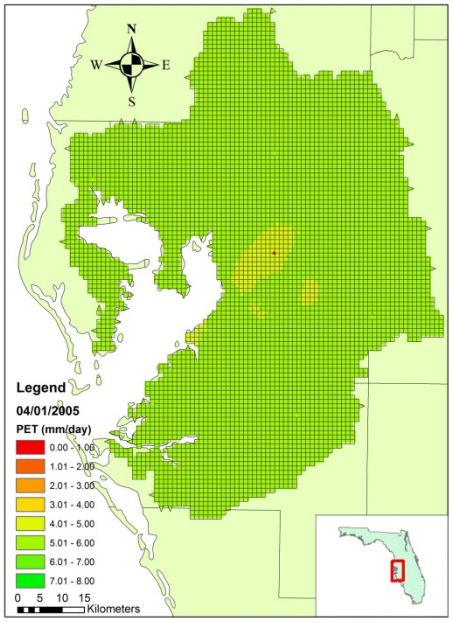
N
W
E
S
Legend
04/01/2005
PET (mm/day)
0.00 - 1.00
1.01 - 2.00
2.01 - 3.00
3.01 - 4.00
4.01 - 5.00
5.01 - 6.00
6.01 - 7.00
7.01 - 8.00
0 5 10 15
Kilometers

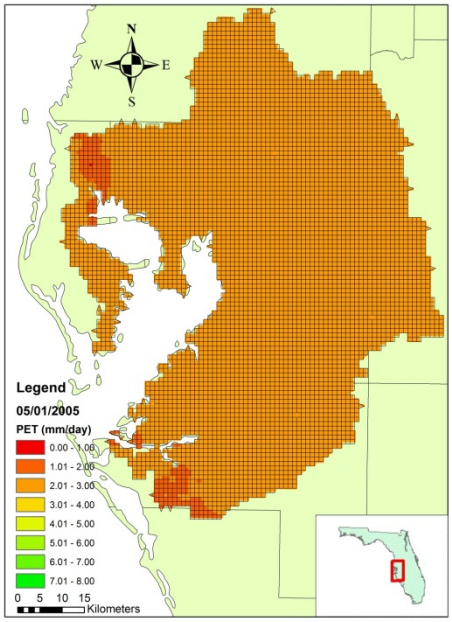
N
W
E
S
Legend
05/01/2005
PET (mm/day)
0.00 - 1.00
1.01 - 2.00
2.01 - 3.00
3.01 - 4.00
4.01 - 5.00
5.01 - 6.00
6.01 - 7.00
7.01 - 8.00
0 5 10 15
Kilometers

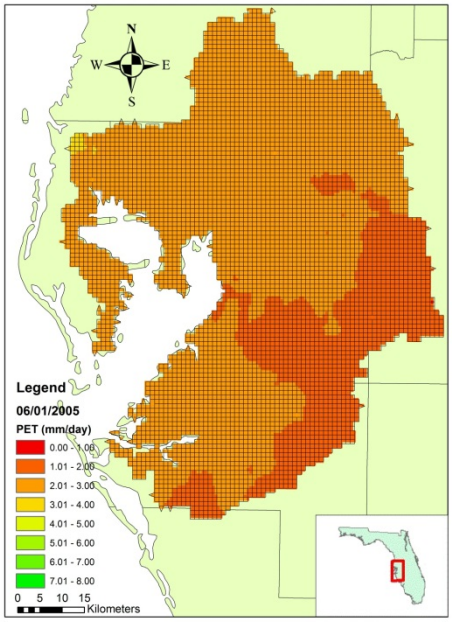
N
W
E
S
Legend
06/01/2005
PET (mm/day)
0.00 - 1.00
1.01 - 2.00
2.01 - 3.00
3.01 - 4.00
4.01 - 5.00
5.01 - 6.00
6.01 - 7.00
7.01 - 8.00
0 5 10 15
Kilometers

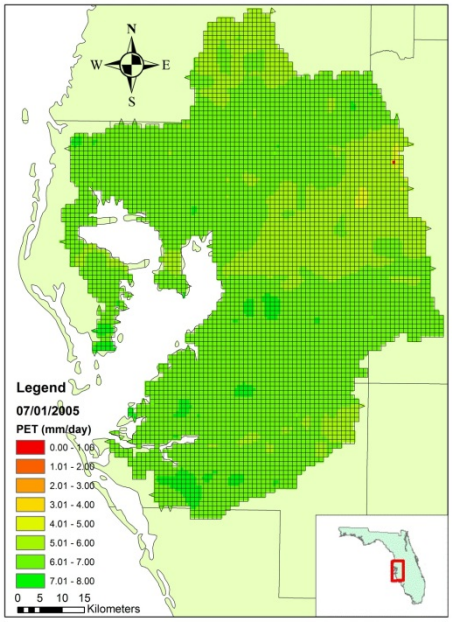
N
W
E
S
Legend
07/01/2005
PET (mm/day)
0.00 - 1.00
1.01 - 2.00
2.01 - 3.00
3.01 - 4.00
4.01 - 5.00
5.01 - 6.00
6.01 - 7.00
7.01 - 8.00
0 5 10 15
Kilometers

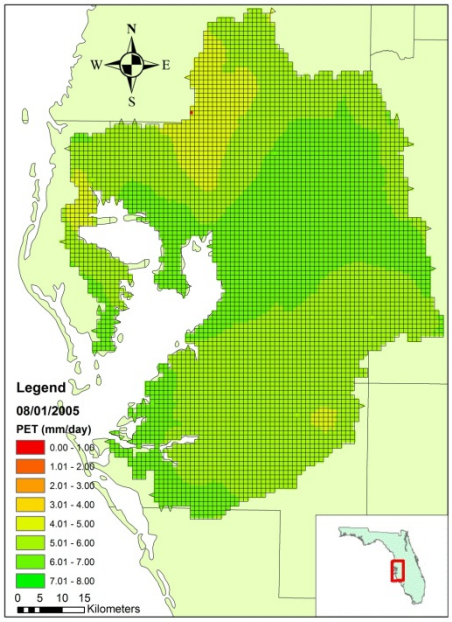
N
W
E
S
Legend
08/01/2005
PET (mm/day)
0.00 - 1.00
1.01 - 2.00
2.01 - 3.00
3.01 - 4.00
4.01 - 5.00
5.01 - 6.00
6.01 - 7.00
7.01 - 8.00
0 5 10 15
Kilometers

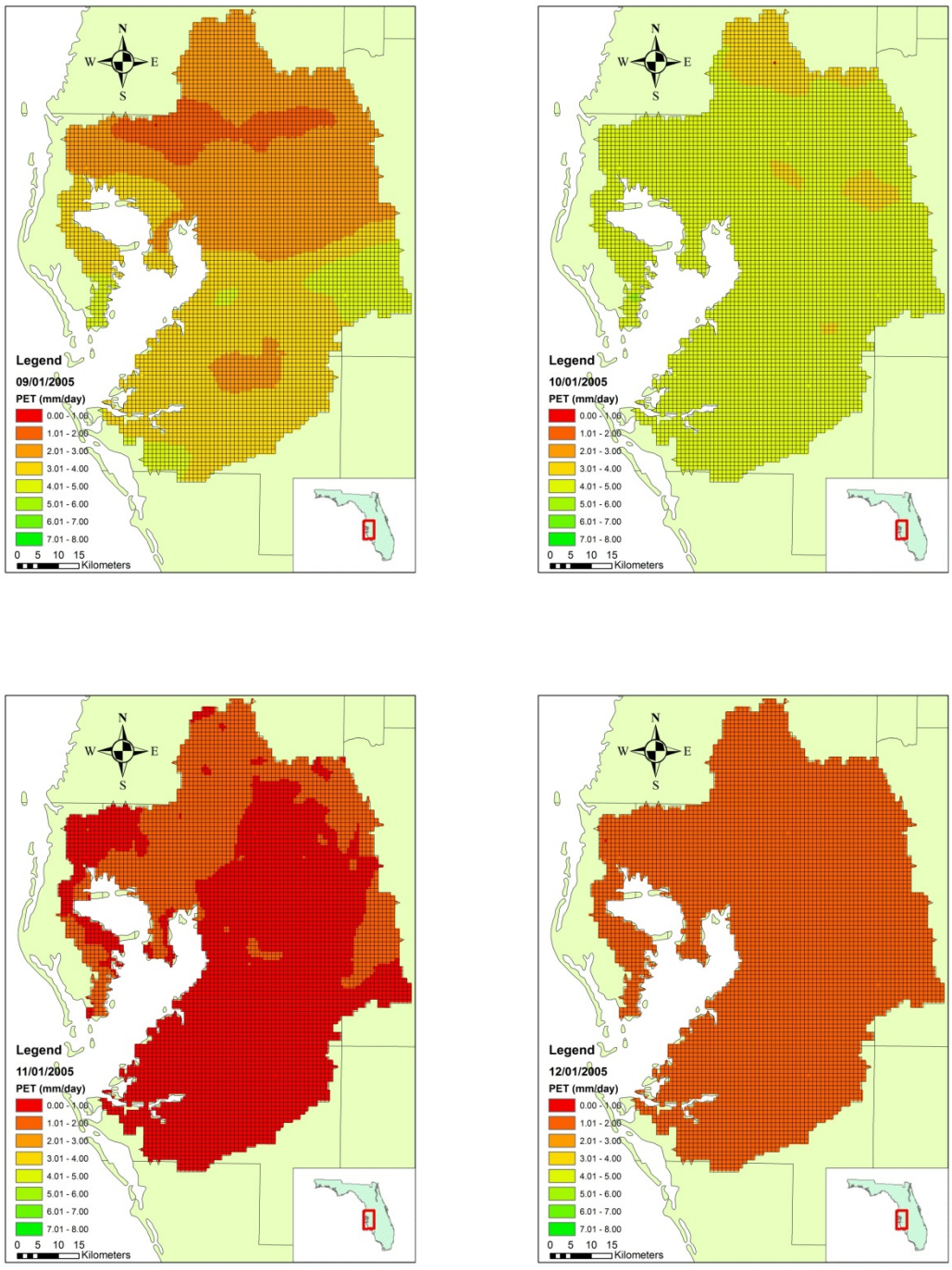

Figure A.7 Daily ET maps for the Tampa Bay watershed for 2005.

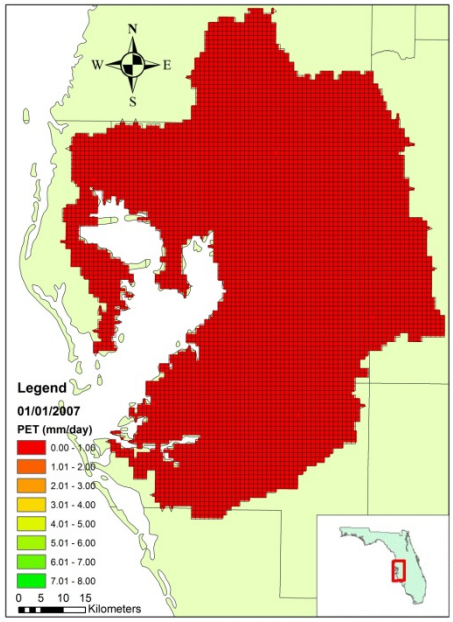
N
W
E
S
Legend
01/01/2007
PET (mm/day)
0.00 - 1.00
1.01 - 2.00
2.01 - 3.00
3.01 - 4.00
4.01 - 5.00
5.01 - 6.00
6.01 - 7.00
7.01 - 8.00
0 5 10 15
Kilometers

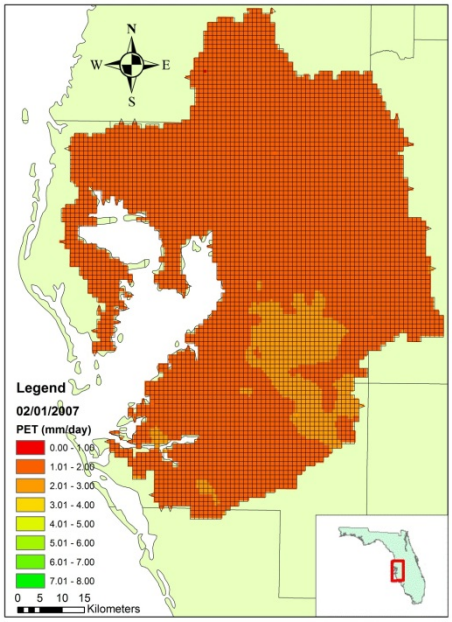
N
W
E
S
Legend
02/01/2007
PET (mm/day)
0.00 - 1.00
1.01 - 2.00
2.01 - 3.00
3.01 - 4.00
4.01 - 5.00
5.01 - 6.00
6.01 - 7.00
7.01 - 8.00
0 5 10 15
Kilometers

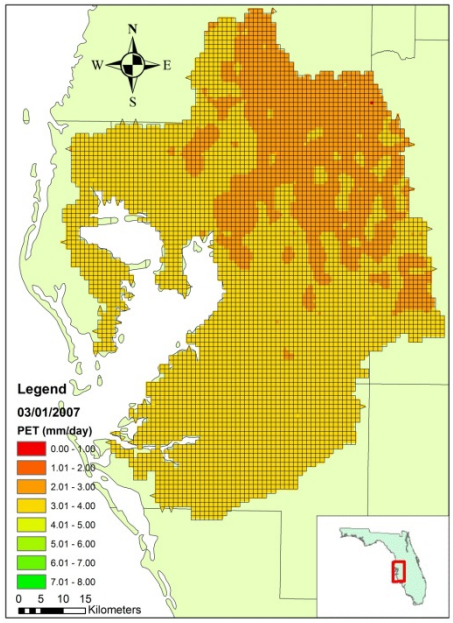
N
W
E
S
Legend
03/01/2007
PET (mm/day)
0.00 - 1.00
1.01 - 2.00
2.01 - 3.00
3.01 - 4.00
4.01 - 5.00
5.01 - 6.00
6.01 - 7.00
7.01 - 8.00
0 5 10 15
Kilometers

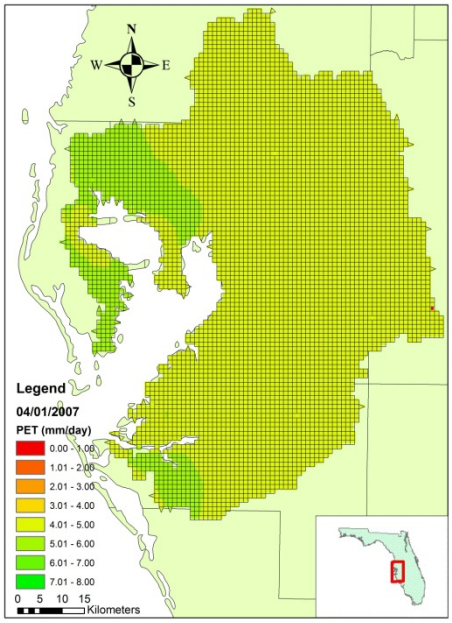
N
W
E
S
Legend
04/01/2007
PET (mm/day)
0.00 - 1.00
1.01 - 2.00
2.01 - 3.00
3.01 - 4.00
4.01 - 5.00
5.01 - 6.00
6.01 - 7.00
7.01 - 8.00
0 5 10 15
Kilometers

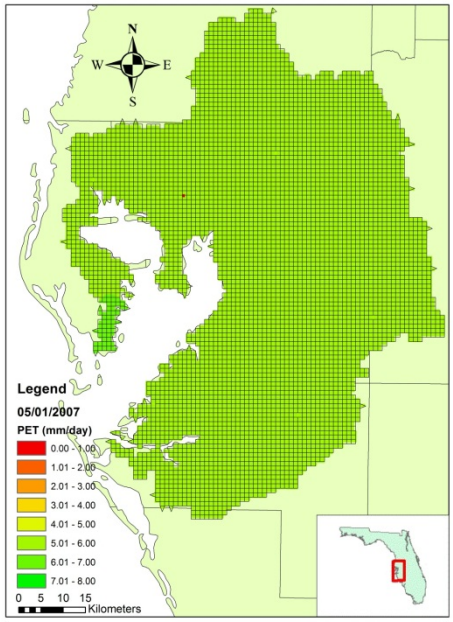
N
W
E
S
Legend
05/01/2007
PET (mm/day)
0.00 - 1.00
1.01 - 2.00
2.01 - 3.00
3.01 - 4.00
4.01 - 5.00
5.01 - 6.00
6.01 - 7.00
7.01 - 8.00
0 5 10 15
Kilometers

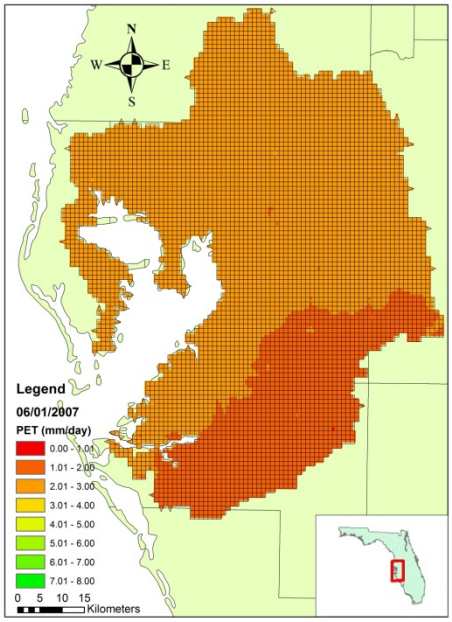
N
W
E
S
Legend
06/01/2007
PET (mm/day)
0.00 - 1.00
1.01 - 2.00
2.01 - 3.00
3.01 - 4.00
4.01 - 5.00
5.01 - 6.00
6.01 - 7.00
7.01 - 8.00
0 5 10 15
Kilometers

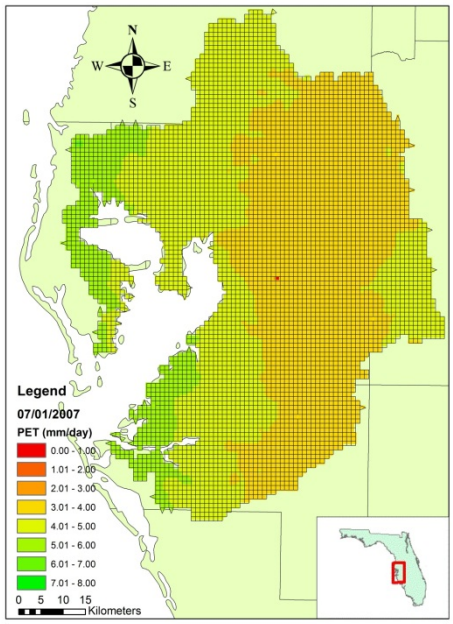
N
W
E
S
Legend
07/01/2007
PET (mm/day)
0.00 - 1.00
1.01 - 2.00
2.01 - 3.00
3.01 - 4.00
4.01 - 5.00
5.01 - 6.00
6.01 - 7.00
7.01 - 8.00
0 5 10 15
Kilometers

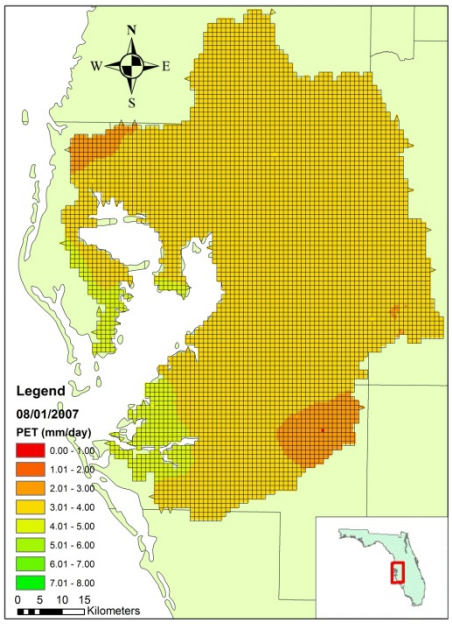
N
W
E
S
Legend
08/01/2007
PET (mm/day)
0.00 - 1.00
1.01 - 2.00
2.01 - 3.00
3.01 - 4.00
4.01 - 5.00
5.01 - 6.00
6.01 - 7.00
7.01 - 8.00
0 5 10 15
Kilometers

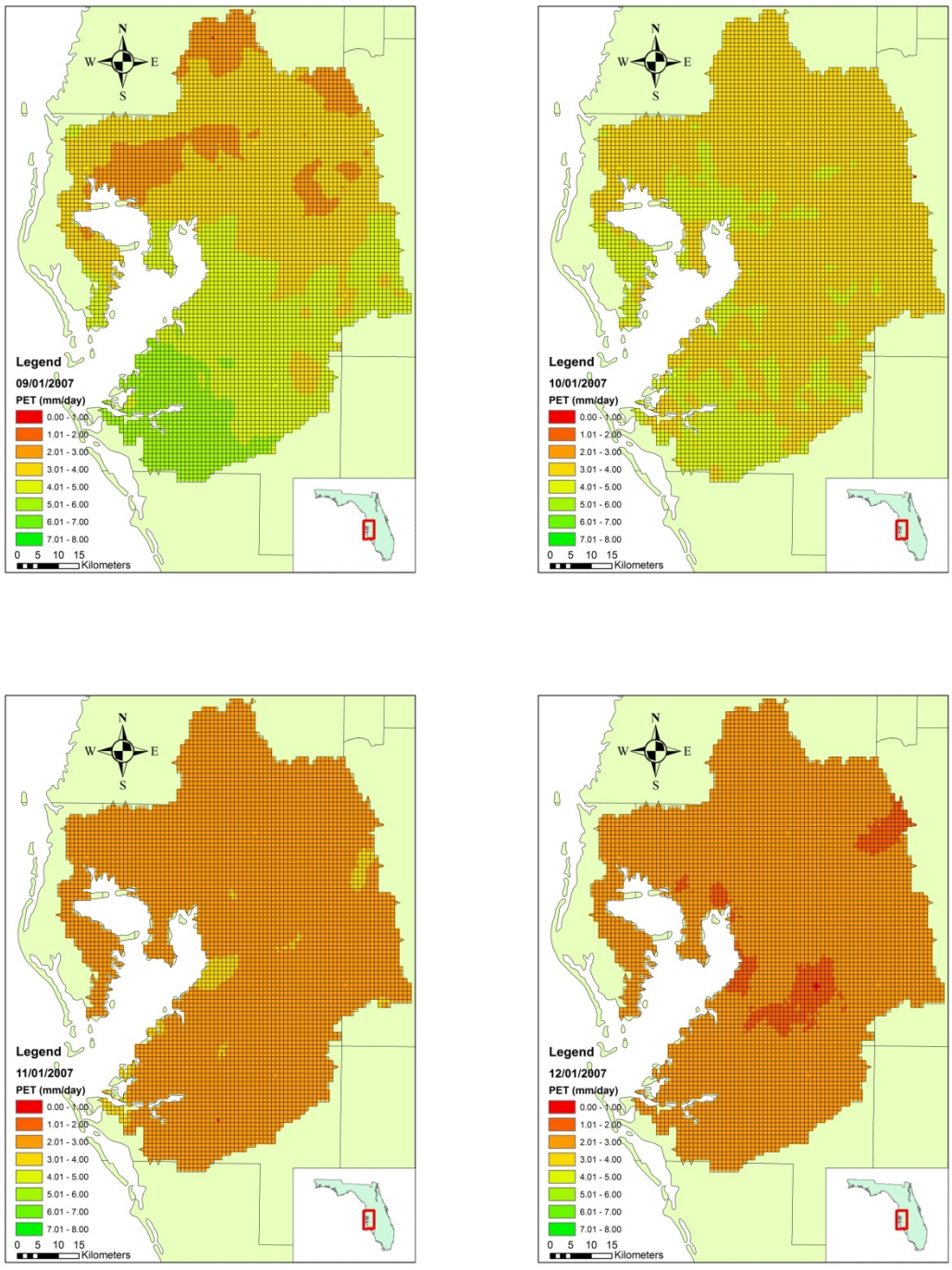

Figure A.8 Daily ET maps for the Tampa Bay watershed for 2007.

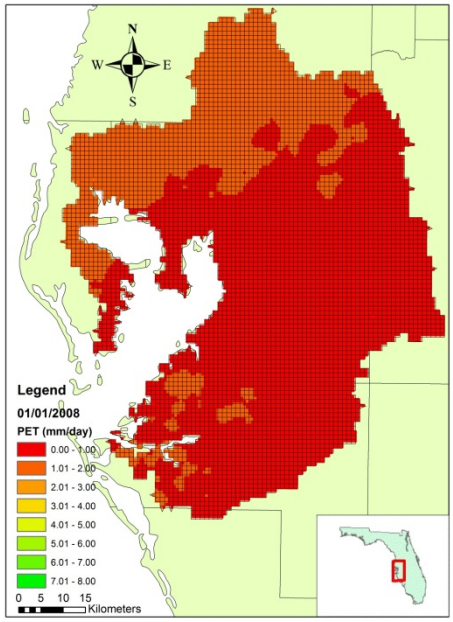
N
W
E
S
Legend
01/01/2008
PET (mm/day)
0.00 - 1.00
1.01 - 2.00
2.01 - 3.00
3.01 - 4.00
4.01 - 5.00
5.01 - 6.00
6.01 - 7.00
7.01 - 8.00
0 5 10 15
Kilometers

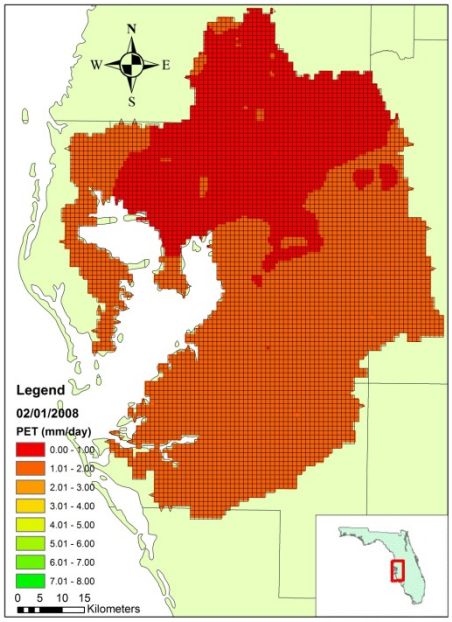
N
W
E
S
Legend
02/01/2008
PET (mm/day)
0.00 - 1.00
1.01 - 2.00
2.01 - 3.00
3.01 - 4.00
4.01 - 5.00
5.01 - 6.00
6.01 - 7.00
7.01 - 8.00
0 5 10 15
Kilometers

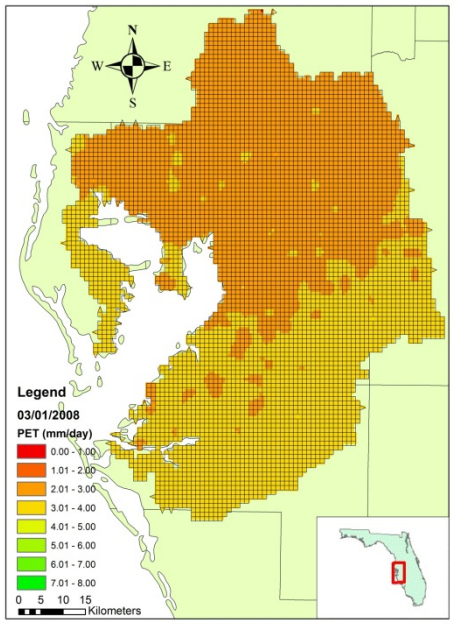
N
W
E
S
Legend
03/01/2008
PET (mm/day)
0.00 - 1.00
1.01 - 2.00
2.01 - 3.00
3.01 - 4.00
4.01 - 5.00
5.01 - 6.00
6.01 - 7.00
7.01 - 8.00
0 5 10 15
Kilometers

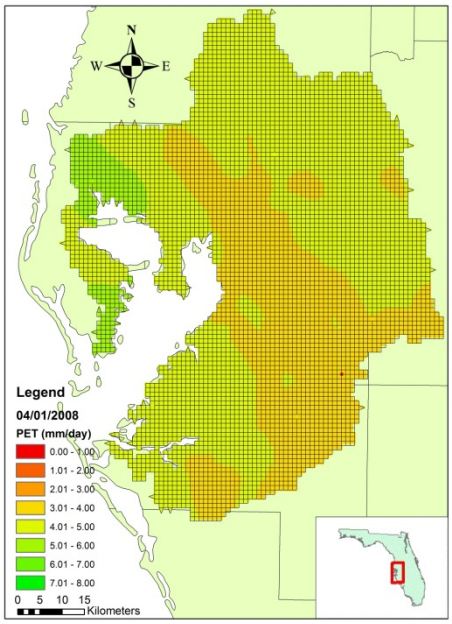
N
W
E
S
Legend
04/01/2008
PET (mm/day)
0.00 - 1.00
1.01 - 2.00
2.01 - 3.00
3.01 - 4.00
4.01 - 5.00
5.01 - 6.00
6.01 - 7.00
7.01 - 8.00
0 5 10 15
Kilometers

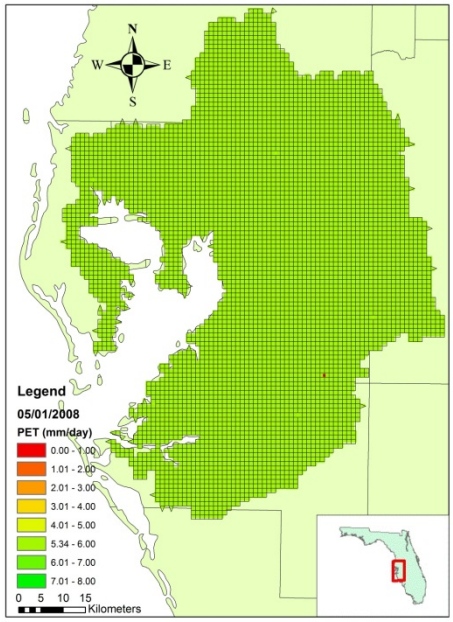
N
W
E
S
Legend
05/01/2008
PET (mm/day)
0.00 - 1.00
1.01 - 2.00
2.01 - 3.00
3.01 - 4.00
4.01 - 5.00
5.34 - 6.00
6.01 - 7.00
7.01 - 8.00
0 5 10 15
Kilometers

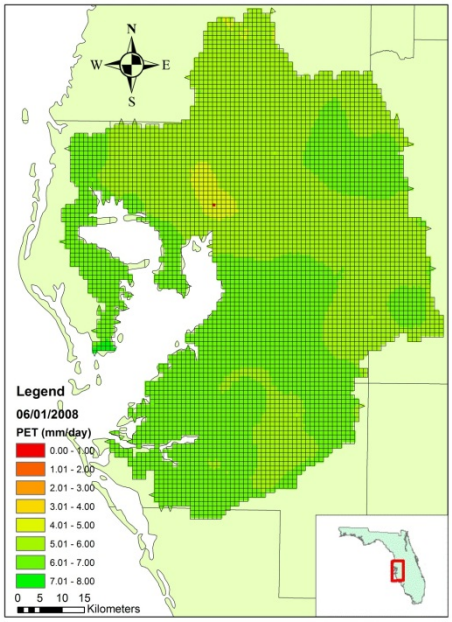
N
W
E
S
Legend
06/01/2008
PET (mm/day)
0.00 - 1.00
1.01 - 2.00
2.01 - 3.00
3.01 - 4.00
4.01 - 5.00
5.01 - 6.00
6.01 - 7.00
7.01 - 8.00
0 5 10 15
Kilometers

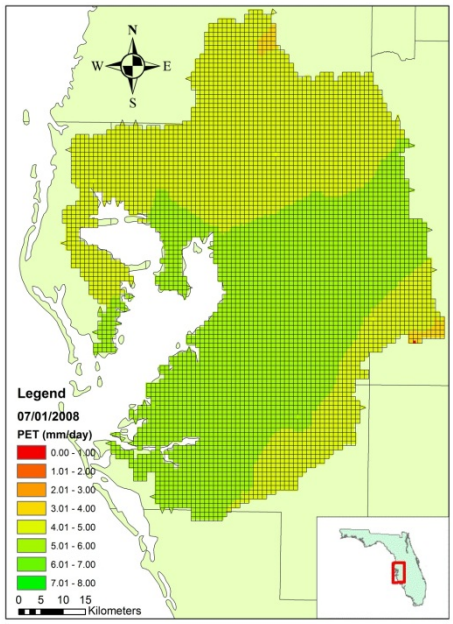
N
W
E
S
Legend
07/01/2008
PET (mm/day)
0.00 - 1.00
1.01 - 2.00
2.01 - 3.00
3.01 - 4.00
4.01 - 5.00
5.01 - 6.00
6.01 - 7.00
7.01 - 8.00
0 5 10 15
Kilometers

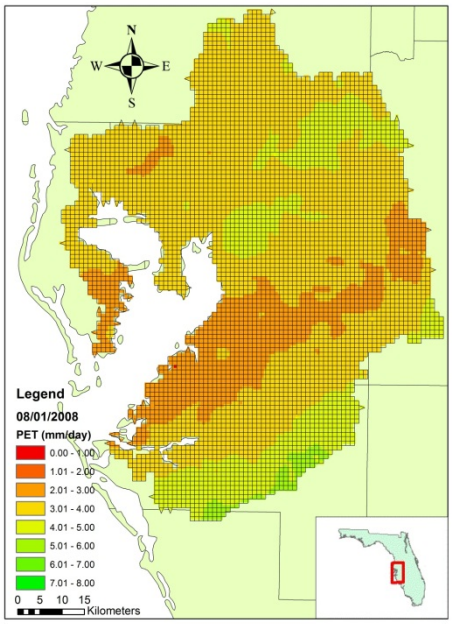
N
W
E
S
Legend
08/01/2008
PET (mm/day)
0.00 - 1.00
1.01 - 2.00
2.01 - 3.00
3.01 - 4.00
4.01 - 5.00
5.01 - 6.00
6.01 - 7.00
7.01 - 8.00
0 5 10 15
Kilometers

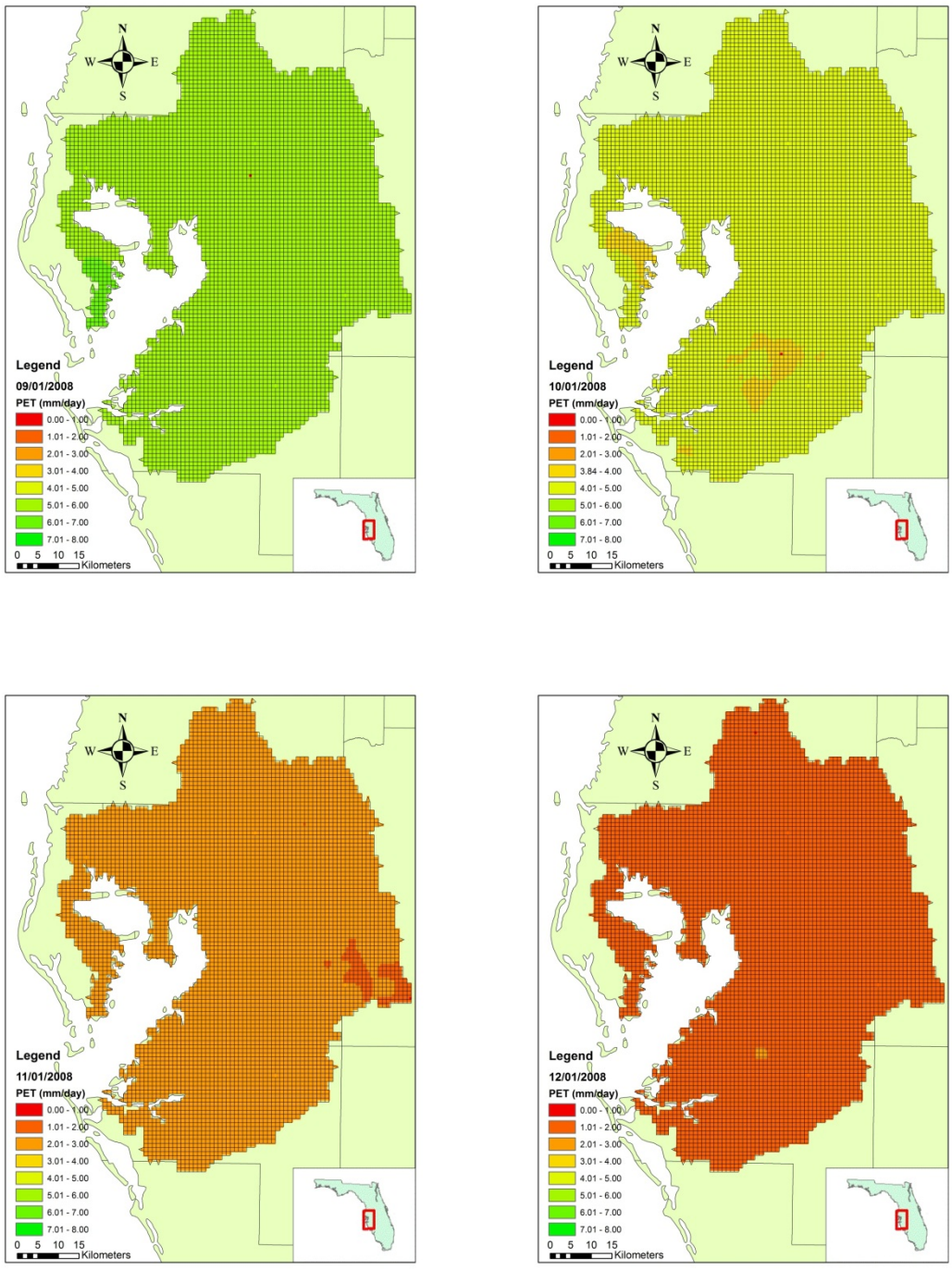

Figure A.9 Daily ET maps for the Tampa Bay watershed for 2008.

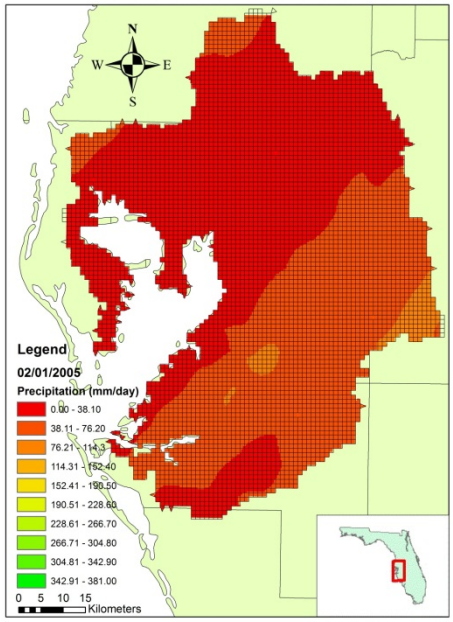
N
W
E
S
Legend
02/01/2005
Precipitation (mm/day)
0.00 - 38.10
38.11 - 76.20
76.21 - 114.30
114.31 - 152.40
152.41 - 190.50
190.51 - 228.60
228.61 - 266.70
266.71 - 304.80
304.81 - 342.90
342.91 - 381.00
0 5 10 15
Kilometers

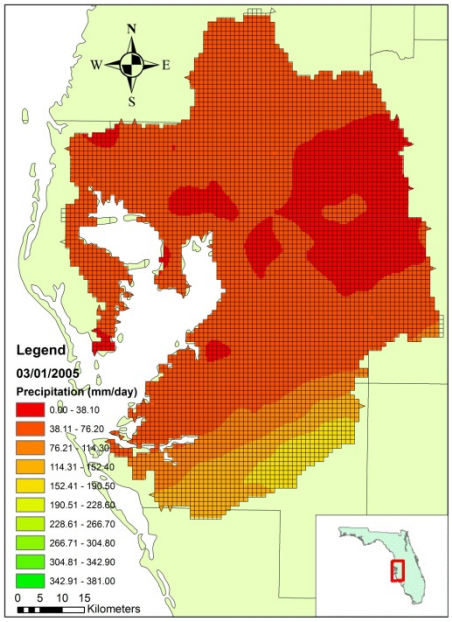
N
W
E
S
Legend
03/01/2005
Precipitation (mm/day)
0.00 - 38.10
38.11 - 76.20
76.21 - 114.30
114.31 - 152.40
152.41 - 190.50
190.51 - 228.60
228.61 - 266.70
266.71 - 304.80
304.81 - 342.90
342.91 - 381.00
0 5 10 15
Kilometers

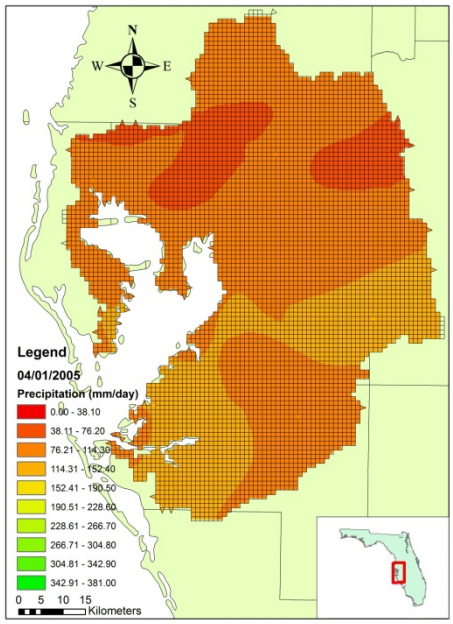
N
W
E
S
Legend
04/01/2005
Precipitation (mm/day)
0.00 - 38.10
38.11 - 76.20
76.21 - 114.30
114.31 - 152.40
152.41 - 190.50
190.51 - 228.60
228.61 - 266.70
266.71 - 304.80
304.81 - 342.90
342.91 - 381.00
0 5 10 15
Kilometers

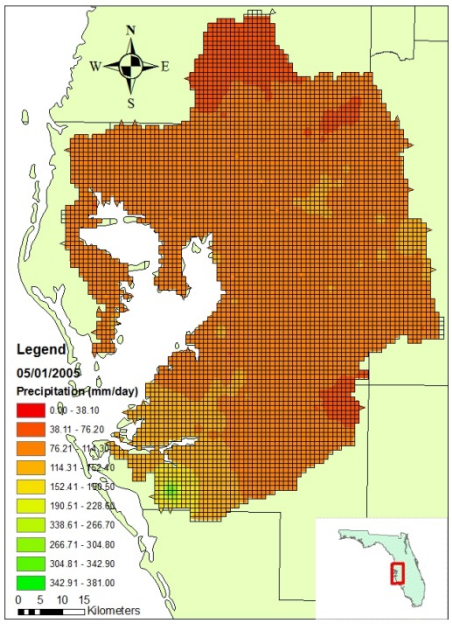
N
W
E
S
Legend
05/01/2005
Precipitation (mm/day)
0.00 - 38.10
38.11 - 76.20
76.21 - 114.30
114.31 - 152.40
152.41 - 190.50
190.51 - 228.60
228.61 - 266.70
266.71 - 304.80
304.81 - 342.90
342.91 - 381.00
0 5 10 15
Kilometers

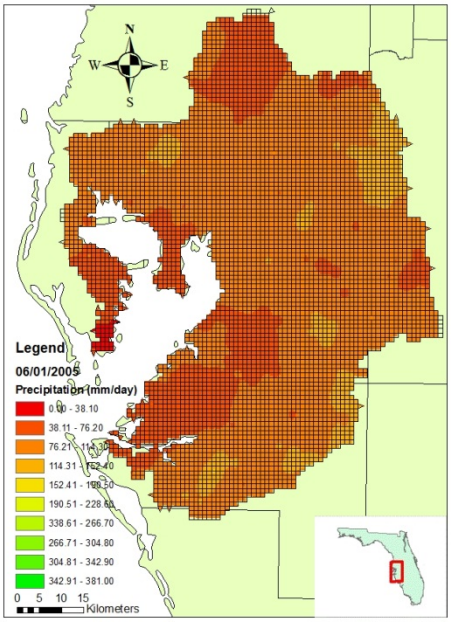
N
W
E
S
Legend
06/01/2005
Precipitation (mm/day)
0.00 - 38.10
38.11 - 76.20
76.21 - 114.30
114.31 - 152.40
152.41 - 190.50
190.51 - 228.60
338.61 - 266.70
266.71 - 304.80
304.81 - 342.90
342.91 - 381.00
0 5 10 15
Kilometers

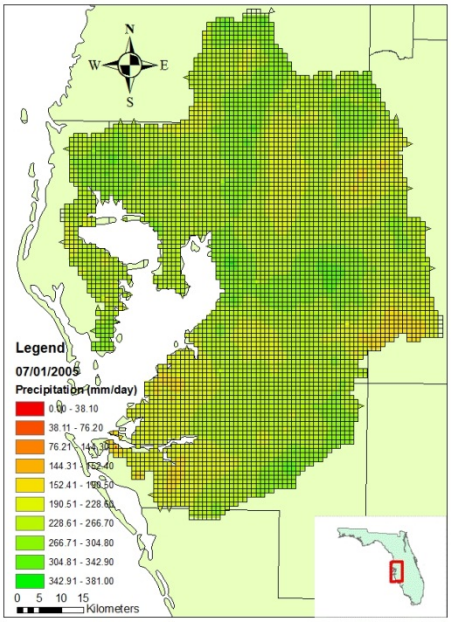
N
W
E
S
Legend
07/01/2005
Precipitation (mm/day)
0.00 - 38.10
38.11 - 76.20
144.31 - 152.40
152.41 - 190.50
190.51 - 228.60
228.61 - 266.70
266.71 - 304.80
304.81 - 342.90
342.91 - 381.00
0 5 10 15
Kilometers

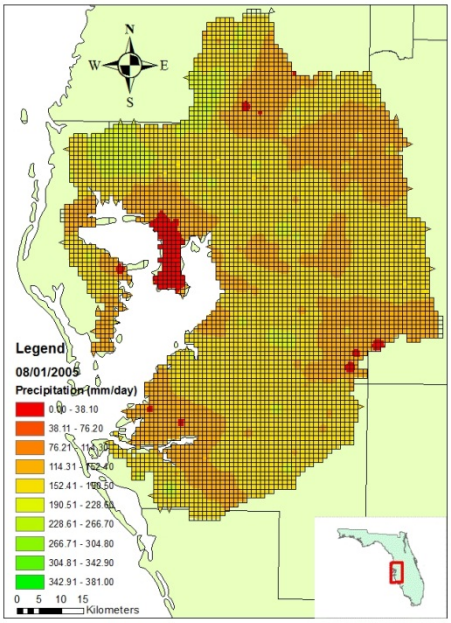
N
W
E
S
Legend
08/01/2005
Precipitation (mm/day)
0.00 - 38.10
38.11 - 76.20
114.31 - 152.40
152.41 - 190.50
190.51 - 228.60
228.61 - 266.70
266.71 - 304.80
304.81 - 342.90
342.91 - 381.00
0 5 10 15
Kilometers

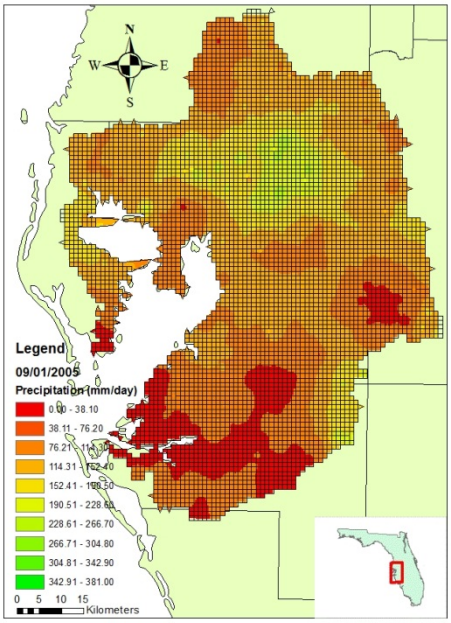
N
W
E
S
Legend
09/01/2005
Precipitation (mm/day)
0.00 - 38.10
38.11 - 76.20
114.31 - 152.40
152.41 - 190.50
190.51 - 228.60
228.61 - 266.70
266.71 - 304.80
304.81 - 342.90
342.91 - 381.00
0 5 10 15
Kilometers

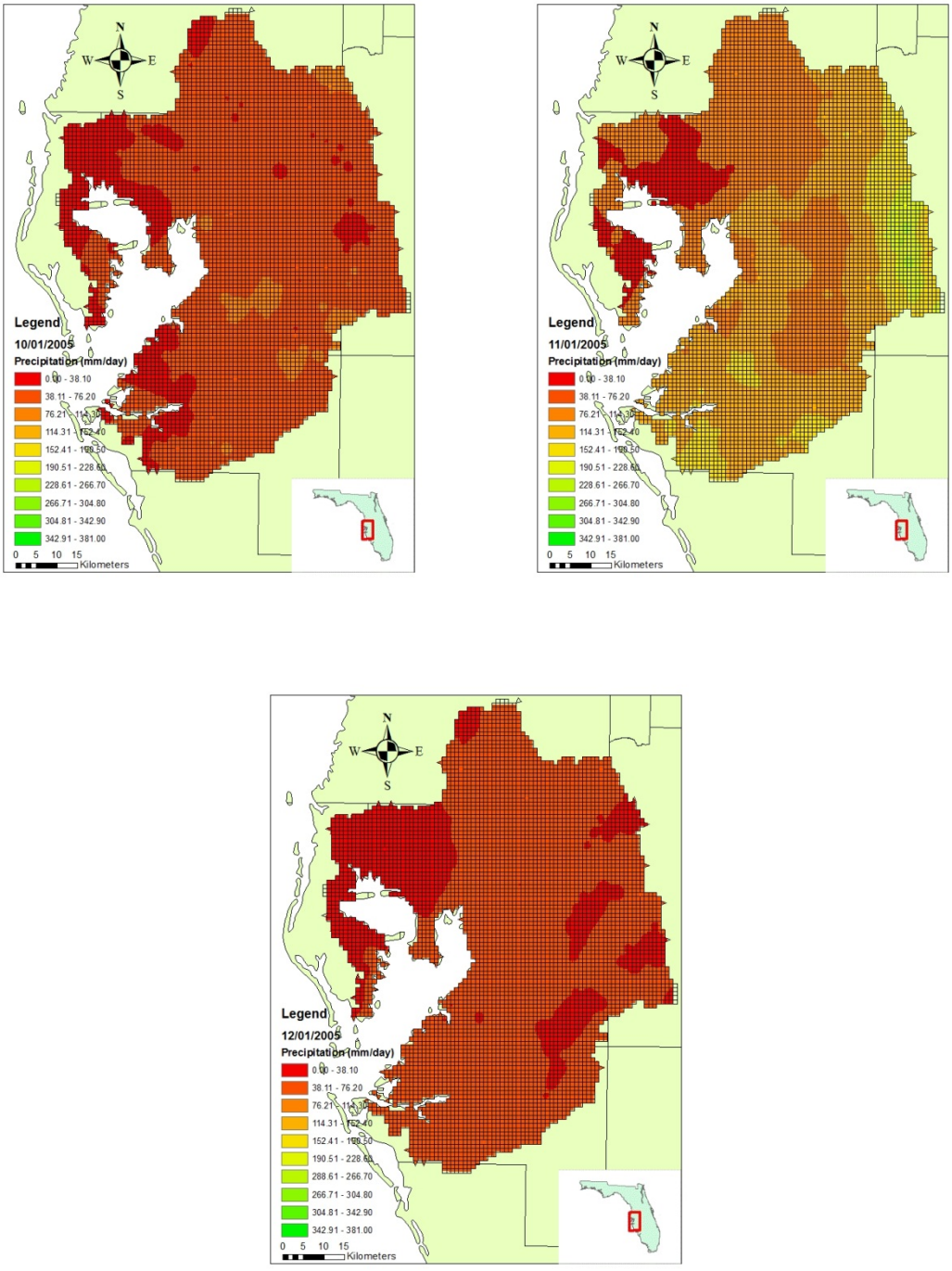

Figure A.10 Month-to-Date Precipitation maps for the Tampa Bay watershed for 2005.

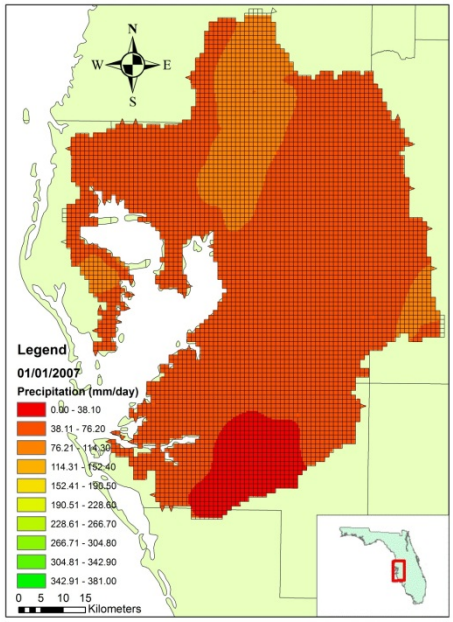
N
W
E
S
Legend
01/01/2007
Precipitation (mm/day)
0.00 - 38.10
38.11 - 76.20
76.21 - 114.30
114.31 - 152.40
152.41 - 190.50
190.51 - 228.60
228.61 - 266.70
266.71 - 304.80
304.81 - 342.90
342.91 - 381.00
0 5 10 15
Kilometers

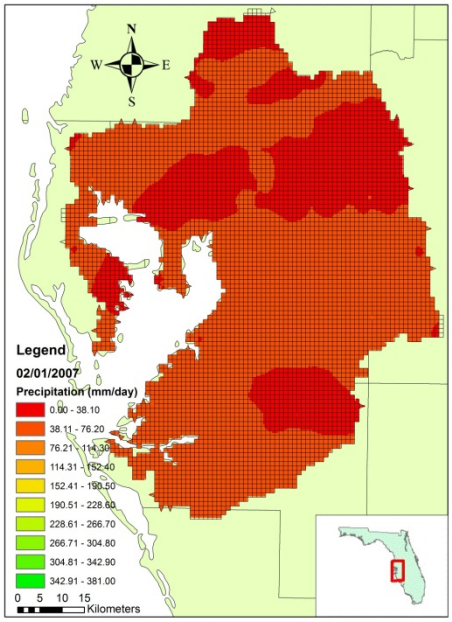
N
W
E
S
Legend
02/01/2007
Precipitation (mm/day)
0.00 - 38.10
38.11 - 76.20
76.21 - 114.30
114.31 - 152.40
152.41 - 190.50
190.51 - 228.60
228.61 - 266.70
266.71 - 304.80
304.81 - 342.90
342.91 - 381.00
0 5 10 15
Kilometers

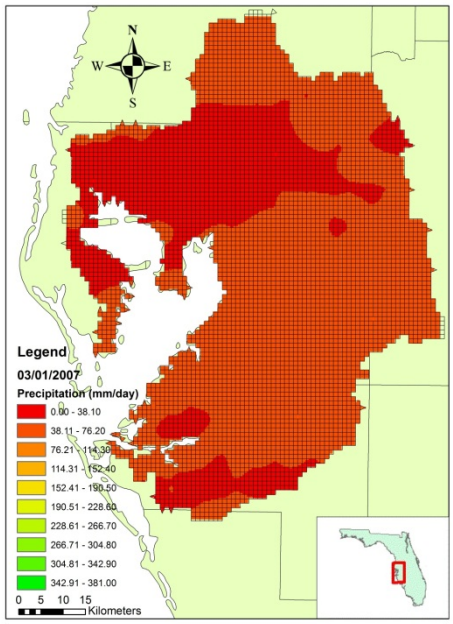
N
W
E
S
Legend
03/01/2007
Precipitation (mm/day)
0.00 - 38.10
38.11 - 76.20
76.21 - 114.30
114.31 - 152.40
152.41 - 190.50
190.51 - 228.60
228.61 - 266.70
266.71 - 304.80
304.81 - 342.90
342.91 - 381.00
0 5 10 15
Kilometers

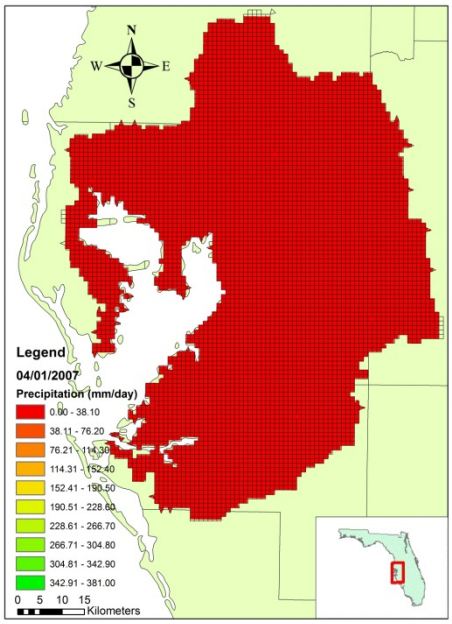
N
W
E
S
Legend
04/01/2007
Precipitation (mm/day)
0.00 - 38.10
38.11 - 76.20
76.21 - 114.30
114.31 - 152.40
152.41 - 190.50
190.51 - 228.60
228.61 - 266.70
266.71 - 304.80
304.81 - 342.90
342.91 - 381.00
0 5 10 15
Kilometers

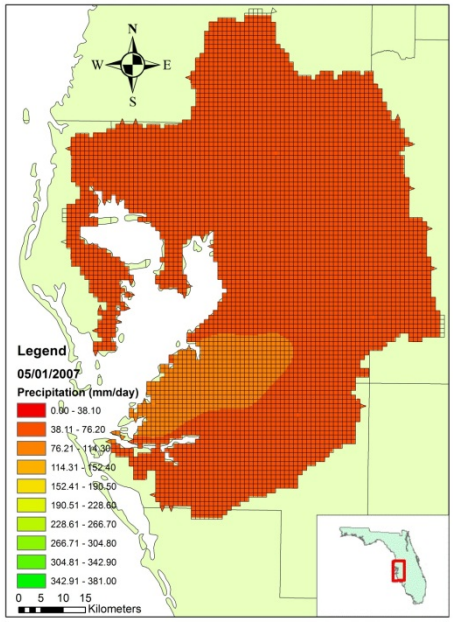
N
W
E
S
Legend
05/01/2007
Precipitation (mm/day)
0.00 - 38.10
38.11 - 76.20
76.21 - 114.30
114.31 - 152.40
152.41 - 190.50
190.51 - 228.60
228.61 - 266.70
266.71 - 304.80
304.81 - 342.90
342.91 - 381.00
0 5 10 15
Kilometers

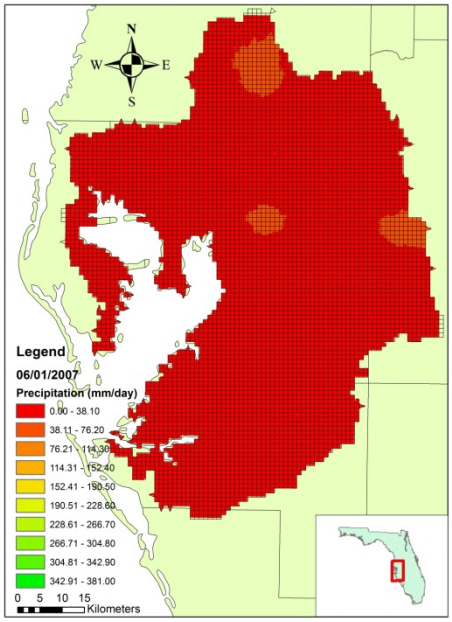
N
W
E
S
Legend
06/01/2007
Precipitation (mm/day)
0.00 - 38.10
38.11 - 76.20
76.21 - 114.30
114.31 - 152.40
152.41 - 190.50
190.51 - 228.60
228.61 - 266.70
266.71 - 304.80
304.81 - 342.90
342.91 - 381.00
0 5 10 15
Kilometers

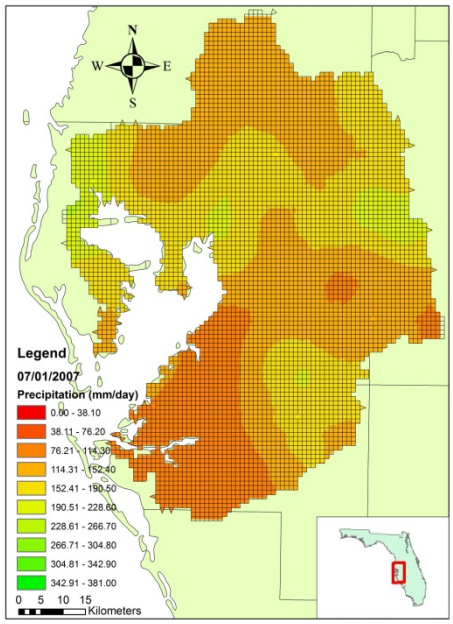
N
W
E
S
Legend
07/01/2007
Precipitation (mm/day)
0.00 - 38.10
38.11 - 76.20
76.21 - 114.30
114.31 - 152.40
152.41 - 190.50
190.51 - 228.60
228.61 - 266.70
266.71 - 304.80
304.81 - 342.90
342.91 - 381.00
0 5 10 15
Kilometers

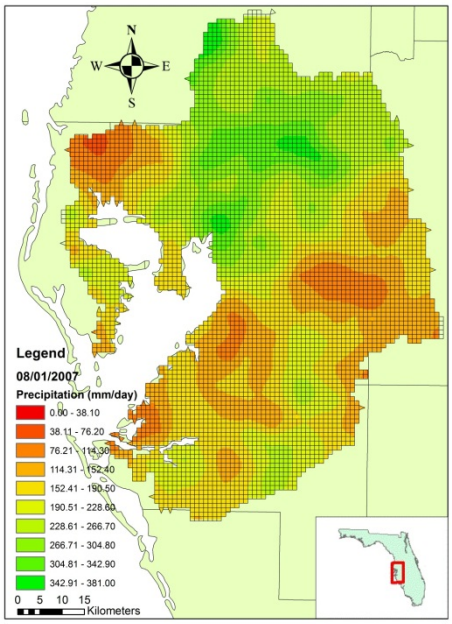
N
W
E
S
Legend
08/01/2007
Precipitation (mm/day)
0.00 - 38.10
38.11 - 76.20
76.21 - 114.30
114.31 - 152.40
152.41 - 190.50
190.51 - 228.60
228.61 - 266.70
266.71 - 304.80
304.81 - 342.90
342.91 - 381.00
0 5 10 15
Kilometers

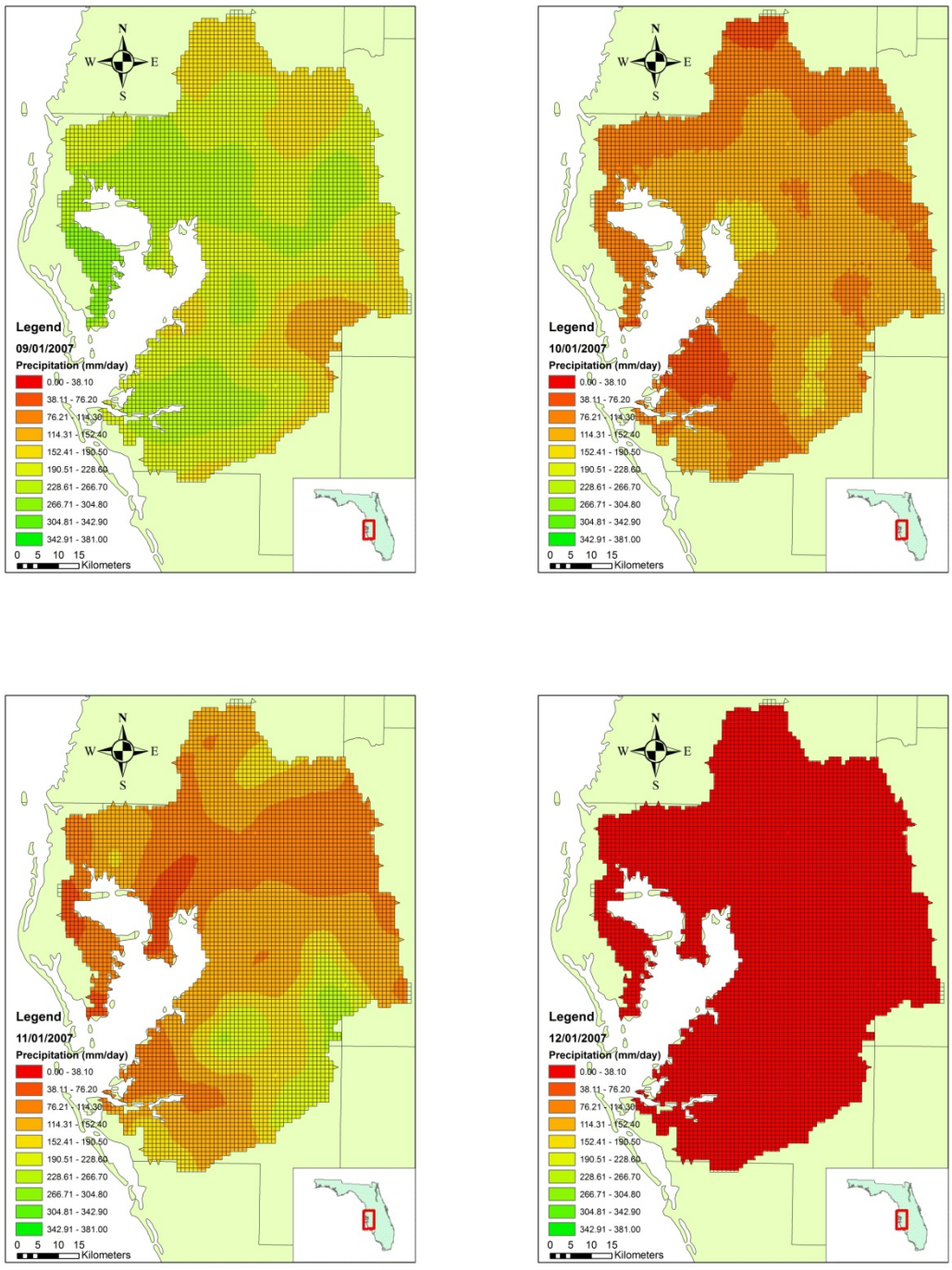

Figure A.11 Month-to-Date Precipitation maps for the Tampa Bay watershed for 2007.

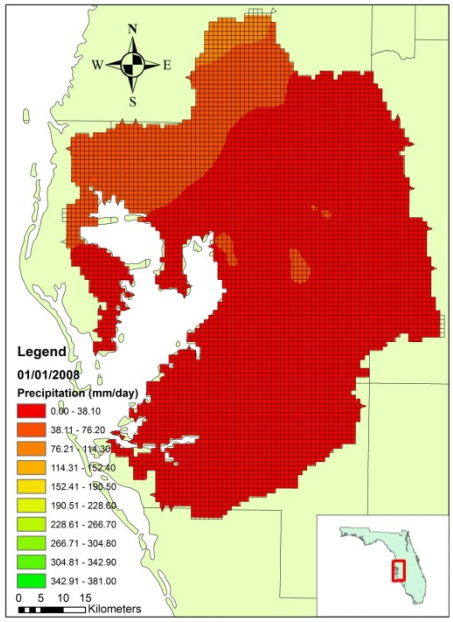
N
W
E
S
Legend
01/01/2008
Precipitation (mm/day)
0.00 - 38.10
38.11 - 76.20
76.21 - 114.30
114.31 - 152.40
152.41 - 190.50
190.51 - 228.60
228.61 - 266.70
266.71 - 304.80
304.81 - 342.90
342.91 - 381.00
0 5 10 15
Kilometers

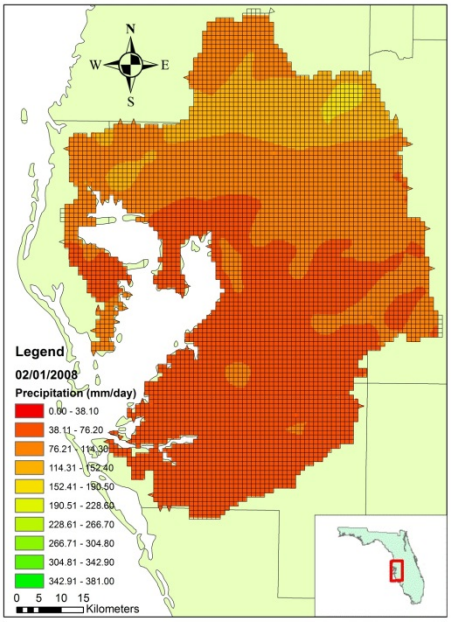
N
W
E
S
Legend
02/01/2008
Precipitation (mm/day)
0.00 - 38.10
38.11 - 76.20
76.21 - 114.30
114.31 - 152.40
152.41 - 190.50
190.51 - 228.60
228.61 - 266.70
266.71 - 304.80
304.81 - 342.90
342.91 - 381.00
0 5 10 15
Kilometers

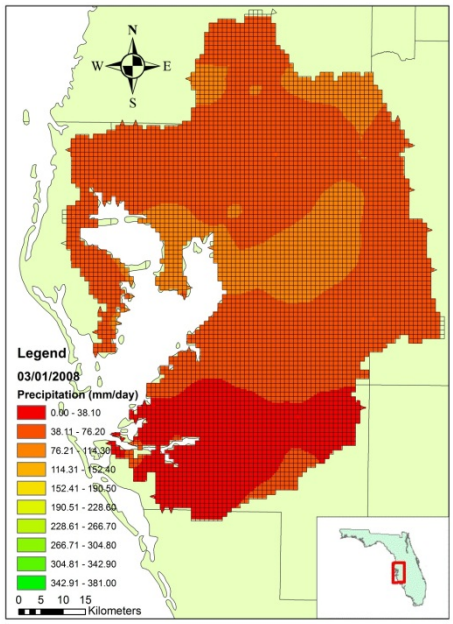
N
W
E
S
Legend
03/01/2008
Precipitation (mm/day)
0.00 - 38.10
38.11 - 76.20
76.21 - 114.30
114.31 - 152.40
152.41 - 190.50
190.51 - 228.60
228.61 - 266.70
266.71 - 304.80
304.81 - 342.90
342.91 - 381.00
0 5 10 15
Kilometers

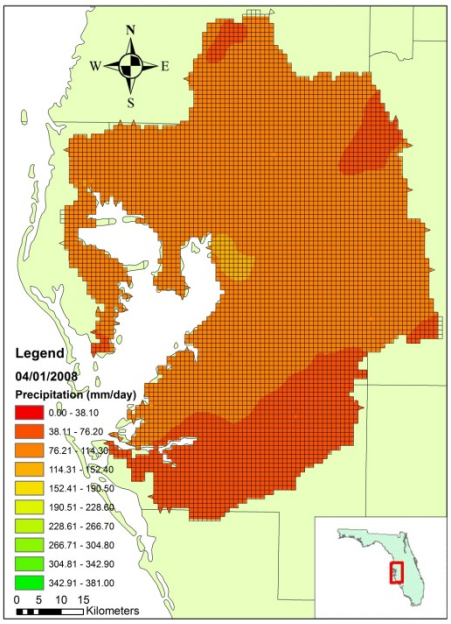
N
W
E
S
Legend
04/01/2008
Precipitation (mm/day)
0.00 - 38.10
38.11 - 76.20
76.21 - 114.30
114.31 - 152.40
152.41 - 190.50
190.51 - 228.60
228.61 - 266.70
266.71 - 304.80
304.81 - 342.90
342.91 - 381.00
0 5 10 15
Kilometers

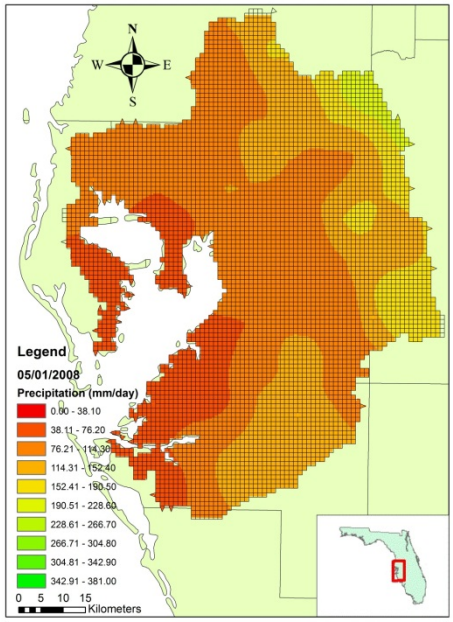
N
W
E
S
Legend
05/01/2008
Precipitation (mm/day)
0.00 - 38.10
38.11 - 76.20
76.21 - 114.30
114.31 - 152.40
152.41 - 190.50
190.51 - 228.60
228.61 - 266.70
266.71 - 304.80
304.81 - 342.90
342.91 - 381.00
0 5 10 15
Kilometers

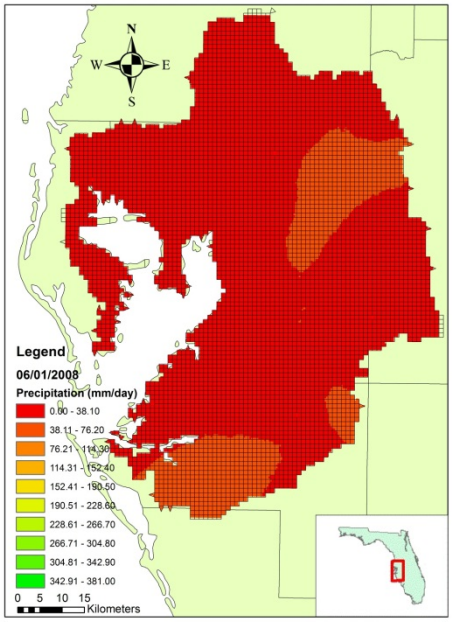
N
W
E
S
Legend
06/01/2008
Precipitation (mm/day)
0.00 - 38.10
38.11 - 76.20
76.21 - 114.30
114.31 - 152.40
152.41 - 190.50
190.51 - 228.60
228.61 - 266.70
266.71 - 304.80
304.81 - 342.90
342.91 - 381.00
0 5 10 15
Kilometers

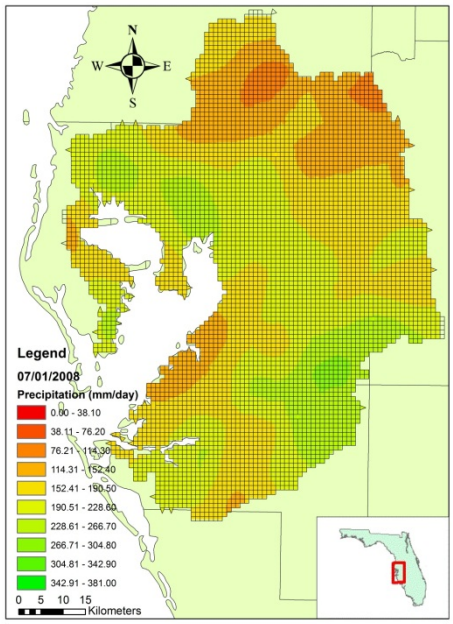
N
W
E
S
Legend
07/01/2008
Precipitation (mm/day)
0.00 - 38.10
38.11 - 76.20
76.21 - 114.30
114.31 - 152.40
152.41 - 190.50
190.51 - 228.60
228.61 - 266.70
266.71 - 304.80
304.81 - 342.90
342.91 - 381.00
0 5 10 15
Kilometers

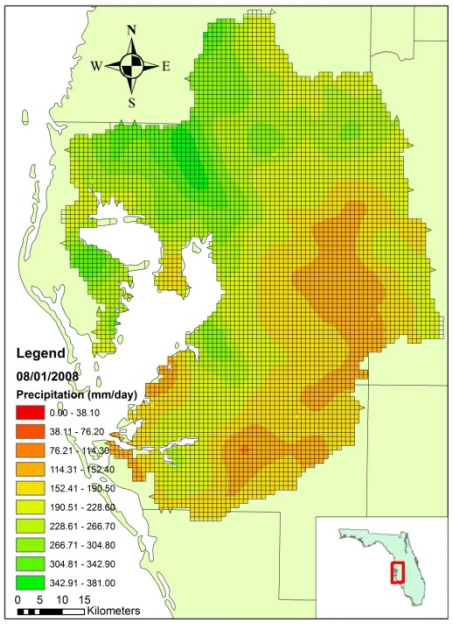
N
W
E
S
Legend
08/01/2008
Precipitation (mm/day)
0.00 - 38.10
38.11 - 76.20
76.21 - 114.30
114.31 - 152.40
152.41 - 190.50
190.51 - 228.60
228.61 - 266.70
266.71 - 304.80
304.81 - 342.90
342.91 - 381.00
0 5 10 15
Kilometers

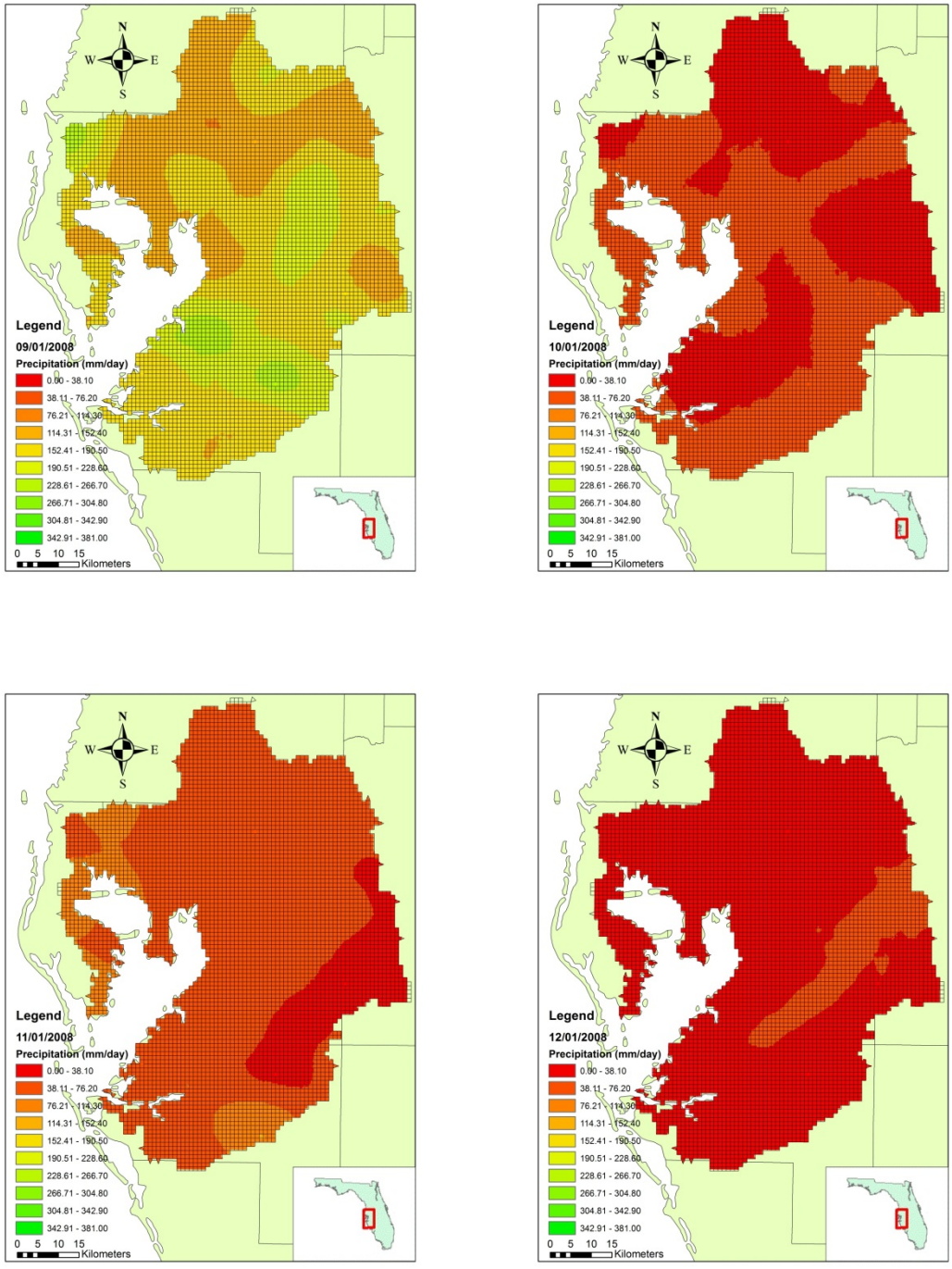

Figure A.12 Month-to-Date Precipitation maps for the Tampa Bay watershed for 2008.

REFERENCES

Adger, W. N., T. P. Hughes, C.Folke, S. R. Carpenter, and J. Rockström, Social-ecological resilience to coastal disasters. Science, 2005, 309 (5737), pp. 1036-1039.

Allenby, B., and J. Fink, Toward inherently secure and resilient societies. Science, 2005, 309 (5737), pp. 1034-1036.

Balling, R. C., and S. W. Brazell, High resolution surface temperature patterns in a complex urban terrain, Photogrammetric Engineering and Remote Sensing, 1988, 54, pp. 1289–1293.

Bannari, A., D. Morin, F. Bonn, and A. R. Huete, A review of vegetation indices. Remote Sensing Reviews, 1995, 13, pp. 95-120.

Bobbin, J., and F. Recknagel, Ecol. Modell, 2001, 146, 253–262.

Bobbin, J., and F. Recknagel, Environ. Int., 2001, 27, 237–242.

Boynton, W. R., and W. M. Kemp 1985. Mar. Ecol. Prog. Ser., 23, pp. 45–55.

Branco, A. B., and J. N. Kremer, Estuaries, 2005, 28 (5), pp. 643–652.

Bricker, S. B., B. Longstaff, W. Dennison, A. Jones, K. Boicourt, C. Wicks, and J. Woerner. Effects of Nutrient Enrichment in the Nation’s Estuaries: A Decade of Change, NOAA Coastal Ocean Program Decision Analysis Series No. 26, Silver Spring, MD: National Centers for Coastal Ocean Science, 2007.

Bricker, S. B., C. G. Clement, D. E. Pirhalle, Orlando, S. P., and Farrow, D. R. G. National Estuarine Eutrophication Assessment, Effects of Nutrient Enrichment in the Nation`s Estuaries. NOAA, 1999.

Burn, D. H., and A. H. E. Mohamed, Detection of Hydrologic Trends and Variability, Journal of Hydrology, 2002, 255.1-4, pp. 107-22.

Camillo, P. J., ‘‘Using one- or two-layer models for evaporation estimation with remotely sensed data,’’ in Land Surface Evaporation: Measurements and Parameterization, ed.

Carrera-Hernández, J. J., and S. J. Gaskin, Spatio temporal analysis of daily precipitation and temperature in the Basin of Mexico, Journal of Hydrology, 2007, 336, (3–4), pp. 231-249.

Cayan, D. R., and Douglas, A. V., Urban influences on surface temperatures in the southwestern United States during recent decades. Journal of Climate and Applied Meteorology, 1984, 23, pp. 1520–1530.

Chang, N. B., and Z. Xuan, Spatiotemporal interactions between soil moisture, vegetation cover and evapotranspiration in the Tampa Bay urban region, Florida, Chapter 6 in Multiscale Hydrological Remote Sensing: Perspectives and Applications, CRC Press, Boca Raton, FL, USA, 2011.

Chang, N. B., Y. Yang, J. A. Goodrich, and A. Makkeasorn, Development of the metropolitan water availability index (MWAI) and short-term assessment with multi-scale remote sensing technologies, Journal of Environmental Management, 2010, 91, pp. 1397-1413.

Chang, N. B., Z. Xuan, and B. Wimberly, "MODIS-based spatiotemporal patterns of soil moisture and evapotranspiration interactions in Tampa Bay urban watershed", Proc. SPIE 8156, 815602, 2011.

Changnon, S. A., Inadvertent weather modification in urban areas: lessons for global climate change. Bulletin of the American Meterological Society, 1992, 73, pp. 621–627.

Cliff, A. D., and J. K. Ord, Spatial and temporal analysis: autocorrelation in space and time, In E. N. Wrigley and R. J. Bennett, editors, Quantitative Geography: A British View, 1981, pp. 104-110.

Cliff, A. D., and J. K. Ord, Spatial Autocorrelation, Pion, London, 1973.

Cloern, J., Mar. Ecol. Prog. Ser., 2001, 210, pp. 223–253.

Conley, D. J., S. Markager, J. Andersen, T. Ellermann, and L.M. Svendsen. Estuaries, 2002, 25, pp. 706–719.

Davis, J., and Y. Sheng, Proc Int CONF Estuarine Coast Model, 2000, 470–484.

D'Esopo, D. A., and B. Lefkowitz. Oper. Res., 1963, 11(6), pp. 901–907.

Diaz, R. J., and R. Rosenberg, Science, 2008, 321, pp. 926–929.

Felip, M., and J. Catalan, J. Plankton Res., 2000, 22, pp. 91-106.

Gallo, K. P., A. L. McNab, T. R. Karl, J. F. Brown, J. J. Hood, and J. D. Tarpley, The use of NOAA AVHRR data for assessment of the urban heat island effect. Journal of Applied Meteorology, 1993, 32, pp. 899– 908.

Gallo, K. P., and T. W. Owen, Assessment of urban heat island: A multi-sensor perspective for the Dallas-Ft. Worth, USA region. Geocarto International, 1998, 13, pp. 35–41.

Gleick, P. H., Climate change, hydrology, and water resources, Reviews of Geophysics, 1989, 27, pp. 329-344.

Goovaerts, P., “Geostatistics For Natural Resources Evaluation,” Oxford University Press, New York, 1997.

Haase, D., Effects of urbanization on the water balance – a long-term trajectory. Environmental Impact Assessment Review, 2009, 29, pp. 211-219.

Houghton, J. T., L. A. Meira Filho, and B. A. Callendar, Climate change 1995: the second IPCC scientific assessment," Intergovernmental Panel on Climate Change, Cambridge University Press, Cambridge, UK, 1996.

Howarth, R., F. Chan, D. J. Conley, Garnier J., S. C. Doney, R. Marino and G. Billen, Front Ecol Environ., 2011, 9 (1), pp. 18-26.

Hu, C., F. E. Muller-Karger, G. A. Vargo, M. B. Neely, E. Johns. Geophys. Res. Lett., 2004, 31.

Huete, A., C. Justice, and W. van Leeuwen, MODIS vegettaion Index (MOD 13): Algorithm Theoretical Basis Document, 1999, 3. http://modis.gsfc.nasa.gov/data/atbd/atbd_mod13.pdf.

Huete, A., K. Didan, T. Miura, E. P. Rodriguez, X. Gao, and L. G. Ferreira, Overview of the radiometric and biophysical performance of the MODIS vegetation indices. Remote Sensing of Environment, 2002, 83, pp. 195–213.

Isaaks, E. H., and R. M. Srivastava, An Introduction to Applied Geostatistics," Oxford University Press, Oxford, (1999).

Jacobs, J., J. Mecikalski, and S. Paech, Satellite-based Solar Radiation, Net Radiation, and Potential and Reference Evapotranspiration Estimates over Florida. Technical Report, Florida Integrated Water Science Center, the United States Geological Survey (USGS), Orlando, FL, USA, 2008.

Janicki, A., R. Pribble, S. Janicki, and M. Winowitch, An Analysis of Long-term Trends in Tampa Bay Water Quality. Technical Report, Tampa Bay Estuary Program, submitted by Janicki Environmental,Inc.

http://www.tampabay.wateratlas.usf.edu/upload/documents/AnalysisLongTermTrendsTampWaterQuality.pdf, accessed by March 2011.

Karl, T. R., and D. R. Easterling, Climate extremes: Selected review and future research directions. Climatic Change, 1999, 42, pp. 309–325.

Karl, T. R., H. F. Diaz, and G. Kukla, Urbanization: its detection and effect in the United States climate record, Journal of Climate, 1988, 1, pp. 1099–1123.

Ketchum, B. H., Distribution of coliform bacteria and other pollutants in tidal estuaries, Sewage Indust. Wastes, 1955, 27, pp. 1288-1296.

Kidder, S. Q., and H. T. Wu, A multispectral study of the St. Louis area under snow-covered conditions using NOAA-7 AVHRR data. Remote Sensing of Environment, 1987, 22, pp. 159–172.

Krige, D. G., A statistical approach to some mine valuations and allied problems at the Witwatersrand, Master's thesis of the University of Witwatersrand, 1951.

Kuo, A., K. Park, S. Kim, and J. Lin. Coastal Management, 2005, 33, pp. 101–117.

Lloyd, S. P., IEEE Trans. Inf. Theory, 1982, 28 (2), pp. 129–137

MacQueen, J. B., Proceedings of 5-th Berkeley Symposium on Mathematical Statistics and Probability, Berkeley, University of California Press, 1967, 1, 281–297.

Milich, L., and E. Weiss, "GAC NDVI interannual coefficient of variation (CoV) images: ground truth sampling of the Sahel along north-south transects," Int. J. Remote Sens., 2000, 21, pp. 235-260.

Moran, P. A., Notes on continuous stochastic phenomena, Biometrika, 1950, 37, 17-23.

National Climatic Data Ceneter (NCDC), Climate of 2004 Atlantic Hurricane Season, National Climatic Data Center, NOAA, 2004. http://www.ncdc.noaa.gov/oa/climate/research/2004/hurricanes04.html.

National Oceanic and Atmospheric Administration (NOAA). State of Coastal Environment. http://oceanservice.noaa.gov/websites/retiredsites/sotc_pdf/EUT.PDF, accessed by March 2011.

NRC (National Research Council). Clean coastal waters: understanding and reducing the effects of nutrient pollution. Washington, DC: National Academies Press. 2000.

Roth, M., T. R. Oke, and W. J. Emery, Satellite derived urban heat islands from three coastal cities and the utilisation of such data in urban climatology. International Journal of Remote Sensing, 1989, 10, pp. 1699–1720.

Running, S. W., ‘‘Computer simulation of regional evapotranspiration by integrating landscape biophysical attributes with satellite data,’’ in Land Surface Evaporation: Measurements and Parameterization, ed.

Russell, M., J. Rogers, S. Jordan, D. Dantin, J. Harvey, J. Nestlerode and F. Alvarez, Prioritization of Ecosystem Services Research: Tampa Bay Demonstration Project, Journal of Coastal Conservation, 2011, 15(4), pp. 647 – 658.

Ryther, J. H., and W. M. Dunstan. Science, 1971, 171, 1008–1013.

Schmugge, T. J., and J. C. André, New York: Springer-Verlag, 1991.

Sellers, P. J., F. G. Hall, G. Asrar, D. E. Strebel, and R. E. Murphy, The first ISLSCP Field Experiment (FIFE), Bull. Amer. Meteorol. Soc., 1988, 69 (1), pp. 22-27.

Steidinger, K. A., J. H. Landsberg, C. R. Tomas, and G. A. Vargo, Four Karenia brevis blooms: A comparative analysis in Harmful Algae 2002: Proceedings of the Xth International Conference on Harmful Algae, Fla. Inst. of Oceanography, St. Petersburg, Fl., 2004.

Steidinger, K. A., Phytoplankton of Tampa Bay: A Review, Florida Department of Natural Resources, Bureau of Marine Research.

Streutker, D. R., A remote sensing study of the urban heat island of Houston, Texas, International Journal of Remote Sensing, 23 (2002), pp. 2595– 2608.

Strickland, J. D., Bull. Fish.Res.Board Can., 1960, 122, 1–172.

Sun, Z. D., N. B. Chang, and C. Opp, Using SPOT-VGT NDVI as a successive ecological indicator for understanding the environmental implications in the Tarim River Basin, China, Journal of Applied Remote Sensing 4, 2010.

Takamura, N., A. Otsuki, M. Aizaki and Y. Nojiri. Archives fur. Hydrobiology, 1992, 24 (2), pp. 129–148.

Tang, P., M. Steinbach, and V. Kumar, Introduction to Data Mining. Boston: Pearson Addison Wesley, 2006.

The Cadmus Group, Inc, comp. Nutrient Control Design: Manual State of Technology Review Report. Rep. no. EPA/600/R-09/012. Environmental Protection Agency, 2009.

Thuraisingham, B. M., Data Mining: Technologies, Techniques, Tools, and Trends. Boca Raton: CRC., 1999.

Tomczak, M., Spatial interpolation and its uncertainty using automated anisotropic inverse distance weighting (IDW) – cross validation/jacknife approach, Journal of Geographic Information and Decision Analysis, 1998, 2, pp. 18–30.

Vicente-Serrano, S. M., J. M. Cuadrat-Prats, and A. Romo, "Aridity influence on vegetation patterns in the middle Ebro Valley (Spain): Evaluation by means of AVHRR images and climate interpolation techniques," J. Arid Environ., 2006, 66, pp. 353-375.

Wackernagel, H., Multivariate geostatistics: An introduction with applications, Springer, New York, (2003).

Wei, B., N. Sugiura and T. Maekawa, Water Res., 2001, 35 (8), pp. 2022–2028.

Weier, J., and D. Herring, Measuring vegetation (NDVI & EVI). Earth Observatory, NASA, 2006. http://earthobservatory.nasa.gov/Library/MeasuringVegetation/printall.php.

Weng, Q., A remote sensing-GIS evaluation of urban expansion and its impact on surface temperature in the Zhujiang Delta, China. International Journal of Remote Sensing, 2001, 22, pp. 1999–2014.

Weng, Q., Estimation of Land Surface Temperature–vegetation Abundance Relationship for Urban Heat Island Studies." Remote Sensing of Environment 2004, 89.4, pp. 467-83.

Weng, Q., Fractal analysis of satellite-detected urban heat island effect. Photogrammetric Engineering and Remote Sensing, 2003, 69, pp. 555-566.

Wu, X., V. Kumar, J. R. Quinlan, J. Ghosh, Q.Yang, H. Motoda, G. J. McLachlan, A. Ng, B. Liu, P. S. Yu, Z. Zhou, M. Steinbach, D. J. Hand, and D. Steinberg, Knowl Inf Syst., 2008, 14, pp. 1–37.

Yassuda, E. A., and Y. P. Sheng, Estuarine and Coastal Modeling, V, American Society of Civil Engineers, 1998, 35–58.

Zhang, L., R. Lemeur, and J. P. Goutorbe, A one-layer resistance model for estimating regional evepotranspiration using remote sensing data,'' in Agricul. and Forest Meteorol., 1995, 77, pp. 241-261.